Mechanistic Investigation of Cytochrome P450 1A2 Catalyzed Metabolism of 8-Alkylxanthines

Jason Boer

A dissertation submitted in partial fulfillment of the requirements for the degree of

Doctor of Philosophy

University of Washington

2003

Program Authorized to Offer Degree:
School of Pharmacy, Department of Medicinal Chemistry

In presenting this dissertation in partial fulfillment of the requirements for the Doctoral degree at the University of Washington, I agree that the Library shall make its copies freely available for inspection. I further agree that extensive copying of the dissertation is allowable only for scholarly purposes, consistent with "fair use" as prescribed in the U.S. Copyright Law. Requests for copying or reproduction of this dissertation may be referred to ProQuest Information and Learning, 300 North Zeeb Road, Ann Arbor, MI 48106-1346, to whom the author has granted "the right to reproduce and sell (a) copies of the manuscript in microform and/or (b) printed copies of the manuscript made from microform."

Signature Jason Roe

Date 3/18/07

University of Washington
Graduate School

This is to certify that I have examined this copy of a doctoral dissertation by

Jason Boer

And have found that it is complete and satisfactory in all respects, and that any and all revisions required by the final examining committee have been made.

Chair of Supervisory Committee:


Kent L. Kunze

Reading Committee:


Kent L. Kunze


William Trager


William Atkins

Date: 3-4-03

University of Washington

Abstract

Mechanistic Investigation of Cytochrome P450 1A2 Catalyzed Metabolism of 8-Alkylxanthines

Jason Boer

Chair of the Supervisory Committee:
Associate Professor Kent L. Kunze
Department of Medicinal Chemistry

The mechanism of CYP1A2 (cytochrome P450 1A2) catalyzed metabolism of 8-alkylxanthines is explored using deuterium isotope effect studies and isotope tracing experiments with an 8-isopropyl analog (isopropylcyclohexylline, IPC) of the CYP1A2 mechanism-based inactivator furafylline. Desaturation of furafylline to an iminium reactive intermediate has been proposed to account for formation of both 1:1 CYP1A2-protein adduct and 8′-carbinol with the majority (80%) of the oxygen sourced to the medium. Reactive intermediate formation with 8-ethyl and 8–isopropyl analogs of furafylline is evident due to H_2O incorporation into their 8′-carbinol metabolites (60% and 43%, respectively), though enzyme inactivation is virtually eliminated. Additionally, 35% and 85%, respectively, of 8-ethyl and 8-isopropyl analog metabolism results in side chain desaturation. Competitive intermolecular deuterium isotope effect studies with IPC in the presence of $H_2{}^{18}O$ suggest that both dual hydrogen atom abstraction and base-catalyzed rearrangement of the reactive intermediate are contributing to olefin metabolite formation, in contrast to the results from similar experiments with the 8-ethyl compound in which rearrangement of the reactive intermediate appears to be the only mechanism of side-chain desaturation. Intramolecular isotope effect analysis of IPC side chain desaturation in the presence of $H_2{}^{18}O$ did not clearly differentiate between the two proposed desaturation pathways. Several mechanistic possibilities to explain the experimental results are discussed. Lastly, the effect of reducing equivalent transfer rate on the sequential metabolism of IPC by two different CYP1A2 enzyme sources was investigated using isotope-tracing experiments.

TABLE OF CONTENTS

LIST OF FIGURES

LIST OF TABLES

CHAPTER 1

INTRODUCTION

1.1 CYTOCHROMES P450

Cytochromes P450 are a super-family of heme-containing monooxygenases primarily involved in the metabolism of xenobiotics. Xenobiotic-metabolizing CYPs are inherently promiscuous, with broad and overlapping substrate specificities (*1*). The native mammalian P450 isoforms have proven to be resistant to crystallization due to their hydrophobicity and membrane-association. To date, a modified rabbit 2C5 enzyme is the only mammalian isoform with x-ray crystallographic three-dimensional structural information (*2, 3*). Structural analysis of all other P450s is derived from homology models based upon few well-characterized soluble bacterial isoforms for which crystal structures have been determined (*1, 4*). The hydrophobic active site pockets of P450s promote binding of hydrophobic xenobiotic substrates, which are usually converted to relatively hydrophilic metabolites, facilitating elimination from the body. In some instances, these metabolites are highly reactive species leading to cellular toxicity, due to binding to cellular macromolecules.

The catalytic power of CYPs is centered about their iron-containing protoporphyrin IX (heme) prosthetic group (Figure 1.1). The hexacoordinate-iron, bound in the heme by the tetrapyrrole nitrogen atoms, has a cysteinate fifth ligand, leaving the sixth position available for binding molecular oxygen (*1*). Activation of bound molecular oxygen to a family of highly reactive heme-oxygen species allows P450s to catalyze a variety of oxidative reactions, including aromatic and aliphatic hydroxylation, N- and O-dealkylation, and olefin epoxidation (*5-8*). Figure 1.2 illustrates some of the more common types of P450 metabolic reactions.

1.2 CYTOCHROME P450 CATALYTIC CYCLE

The classic cytochrome P450 catalytic cycle (Figure 1.3) begins with the enzyme in its resting low spin, hexacoordinate, ferric state **1** (*1*). An active site water molecule, which is believed to occupy the sixth ligand position, is displaced by the substrate binding. Loss of the sixth ligand shifts the heme to a high spin state **2**, facilitating a one-electron reduction by NADPH-P450 reductase to generate the ferrous state **3**. At this point, molecular oxygen binds to the iron in the sixth ligand position creating the ferrous dioxygen complex **4**. Subsequent second electron transfer from NADPH-P450 reductase leading to the ferric peroxide species **5** is generally regarded as the rate-limiting step of the cycle. Up to this point in the cycle, the intermediates and processes have been thoroughly characterized, however after the rate-limiting second electron transfer, the transient nature of the states leading back to the resting enzyme has precluded their complete elucidation. What is believed to happen is that the iron-peroxide species **5** experiences two rapid and sequential protonations of the distal oxygen, followed by the loss of a water molecule, generating the iron-oxenoid species **6**. A recent x-ray crystallography study of P450cam catalysis at cryogenic temperatures supports this sequence of events (*9*). After addition of the second electron, O-O bond cleavage was observed, leaving a single oxygen atom bound to the iron. In addition, evidence for a proton shuttle involving active site water molecules and active site protein residues was observed (*9*). While the iron-oxenoid species **6** is believed to be the active oxidant in most P450 reactions, there is a growing body of evidence suggesting that the iron-peroxy anion **5** and perhaps the mono-protonated iron-hydroperoxy species are involved in certain types of P450-catalyzed oxidation reactions.

1.3 MECHANISM OF CYP-MEDIATED HYDROXYLATION

Cytochromes P450 readily catalyze alkane hydroxylation at ambient temperatures, overcoming a significant energy barrier (96, 99, 101 kcal/mol for C-H bond dissociation energies of 3°, 2°, and 1° carbons, respectively) (*10*). The mechanism of hydroxylation by P450s has been the focus of intense mechanistic investigation. Initially an insertion mechanism (Figure 1.4a) was proposed for this reaction, based on early studies that showed that the process usually involved retention of stereochemistry and displayed small kinetic isotope effects (*11-13*). Subsequent experiments, however, refuted the insertion mechanism, while supporting a stepwise "oxygen-rebound" mechanism (Figure 1.4a). Hydroxylation of exo, exo, exo, exo-tetradeuteronorbornane **1.5.1** by $P450_{LM2}$ gave the trideutero-endo-alcohol **1.5.2** and the tetradeutero-exo-alcohol **1.5.3**, both of which require stereochemical scrambling *in route* to product formation, and therefore support a stepwise mechanism (*14*). In addition, the high deuterium isotope effects associated with hydroxylation of norbornane (11.5 ± 1) are inconsistent with an insertion mechanism (*14*). Allylic rearrangement in the hydroxylated product **1.5.5** of tetradeutero-cyclohexene **1.5.4** also supports a stepwise process (*15*). Lastly, high isotope effects and stereochemical inversion associated with benzylic hydroxylation of ethylbenzene **1.5.6** suggest the existence of a discrete radical intermediate (*16*). As a result of these findings, the stepwise oxygen rebound mechanism (Figure 1.4b) has been the consensus mechanism of P450-catalyzed hydroxylation for over a decade.

With the acceptance of the oxygen rebound mechanism, investigators then turned their attention to 'timing' of the substrate radical lifetime and recombination process using new mechanistic probes, the free-radical clocks (*17*). These probes were used

because of their ability to undergo rapid irreversible structural rearrangement or isomerization reactions upon generation of a radical intermediate (Figure 1.6). Detection of rearranged products indicated the existence of a radical intermediate, the lifetime of which may be estimated by comparison to the known rate of rearrangement of the probe substrate radical. For instance, if a probe substrate radical is known to rearrange at a rate of $5 \times 10^5\ s^{-1}$ and no rearrangement products are observed in incubations, then the rate of oxygen rebound or recombination must be in great excess of $5 \times 10^5\ s^{-1}$. If another probe with a rate of radical rearrangement of $5 \times 10^8\ s^{-1}$ is chosen, and the ratio of unrearranged to rearranged carbinols is 5/1, then the rate of oxygen rebound must be approximately five times that of radical rearrangement ($2.5 \times 10^9\ s^{-1}$).

Initial studies with radical clock substrates, methylcyclopropane **1.6.1**, nortricyclane **1.6.3**, and bicyclo[2.1.0]pentane **1.6.5**, showed that radical recombination must be significantly faster than cyclopropylmethyl radical rearrangement ($1.3 \times 10^8\ s^{-1}$); only unrearranged carbinol products of methyl cyclopropane and nortricyclane (**1.6.2** and **1.6.4**, respectively) were detected (*18*). Hydroxylation of bicyclo[2.1.0]pentane, on the other hand, produced a 7:1 mixture of unrearranged **1.6.6** and rearranged **1.6.7** alcohols. Later determination of the rate of bicyclo[2.1.0]pentane rearrangement ($2.4 \times 10^9\ s^{-1}$) indicated that the rate of recombination was $2 \times 10^{10}\ s^{-1}$ (*19*).

Continued efforts with radical clock probe substrates with ever increasing rates of rearrangement lead to increasingly fast estimates of recombination rate, up to $7 \times 10^{12}\ s^{-1}$ (*20, 21*). Initially, these results were believed to be misleading, as many of the faster radical clocks were also large compounds, and therefore the radical rearrangement process may be impeded by active site constraints. This would lead to less detected

rearranged product and an overestimation of the rate of recombination. However, studies with radical probes immune to such active site constraints also reacted with exceedingly fast recombination rates, now up to 1.4 x 10^{13} s^{-1} (*21, 22*). Ultimately, this lead to the proposal that a carbocation intermediate may play a role in hydroxylation by P450s (*22*).

Newcomb and coworkers, in a series of studies using hypersensitive mechanistic probes with divergent radical and cationic rearrangement pathways (Figure 1.6d), have obtained evidence consistent with the existence of a cationic intermediate in P450-catalyzed hydroxylation reactions, in addition to a recombination rate of 1.5 x 10^{13} s^{-1} (*23-26*). These results, however, require a radical intermediate lifetime of 80-200 fs, too short for a true intermediate, suggesting a competing pathway in which cation generation is possible, but not obligatory. From this work, a "unified mechanistic view of P450-catalyzed hydroxylations" has been proposed, wherein: 1) both the iron-oxenoid and the iron-hydroperoxy species can participate in hydroxylation reactions, 2) no radical intermediates are produced in hydroxylation by either species, both are insertion processes, and 3) hydroxylation by the iron-oxenoid species results in a neutral product, whereas hydroxylation by the iron-hydroperoxy species involves insertion of OH^+ to form a protonated alcohol, which can lead to cationic rearrangement (*26*).

A "two-state reactivity" paradigm, which accounts for all of the divergent observations, has recently been proposed (*27-30*). In this proposal, the low-spin and high-spin states of the iron-oxenoid species are proposed to both participate in hydroxylation reactions, albeit by different physical processes. The low-spin state is prone to concerted mechanisms, whereas the high-spin participates in hydrogen atom-abstraction processes. Spin-state inversion in the process of hydroxylation is marshaled

to explain some of the disparate mechanistic findings to date. Interestingly, Newcomb and coworkers (previous paragraph) seem amenable to adoption of the two-state reactivity paradigm to explain some of their results (*26*).

Finally and most recently, Auclair, *et al.* have shown clear evidence for the involvement of a radical intermediate in hydroxylation reactions by four different CYPs (*31*). Depending on the particular P450 isoform used, the radical lifetime ranged from 16 to 52 ps, corresponding to a recombination rate on the order of 2×10^{10} s^{-1}. Trace amounts of cationic rearrangement products were also observed. The authors conclude that their results are consistent with Shaik's two-state reactivity paradigm, with the mechanism of any particular hydroxylation existing on a continuum of mechanisms ranging from insertion to generation of a discrete substrate radical intermediate. Where a particular hydroxylation lies on this continuum depends upon the stability of the incipient substrate radical. Contrary to Newcomb and coworkers, cation generation is believed to be due to a second electron transfer from the substrate radical, and the notion of iron-hydroperoxy species involvement is deemed improbable (*31*).

Overall, these and other studies support the view that the mechanism of hydroxylation by P450s may be far more complex than originally thought. Great strides are being made in the analysis of the experimental observations, including convergence of different mechanistic proposals and the involvement of multiple oxidants (*26, 31*). As it stands, it is the author's opinion that the overwhelming majority of evidence supports a hydroxylation mechanism like that proposed by Auclair, *et al.*, involving a discrete radical intermediate, the lifetime and fate (possible second electron transfer) of which is highly dependent upon substrate structure. The two-state reactivity of the iron-oxenoid

complex proposed by Shaik, *et al.* is an intriguing possibility and warrants further consideration.

1.4 MECHANISM OF P450-CATALYZED DESATURATION

P450s are capable of dehydrogenation of substrates yielding desaturated metabolites. P450-mediated desaturation is of toxicological importance due to its involvement in bioactivation processes. Olefinic products may be further converted to epoxides which are known alkylating agents. Drawing upon what is known about hydroxylation by P450s and that desaturation is often accompanied by hydroxylation, mechanistic convergence is likely. Figure 1.7 shows two proposed mechanisms of P450-catalyzed dehydrogenation (*1*). Both mechanisms are initiated by a hydrogen atom transfer, resulting in a carbon radical that may undergo recombination to generate the hydroxylated product. Alternatively, the intermediate radical may be decomposed by the iron bound hydroxyl radical through either a second electron transfer (SET) (followed by deprotonation) or a second hydrogen atom transfer (HAT) leading to the desaturated product.

Perhaps the most complete mechanistic exploration of desaturation by P450s has been on that of valproic acid (VPA) (*32-37*). Desaturation of VPA to its hepatotoxic $\Delta^{4,5}$-olefin metabolite is accompanied by hydroxylation of both the 4 and 5- positions (Figure 1.8) (*34*). Intramolecular deuterium isotope effect analysis of the formation of the desatured product and carbinols clearly indicate that 4-hydroxylation and $\Delta^{4,5}$-desaturation both require the initial removal of the 4-hydrogen atom. Both 4-hydroxy- and 4-ene-VPA formation display large normal isotope effects (5.05 and 5.58,

respectively) when formed from [4,4-$^2H_2$]VPA, whereas low normal isotope effects are observed when these same metabolites are formed from [5,5,5-$^2H_3$]VPA (1.09 and 1.62, respectively) (*35*). Thus, the C-4 carbon radical is the most likely intermediate for 4-hydroxylation and $\Delta^{4,5}$-desaturation, and the second HAT from the 5-position is isotopically sensitive. Terminal 5-hydroxylation appears to be a separate metabolic process, with no desaturation resulting from the initial removal of the 5-hydrogen atom (*35*). These results indicate that desaturation in this case involves a dual hydrogen atom transfer mechanism (sequential HAT reactions), although formation of a carbocation remains a possibility, as discrimination between dual HAT and HAT/SET mechanisms was not possible with these studies (*38*). Even with the relatively large amounts of desaturation occurring in VPA metabolism, product ratios indicate that the vast majority of the initially formed carbon radical undergoes oxygen-rebound to form the carbinol product.

Deuterium isotope effect studies on testosterone desaturation to Δ^6-testosterone by CYP2A1 indicate that, like VPA, the dehydrogenation of testosterone is through a dual HAT mechanism (Figure 1.9) (*39*). The metabolic profile of this reaction is similar to that of VPA, in that both 6α- and 7α-hydroxylation, as well as Δ^6-desaturation, are observed. Isotope effects suggest that Δ^6- and 6α-hydroxytestosterone share a common intermediate, presumably the 6-carbon radical. Interestingly, the isotope effects associated with 6α- and 7α-hydroxylation from 6α,7α-d_2-testosterone are significantly different (2.6 and 9.2, respectively) (*39*). The differential isotope effects on seemingly identical reactions are explained by the potential for resonance stabilization of the C6-

radical by the adjacent conjugated 3,4,5-enone system of testosterone (*39*). Resonance stabilization of the carbon radical intermediate is also invoked to account for the larger desaturation to oxygen rebound ratio observed with testosterone metabolism (≈ 1), as compared to an aliphatic system like VPA (< 0.02 in phenobarbital-induced rat liver microsomes) (*34, 39*). Radical delocalization could allow the enzyme to sample other mechanistic possibilities besides recombination, such as a second HAT.

The electrophilic 3-methylindole dehydrogenation product, 3-methyleneindolenine, is believed to be the primary cause of the its associated pulmonary toxicity (*40*). Deuterium isotope effects on 3-methyleneindolenine and indole-3-carbinol formation from [d_3-methyl]-3-methylindole were large, normal, and similar in magnitude (5.5 and 5.0, respectively), suggesting that the formation of both products begins with initial hydrogen atom abstraction from the exocyclic methyl group, followed by second electron transfer, second hydrogen atom transfer, or recombination (Figure 1.10) (*40*). Interestingly, the desaturation/oxygen rebound ratio of 3-methylindole metabolism (10) is extraordinarily high by comparison to other well-known desaturation processes, such as Δ^6-testosterone formation (≈1.0) [Korzekwa, 1990 #11] and Δ^2,Δ^4-valproic acid formation (0.5) (Δ^2-VPA is desaturated to Δ^2,Δ^4-VPA) (*37*). In addition, as much as 85% of the 3-methyl carbinol product of 3-methylindole stemmed from addition of oxygen from the medium to the desaturated product. When one factors this into the desaturation to oxygen rebound ratio, the resultant ratio (50) is far above any observed in the literature. Again, delocalization of the substrate radical intermediate following initial HAT is invoked to explain the exceedingly large amounts of desaturated product (*40*). In

the case of 3-methylindole, potential conjugation with the aromatic indole appears to enhance resonance stabilization.

P450-catalyzed desaturation reactions are not limited to C-C bonds. C-N bonds are also susceptible through a third proposed mechanism of P450-catalyzed desaturation, initiated by a single electron transfer from the heteroatom (*5*). 1,4-Dihydropyridines are known to undergo aromatization through a CYP-dependent process. The mechanism is thought to involve initial formation of a nitrogen radical cation by P450-mediated electron abstraction (Figure 1.11). Initial electron transfer, rather than HAT, is believed to occur because of 1) the observed liberation of 4-alkyl radicals, 2) the lack of selectivity for loss of the 4-hydrogen atom, indicative of a non-enzymatic process, and 3) the low isotope effects on 4-hydrogen atom removal (1-3), consistent with isotope effects for oxidation of amines, which are believed to experience initial electron transfer from the nitrogen atom (*41-43*). The radical cation intermediate can then undergo aromatization by subsequent transfer of a hydrogen atom (path A in figure 1.11), transfer of a second electron plus a proton (path A in figure 1.11), or by loss of a 4-alkyl radical plus a proton (path B in figure 1.11) (*42, 44-46*).

Desaturation by P450s is a reaction that seemingly has no single mechanism and, like all chemical reactions, follows the path of least resistance. Whether initiated by a HAT or an electron transfer, radical stabilization appears to play a major role in dictating the metabolic flux between recombination and desaturation pathways

1.5 MECHANISM OF P450-MEDIATED EPOXIDATION

Epoxidation reactions by P450s are of particular toxicological interest because the products are potentially highly reactive toward nucleophilic moieties of cellular macromolecules. As with hydroxylation and desaturation, much controversy surrounds the mechanism of P450-catalyzed epoxidation. Initially, epoxidation was thought to involve simultaneous formation of both C-O bonds, due to the retention of olefin substrate stereochemistry (*5*). However, differential isotope effects on epoxide formation from internal- and external-carbon deuterated analogs of styrene suggested the asynchronous transfer of oxygen to the π-bond (*47*). Similar isotope effects from deuteration in either position would be expected if the mechanism involved simultaneous C-O bond formation.

Support for a nonconcerted epoxidation mechanism primarily comes from the observation of prosthetic heme alkylation associated with the oxidation of certain terminal olefins (Figure 1.12) (*5*). Additional support is provided by the direct formation of carbonyl rearrangement products during oxidation of some olefins, a process indicative of cation formation (Figure 1.12) (*5*). A final observation by Groves, *et al.* that epoxidation of trans-1-deuteriopropene is accompanied by significant loss of the deuterium suggests the formation of a metallaoxetane intermediate (Figure 1.12) (*5, 48*). Figure 1.12 shows a mechanistic scheme covering most of the currently proposed mechanisms of epoxidation, beginning with the generally accepted initial formation of a charge transfer complex between the iron-oxenoid and the olefin. However, the mechanistic controversy expands beyond the mechanism of oxygen addition to the identity of the iron-oxygen species involved in epoxidation.

In a series of mutation studies on mammalian P450s, disruption of the proton shuttle necessary for conversion of the peroxo-iron to oxenoid-iron was found to diminish reactions thought to require the iron-oxenoid species, while enhancing those thought to involve the iron-hydroperoxy or –peroxy species (*49-51*). These results suggest that the iron-oxenoid species is not the only oxidant produced in the P450 cycle; rather all three iron-oxygen complexes are capable of catalyzing certain P450 reactions, depending on the nature (electrophilic or nucleophilic) of the oxidant required (Figure 1.13a) (*50*). In particular, the iron-hydroperoxy species is proposed to be involved in epoxidation reactions, through an insertion process (Figure 1.13b) (*50*). These results are corroborated by the results obtained with iron-porphyrin model systems, which also indicate that both the iron-oxenoid and iron-hydroperoxy participate in olefin epoxidation (*52, 53*).

Finally, and most recently, computational studies performed by Shaik and coworkers indicate that the iron-oxenoid species is the sole oxidant involved in P450-catalyzed epoxidation reactions (*54*). Two-state reactivity (quartet and doublet spin states) of the iron-oxenoid complex, in addition to two heme oxidative states (Fe^{IV} with a neutral porphyrin ring and Fe^{III} with a cation radical porphyrin ring), are invoked to explain previously observed experimental results (*55*). Like these authors' proposed mechanism of hydroxylation (*29, 30*), the doublet spin state is thought to participate in insertion-type reactions, whereas catalysis by the quartet spin state involves a more stepwise process with transient radical intermediates (*55*). In addition, significant participation of a cationic intermediate (see figure 1.12) is considered unlikely, due to

unfavorable energetics (the corresponding radical will be lower in energy, and therefore favored) (*55*).

While the exact mechanism of CYP-mediated epoxidation remains ambiguous, sufficient evidence has been presented to warrant the consideration of multiple oxidants or multiple spin states when investigating the mechanism of any P450-catalyzed reaction.

1.6 SEQUENTIAL METABOLISM BY CYTOCHROMES P450

It is not uncommon for cytochromes P450 to catalyze several oxidation reactions on one substrate, generating several different metabolites. Sequential metabolism refers to the process in which one metabolite serves as the precursor for oxidative formation of another. The two possible mechanisms of sequential metabolism (dissociative and non-dissociative) differ only in the retention or release of intermediate metabolites (*56*). Dissociative sequential metabolism is the situation where the primary metabolite is released from the enzyme active site, after which it must rebind for oxidation to the secondary metabolite. In non-dissociative sequential metabolism, the primary metabolite remains in the enzyme active site for additional catalytic processing. Non-dissociative sequential metabolism by xenobiotic-metabolizing P450s is uncommon, whereas it is often observed with steroidogenic P450s, which are known to catalyze sequences of 2 or 3 oxidative reactions (*5, 6*).

$P450_{SCC}$, cholesterol side-chain cleavage enzyme, in believed to catalyze C_{22}- and C_{20}-hydroxylation followed by oxidative C_{20}-C_{22} bond scission (in that order) while converting cholesterol to pregnenolone (Figure 1.14). Each of the oxidative steps consumes one molecule of oxygen and one of NADPH (*57*), thus the process seemingly

follows normal P450 chemistry. Indeed, most mechanistic investigation of cholesterol oxidation to pregnenolone suggests that 22-hydroxycholesterol and subsequently 20,22-dihydroxycholesterol are formed via the 'normal' P450-hydroxylation mechanism, with the oxygen in both hydroxyl groups sourced to molecular oxygen (*58, 59*). However, contradictory results generated by Kraaipoel, *et al.* suggested otherwise (*60-62*).

Kraaipoel and coworkers found that a significant amount of ^{18}O from the medium (60%) was incorporated into the C22-hydroxyl group of the diol intermediate (*60*). From this and other experimental observations, the epoxide-diol mechanism of cholesterol oxidation was proposed (Figure 1.15). In this mechanism, cholesterol is desaturated to $\Delta^{20,22}$-cholesterol, which can be hydrated, explaining the formation of 22-hydroxycholesterol, or converted to 20,22-epoxycholesterol. Water addition to the epoxide intermediate explains their ^{18}O incorporation results, and generates 20,22-dihydroxycholesterol, which then undergoes oxidative C-C bond cleavage. Generation of water with its oxygen sourced to molecular oxygen in the catalytic processing of cholesterol by $P450_{SCC}$ is used to explain the less than 100% ^{18}O (60%) incorporation in the C22-hydroxyl group of 20,22-dihydroxycholesterol formed in the presence of $H_2{}^{18}O$ (*60*). While intriguing, particularly with foreknowledge of the data to be presented in this thesis, subsequent testing of the proposed epoxide and olefin intermediates showed that this mechanism is unlikely (*63-65*). Incubation of $P450_{SCC}$ with synthetic olefin and epoxide (all possible isomers) showed poor (20 to 66% of the rate of cholesterol conversion under the same conditions) to no conversion to pregnenolone, depending on the extent of purification of the enzyme used. Crude enzyme preparations showed conversion of these proposed intermediates to pregnenolone, whereas purified enzyme,

which was considered to be a truer representation of the catalytic activity of $P450_{SCC}$, did not. Thus, these investigators concluded that olefin and epoxide intermediates do not participate in the biosynthetic pathway of pregnenolone.

The mechanism of the final step in conversion of cholesterol to pregnenolone (C_{20}-C_{22} bond cleavage) remains unresolved. Figure 1.16 illustrates two viable mechanisms, one heterolytic (path A) and one homolytic (path B) (*5*). Both mechanisms invoke the iron-oxenoid species as the active oxidant. In path A, the electrophilic iron-oxenoid species is intercepted by one of the hydroxyl groups of 20,22-dihydroxycholesterol. Subsequent heterolytic rearrangement results in C-C bond cleavage. Path B involves an initial HAT from one of the hydroxyl groups, radical rearrangement leading to homolytic C-C bond scission, and finally, electron transfer from the generated carbon radical to the iron-oxygen complex. Unfortunately, resolution of the $P450_{SCC}$-catalyzed C-C bond cleavage mechanism does not appear to be forthcoming, as most of the research dates from the 1970s and little has been done since.

In the case of $P450_{SCC}$, factors that promote retention of intermediates include 1) the high affinity of hydroxylated intermediates, which bind to the enzyme 100-300 times more tightly than cholesterol (*66*), and 2) enhanced stability of the ferrous-dioxygen complex (Fe^{2+}-O_2) when complexed with the hydroxy-cholesterols while waiting for the second electron transfer to complete the reaction (*67, 68*). Thus, $P450_{SCC}$ is an example of a highly directed reaction sequence with little opportunity for leakage, which virtually guarantees complete sequence catalysis once cholesterol binds (*67, 68*). Xenobiotic-metabolizing P450s, on the other hand, have to be able to accommodate a multitude of substrates, and therefore often do not have the precise substrate/enzyme binding

interactions that might support non-dissociative sequential metabolism. Accordingly, few examples of non-dissociative sequential metabolism by xenobiotics metabolizing P450s are found in the literature (*69-71*).

In the case of CYP2E1 oxidation of ethanol to acetic acid via acetaldehyde, approximately 90% of the acetaldehyde intermediate remains bound in the active site for oxidation to acetic acid (*71*). Studies on $P450_{17\alpha,lyase}$, a steroidogenic P450, showed an enhancement of non-dissociative sequential metabolism with increasing NADPH-P450 reductase concentration (*72*). This observation is in agreement with the findings of Grogan, *et al.* on the multi-step conversion of androstenedione to estrogen, where the extent of non-dissociate sequential metabolism was found to be dependent on the rate of electron transfer from NADPH-P450 reductase (*73*). In addition, while comparing bovine and guinea pig $P450_{17\alpha,lyase}$, Yamazaki, *et al.* found that the dissociation rates of sequence intermediates also plays a role in regulation of successive reactions (*74*). From these studies, it seems likely that the extent of non-dissociative sequential metabolism by xenobiotic-metabolizing P450s would also be controlled by rates of reduction and of intermediate dissociation.

1.7 CYTOCHROME P450 1A2

Cytochrome P450 1A2 is inducible and primarily hepatically expressed, making up approximately 13% of the total hepatic P450 content (*75*). Even so, CYP1A2 is of relatively little pharmacological significance, as it is involved in the metabolism of only ≈8% of commonly used drugs (*1, 75, 76*). In general, CYP1A2 substrates are planar, aromatic, lipophilic, and polycyclic. Common drugs that are metabolized by CYP1A2

include warfarin, theophylline, caffeine, phenacetin, acetaminophen, and 7-ethoxyresorufin (*1*). The primary importance of CYP1A2 is in its integral role in the bioactivation of chemical environmental contaminants; over 90% of known carcinogens can be activated through CYP1A2-catalyzed metabolism (*75*). In particular, CYP1A2 catalyzes the N-hydroxylation of carcinogenic aryl amines and heterocyclic amines found in charbroiled foods and cigarette smoke (*1*). Accordingly, the toxicological significance of CYP1A2-mediated oxidation is the primary driving force behind investigation of its activity and expression.

1.8 MECHANISTIC INVESTIGATION WITH DEUTERIUM ISOTOPE EFFECTS

Deuterium isotope effect analysis of enzyme-mediated reactions has proven to be an invaluable tool for elucidation of the underlying chemical mechanisms. Kinetic deuterium isotope effect experiments are designed to observe a difference in the rate of the reaction as a result of selective deuteration of the substrate. In essence, isotope effects are a consequence of the difference in mass between hydrogen and deuterium atoms, resulting in lower zero-point vibration energies for C-D bonds versus C-H bonds. The difference in zero-point energies, in turn, results in more energy being required to break a C-D bond versus a C-H bond (i.e. it is 'harder' to remove a deuterium atom) (*77*).

The magnitude of the intrinsic isotope effect (the isotope effect associated solely with the bond-breaking event) directly reflects the symmetry of the transition state, which may contribute to the understanding of the reaction mechanism (*77, 78*). As a C-H or C-D bond is broken, some or all of the stretching vibration of that bond is lost in the transition state. With a symmetric transition state, the stretching vibration is completely

lost as the hydrogen or deuterium atom undergoes translation toward the acceptor atom. If no ground-state zero-point energy is contributed to the transition state zero-point energy, there will be no isotope-dependent difference in the transition state, resulting in a large isotope effect. On the other hand, if the transition state is asymmetric, significant stretching vibration may be maintained in the transition state. Accordingly, because C-H and C-D bonds have different ground-state zero-point vibrational frequencies, the transition state zero-point energies for transfer of a hydrogen or deuterium atom will differ. The resulting isotope-dependent difference in the transition state leads to a reduced isotope effect (*77, 78*). While the magnitude of the intrinsic isotope effect correlates to the symmetry of the transition state of any given reaction, the intrinsic isotope effect for different reactions will vary depending on the relative transition state energies, which must be taken into account when comparing isotope effects (*79*).

Application of kinetic deuterium isotope effect analysis to enzymatic reactions has proven to be inherently complex. The multi-step nature of enzymatic reactions results in a situation in which the observed isotope effect is a function of various isotopically sensitive, partially rate-limiting events. Ultimately, this may lead to lowering, or masking, of the intrinsic isotope effect of the bond-breaking event and incorrect assignment of the underlying mechanism (*80*). Masking may result in experimentally observed isotope effects ranging from 1 (no observable isotope effect) to the intrinsic value.

The apparent isotope effect on V_{max} (^{D}V) and K_m/V_{max} ($^{D}V/K$) of most enzymatic systems with only one isotopically sensitive step can be described using equation 1:

$$^{D}V \text{ or } ^{D}V/K = \frac{k_H/k_D + C}{1 + C} \qquad \text{eq. 1}$$

where k_H/k_D is the intrinsic isotope effect and the definition of C depends on the nature of the isotope effect observed (^{D}V or $^{D}V/K$) (*39, 81*). For ^{D}V isotope effects, C is the "catalytic ratio," the ratio of rate constants for the isotopically sensitive step to the sum of all other enzymatic steps (*39*). In the case of $^{D}V/K$ isotope effects, C is the commitment to catalysis, or a measure of the enzyme's propensity to proceed with production of a certain metabolite vs. reverting to its previous state or forming alternate products (*39*). From eq. 1, one can see that as C becomes large, the observed isotope effect will diminish (masking), whereas, as C decreases, the observed isotope effect will approach the intrinsic value, k_H/k_D. Thus, isotope effect analysis of an enzymatic system in which multiple product formation pathways are available from a single intermediate will provide the best opportunity to observe near intrinsic isotope effect values.

Model I

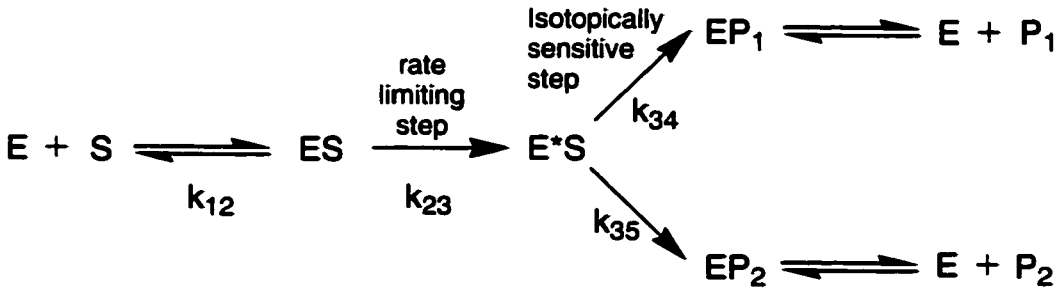

Fortuitously, as shown in model I, the activation of the cytochrome P450 iron-oxygen complex is believed to be irreversible (k_{23}), and multiple products are often

formed from this single E*S complex (*39, 81-83*). Because CYPs have multiple routes of E*S decomposition (sometimes including, but not shown, the nonproductive decomposition of E*S), the commitment to formation of one particular product is potentially low. In model I, the competing routes of oxidation (k_{34} and k_{35}) have different rate constants, and only formation of P_1 (k_{34}) is isotopically sensitive. Retardation of k_{34} due to substrate deuteration will result in a buildup of the E^*S_D complex. However, P_2 formation is non-isotopically sensitive, and the rate constant for its formation (k_{35}) will not change upon substrate deuteration. Therefore, P_2 formation will increase with the buildup of E^*S_D, reflecting the degree to which P_1 formation (k_{34}) has slowed, and unmasking the intrinsic kinetic deuterium isotope effect. This phenomenon of metabolic flux being directed through a pathway that is not influenced by deuteration of the substrate is referred to as isotopically sensitive branching or metabolic switching (*82*). As a result of metabolic switching, isotope effects are observed on both metabolites, with a normal isotope effect (>1) observed on P_1, as k_{34} slows with deuteration, and an inverse isotope effect (<1) on P_2, as the concentration of E^*S_D increases. Because P_1 and P_2 are formed from the same E*S complex, the ratio of their formation (P_1/P_2) directly correlates to the ratio of k_{34} and k_{35}. This allows the calculation of a lower estimate of the intrinsic isotope effect for P_1 formation from the observed isotope effects on the two products (*83*).

$$\frac{P1H/P2H}{P1D/P2D} = \frac{P1H/P1D}{P2H/P2D} = \frac{{}^{D}V/K_{P1}}{{}^{D}V/K_{P2}} = k_{34H}/k_{34D} = \text{Intrinsic Isotope Effect}$$

In intramolecular isotope effect experiments, a substrate with two symmetric sites of oxidation is chosen (*84*). Upon deuteration of one of these sites, the observed isotope effect then reflects the enzymes 'choice' or the competition between the two equivalent sites. Assuming rapid equilibration of the two equivalent sites within the enzyme active site, the intramolecular isotope effect design provides the enzyme with a readily available "switch to" site of metabolism (k_{35} in model I), leading to unmasking of the intrinsic isotope effect.

1.9 CYP1A2 METABOLISM OF 8-ALKYL XANTHINES

Cytochrome P450-catalyzed oxidation of xenobiotics usually forms unreactive, relatively hydrophilic products that are eliminated from the body without incident. In some cases, however, highly electrophilic metabolites, which form adducts to intracellular sites or to the P450 itself, are generated. Mechanism-based inactivators (or suicide substrates) are substrates that, through the metabolic action of the enzyme, are converted to a reactive intermediate that effectively 'kills' that enzyme, often through alkylation of active site protein residues or the heme prosthetic group. As such, suicide substrates present the opportunity for mechanistic elucidation of the events leading to formation of the reactive intermediate, and therefore of the enzyme mechanism.

Furafylline (FF, Figure 1.17), an 8-methyl xanthine, was designed to be a long-acting derivative of theophylline (Figure 1.17) for the treatment of asthma (*85*). However, FF was found to be a potent inhibitor of CYP1A2 activity (*86, 87*). Further study in our laboratory showed that FF is a mechanism-based inactivator of CYP1A2, causing time and concentration-dependent loss of enzyme activity and formation of a 1:1

CYP1A2-protein adduct (*88, 89*). The metabolism of furafylline and cyclohexylline (CH) (Figure 1.17), a 3-cyclohexylmethyl analog of FF, results in either 8-methyl hydroxylation or protein adduction (partition ratio = 5.5 and 7.5, respectively). Interestingly, oxygen-tracing experiments indicate that the majority of the oxygen incorporated into the 8′-carbinol metabolite comes from H_2O (FF,80%; CH,70%). The metabolism of furafylline by CYP1A2 is an unusual system with parallels to 3-methylindole in which normal P450 oxygen rebound has become a minor process, in favor of a process that allows the addition of a water molecule or protein nucleophile to a reactive metabolic product. In addition, all metabolic products (8′-OH from O_2, 8′-OH from H_2O, and protein inactivation) were found to be isotopically sensitive to deuterium substitution on the 8-methyl group, displaying large normal intramolecular isotope effects ($k_H/k_D \approx 9$) (*88, 89*). To account for the experimental results, a desaturated iminium reactive intermediate, the 'imidazomethide', formed by a hydrogen atom transfer (HAT) or by a second electron transfer (SET) from the initially formed 8′-carbon radical has been proposed (Figure 1.18) (*89*). The imidazomethide is quenched by reaction with a water molecule to form the carbinol with the oxygen from the medium or by reaction with a protein nucleophile to form the adduct. The carbinol with oxygen from molecular oxygen is generated by the consensus P450 oxygen rebound mechanism. CYP1A2-catalyzed oxidation of the N^7-methylated derivatives of FF and CH produce N-methyl-8′-carbinols with the oxygen sourced entirely to molecular oxygen and no enzyme inactivation. This indicates that reactive imidazomethide intermediate formation is

completely blocked and supports the idea that it is formed by removal of a second hydrogen atom from the imidazole nitrogen, rather than a SET process (*89*).

Negative results of trapping experiments suggest that both adduction and water incorporation occur within the enzyme active site. In support of this idea, water is found to be stereoselectively incorporated into the 8′-carbinol of ethylcyclohexylline (S/R=20), indicative of water addition to the imidazoethide reactive intermediate within the chiral confines of the enzyme active site (*90*). Interestingly, while water incorporation (60%) with ethylcyclohexylline (ETC, Figure 1.17) implicates desaturated reactive intermediate formation, enzyme inactivation is virtually nonexistent (partition ratio > 700). In addition, predominantly S-carbinol was produced whether oxygen from water or molecular oxygen was added (*90*), and minimal inversion of stereochemical configuration in the course of oxygen addition from either source was observed (i.e. pro-S HAT results in S-carbinol from both oxygen sources) (unpublished ETC results). This is in sharp contrast to the results of White, *et al.* who showed that ethyl benzene oxidation resulted in significant inversion of configuration (see 1.5.6 of figure 1.5) (*16*). Thus, the results with ETC show that rotation about the C8-C8′ bond in the putative substrate radical does not occur, that the substrate ω-1 radical does not reorient to present the opposite face to the Fe-OH radical for recombination, and that the active site water molecule responsible for decomposition of the reactive intermediate must be located in close proximity to the iron-oxygen complex. As expected, N^7-methyl-ethylcyclohexylline incubation with CYP1A2 showed a complete lack of water

incorporation into the 8′-carbinol, and like its N-protio analog, a very high degree of stereochemical configuration retention (unpublished results).

Further emphasizing the unique nature of this system, relatively large amounts of vinylcyclohexylline and diol-ethylcyclohexylline metabolites are produced from ETC (35% of total metabolic turnover), with the diol being a secondary oxidation product via putative epoxidation of the olefin (Figure 1.19). Evidently, while only slightly decreasing water incorporation and the total desaturation (olefin+diol+carbinol from H_2O) to oxygen rebound ratio (ETC = 2.4, CH = 2.8), the additional methyl group of ETC renders its reactive intermediate unable to inactivate CYP1A2 and presents the enzyme with a second desaturation pathway.

Competitive ($^DV/K$) and non-competitive (^DV) deuterium isotope effects analysis of ethylcyclohexylline metabolism using ω-1 D_2 and ω D_3 substrates in the presence of $H_2{}^{18}O$ were performed to construct a mechanistic scheme that included olefin and diol formation. The three reasonable routes of olefin formation are shown in Figure 1.20. Path A, which involves initial ω-hydrogen atom abstraction, can be excluded as a possibility due to: 1) only minute amounts of primary carbinol (8″-OH-ethylcyclohexylline) formed in incubations with ETC, 2) incubations with vinylcyclohexylline produce the primary alcohol, in addition to the diol, and 3) the ratio of diol/8″-OH produced in incubations with ETC and vinylcyclohexylline are similar. These results indicate that the minor amounts of 8″-OH formed in incubations with ETC actually stem from the olefin via a poorly understood non-oxidative but NADPH- and O_2-dependent mechanism for which precedent now exists (*91*). One would expect

significantly more primary carbinol formation via oxygen rebound if the terminal carbon radical exists, as implicated in path A. In Path B, a second HAT from the ω-position follows initial 8′-hydrogen atom abstraction. Path C shows the olefin being formed by a rearrangement of the proposed reactive intermediate, possibly by an active site base-catalyzed terminal proton removal.

Deuterium isotope effect experiments with ω-perdeuterated substrates allow discrimination between the two plausible pathways (B and C in Figure 1.20), both of which would have a different isotopically sensitive branching point and therefore different isotope effect profiles. If path B is operative, the isotopically sensitive branching point is the 8′-carbon radical, therefore one would expect a normal isotope effect on vinyl formation with a concomitant inverse isotope effect on the non-isotopically sensitive formation of 8′-carbinol from both dioxygen and water. Path C, with the isotopically sensitive branching point at the reactive intermediate and assuming irreversibility of reactive intermediate formation, would be expected to produce a normal isotope effect on vinyl formation, an inverse isotope effect on 8′-carbinol from H_2O, and no isotope effect on 8′-carbinol from oxygen rebound.

The deuterium isotope effect experimental results with ETC (Table 1.1) indicate that path C (Figure 1.20) is the mechanism of olefin formation with this substrate; that is, a postulated active site base catalyzes the rearrangement of the reactive intermediate by the isotopically sensitive removal of an ω-proton. The key observations from these incubations implicating this mechanism are 1) the absence of an isotope effect on formation of 8′-carbinol from O_2, 2) the inverse isotope effect on formation of 8′-OH

from water incorporation, and 3) the reasonably large normal isotope effect on olefin formation (3.3-3.9). As discussed above, these results argue against the reversibility of reactive intermediate formation and indicate that the isotopically sensitive branching point is between the olefin and 8′-carbinol from water incorporation (i.e. at the reactive intermediate, path C in figure 1.20). Taking advantage of the observed metabolic switching between these two metabolites on opposite sides of the branching point, we are able to calculate a lower limit of the intrinsic isotope effect for ω-hydrogen atom removal of 5.5-5.8 (3.52/0.64 and 3.86/0.66). This large isotope effect for ω-HAT is not consistent with normally observed isotope effects for desaturation by P450s via dual hydrogen atom transfer ($^{D}V/K \approx 1$-2) and more indicative of a base-catalyzed proton removal via an E_1Cb (elimination, first-order, conjugate base)-type mechanism (see discussion) [Lowry, 1976 #100]. Interestingly, the same postulated base that is responsible for the decomposition of FF's imidazomethide reactive intermediate to form the protein adduct could be responsible for rearrangement of ETC's reactive intermediate. ETC is a much poorer inactivator of CYP1A2 than CH (partition ratios of >700 and 7.5, respectively), which could be explained by the ω-methyl of ETC being positioned such that quenching of the reactive intermediate by the protein nucleophile is impeded, while ω-proton removal is facilitated. Additional support for the hypothesis of a common intermediate between vinylcyclohexylline and 8′-carbinol from H_2O comes from the observation of similar olefin to carbinol from water ratios following S-deuterium or hydrogen abstraction (0.63 and 0.62, respectively; unpublished results).

In contrast to these results, deuterium isotope effect analysis of N^7-methyl-ethylcyclohexylline indicated that olefin formation is via path B (dual hydrogen atom transfer) of Figure 1.20 (data shown in table 1.2). Large and normal isotope effects on ^{D}V and $^{D}V/K$ were observed for formation of 8′-OH and olefin for the ω-1 D_2 substrate. These results are consistent with the consensus hydrogen atom abstration mechanism for hydroxylation. Small normal isotope effects on ^{D}V and $^{D}V/K$ were observed for olefin formation from the ω D_3 deuterated substrate, whereas low to slightly inverse isotope effects were observed for 8′-OH. All together, these results indicate a small normal isotope effect for desaturation via second hydrogen atom removal and are consistent with literature results. In addition, carbinol to olefin ratios were found to be highly dependent on hydrogen abstraction stereochemistry; pro-I and pro-(S) hydrogen abstraction resulted in alcohol to olefin ratios of 1.3 and 9.6, respectively. This is consistent with the presence of stereochemically distinct 8′-substrate radicals (cis and trans). Overall these observations are consistent with a mechanism where carbinol and olefin are formed as a result of a branching reaction in which the substrate ω-1 radical and the heme iron hydroxyl radical decompose via recombination at the ω-1 position and an isotopically sensitive ω hydrogen atom abstraction, respectively. This is in agreement with the results of N-methyl furafylline and N-methyl cyclohexylline, in that N-methylation appears to block the formation of the reactive intermediate.

The results with ethylcyclohexylline suggest the possibility that rearrangement of the desaturated reactive intermediate is a generally observed process in the desaturation of 8-alkylxanthines by CYP1A2. In order to assess this prospect and to expand the 8-

alkylxanthine SAR studies of our laboratory, we explored the metabolism of isopropylcyclohexylline (IPC, Figure 1.17) by CYP1A2 using deuterium isotope effect analysis in conjunction with $H_2{}^{18}O$-incorporation studies, under the premise that the additional methyl group of isopropylcyclohexylline will potentially present the enzyme with another opportunity for desaturation; it is possible that we may be able to observe both desaturation mechanisms occurring on the same substrate. In order to establish a benchmark of "normal" P450-catalzyed metabolism, N^7-methyl-isopropylcyclohexylline metabolism by CYP1A2 was also studied. The metabolic end products from N^7-methyl- and N^7-protio-xanthine metabolism are often quite similar, though manifestly derived from different biochemical processes. Accordingly, the study of N^7-methyl-isopropylcyclohexylline should provide a convenient point of reference.

The Nature of the Imidazomethide Reactive Intermediate

Desaturation of FF and its analogs to the proposed iminium-reactive intermediate could proceed via an overall $-2e^-/-2H^+$ or a $-2e^-/-1H^+$ process, resulting in an uncharged or a charged species, respectively (Figure 1.21). The difference between the two processes lies in the second step following initial 8′-hydrogen atom abstraction. This second step could be a second hydrogen atom transfer (HAT) or a second electron transfer (SET). To differentiate between these two possibilities, metabolic studies with cyclopropylmethylcyclohexylline (CPMC) were employed.

The structure and nonclassical nature of cyclopropyl carbinyl cations have been extensively studied for several decades (*92-98*). (A complete discussion of the evolution

of ideas in this field is beyond the scope of this thesis, due to the volume of research. For an excellent introduction to "nonclassical" ions see (*97*), and for general discussion of classical and nonclassical ions see (*98*).) Any particular carbocation can be thought of as existing somewhere on a continuum of carbocationic species with differing degrees of charge delocalization (Figure 1.22). The limiting classes of this continuum are trivalent "classical" carbenium ions and penta- (or tetra-) coordinated "nonclassical" carbonium ions (*97*). The former contains an sp^2-hybridized electron deficient central carbon atom, usually with three directly bound atoms in a planar configuration (eg. The triphenylmethyl cation shown in Figure 1.22). The charge delocalization is usually by p π-orbital overlap (*94*). Nonclassical carbonium ions, on the other hand, have a central carbon atom bound to 4 or 5 atoms by three single bonds and a 2-electron 3-center bond (eg. The norbornyl cation shown in Figure 1.22) (*95*). These nonclassical ions live up to their namesake by involving partly nonclassical electron delocalization through overlap of orbitals between atoms that are not connected by a σ-bond. The resulting bond is usually a combination of σ and π bond character (*94*). Substituents play a critical role in determining where a carbocation lies on this continuum. For example, the norbornane cation is a prototypic nonclassical cation, however the 2-phenyl-norbornyl cation was found to be classical in nature due to predominant delocalization of the positive charge by the phenyl ring (i.e. over σ-bond participation that would result in nonclassical nature) (*95*). Even 2-methyl-norbornane was found to have decreased nonclassical-type σ-delocalization of the positive charge over that of unsubstituted norbornyl cation. Trivalent carbenium ions can show varying degrees of charge delocalization to adjacent functional groups without becoming pentacoordinated carbonium ions. As pointed out by

Roberts and Mazur, interpretation of products from a new carbonium ion may be made from carbonium ion theory, but prediction of the products depends on 1) the carbonium ion stability, 2) the energy barriers to interconversion of the carbonium ions, 3) the reactivities of the carbonium ion toward nucleophilic attack, 4) the reversibility of the reaction, and 5) the stability of the products (*96*).

Solvolysis of cyclopropylmethyl alcohols is known to lead to an equilibrium of cyclopropylmethyl, cyclobutyl, and homoallyl products (*99, 100*), with substituents playing a major role in deciding the course of the cationic rearrangement reaction (*97*) (For further reading on ` ubstituents effects on cyclopropylcarbinyl and cyclobutyl cations, see (*101*).). This is believed to be due to the nonclassical nature of cyclopropylcarbinyl cations. Olah, *et al.* found that the cyclopropylcarbinyl cation exists in an equilibrium between 3 nonclassical species due to the overlap of the carbenium carbon empty p-orbital with a C-C σ-bond (Figure 1.23) (*93*). Therefore, if a charged intermediate lending cationic character to the 8′-position is formed in incubations of CPMC with CYP1A2 and if delocalization of the positive charge to the adjacent imidazole ring does not prohibit nonclassical charge delocalization by the cyclopropyl ring, rearrangement would be expected (Figure 1.24). As shown in figure 1.24, active site water, which previous studies with ethylcyclohexylline (*90*) indicate is in the immediate vicinity of the reactive intermediate, is the ideal agent for trapping any cation formed. In this way, any ring-rearranged cyclobutylcyclohexylline carbinol or ring-opened butenol products generated in the incubations with cyclopropylmethylcyclohexylline should contain oxygen solely from the medium and be indicative of generation of a cation in the 8′-position.

On the other hand, radical-rearrangement due to an 8′-carbon radical is unlikely, because the lifetime of the closest analog in the literature, the benzyl cyclopropyl radical, is sufficiently long that it does not rearrange to any significant extent in P450-hydroxylation reactions (*20, 102*). In fact, studies have shown that ring-opening of the cyclopropylbenzyl radical is reversible, and that the equilibrium favors the ring-closed form (*20, 102-104*). Finally, Beckwith, *et al.* found that that ring-closed form of the cyclopropylmethyl radical is thermodynamically favored when radical-stabilizing moieties, such as a phenyl group, are present; the estimated isokinetic temperature of phenylcyclopropane is approximately 500 °C (*105*). Hence, any rearranged product seen with CPMC can be attributed to a cationic intermediate.

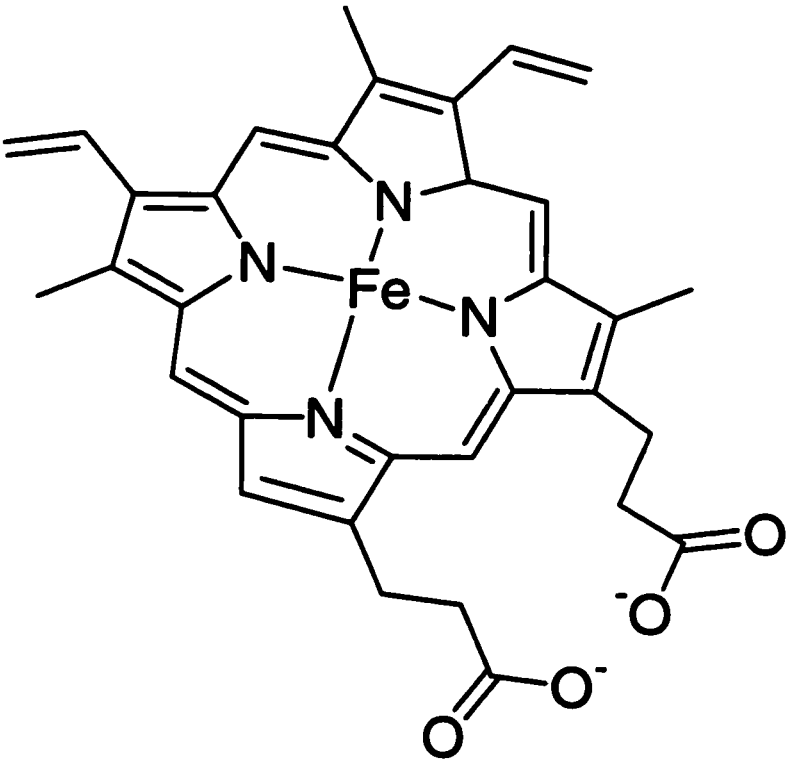

Figure 1.1 Iron protoporphyrin IX.

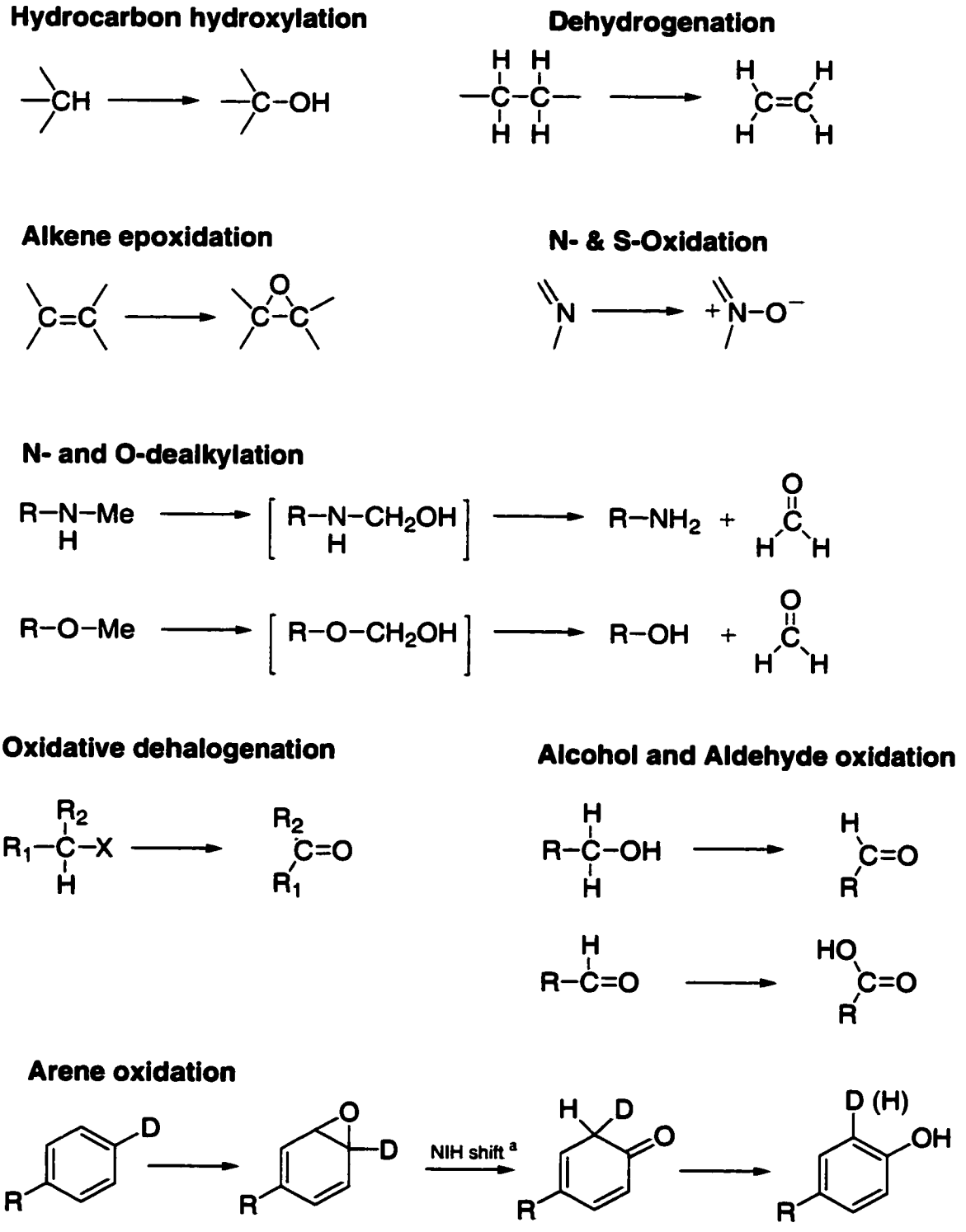

Figure 1.2 Major types of P450-catalyzed reactions.

[a] (*106*).

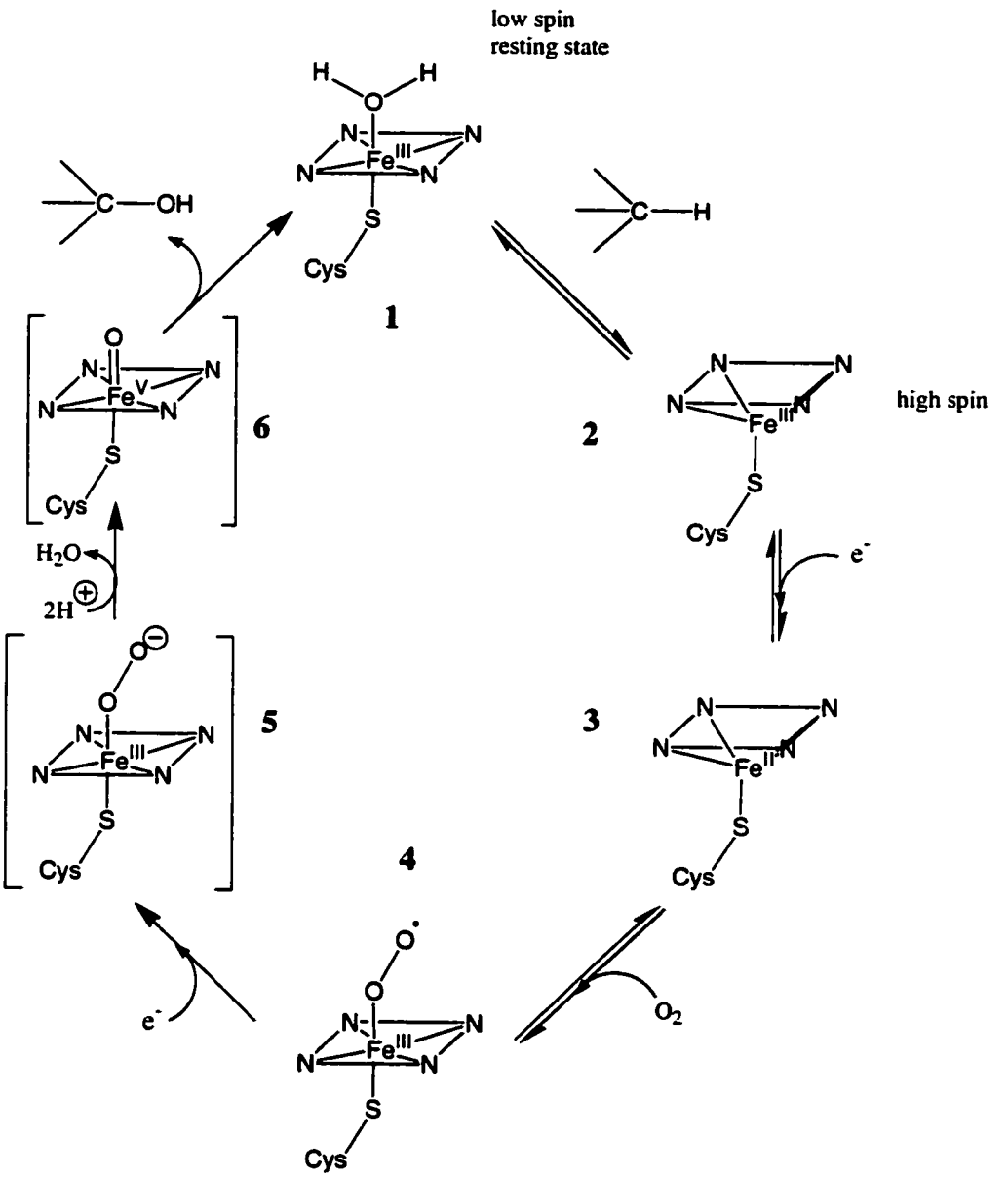

Figure 1.3 Cytochrome P450 catalytic cycle.

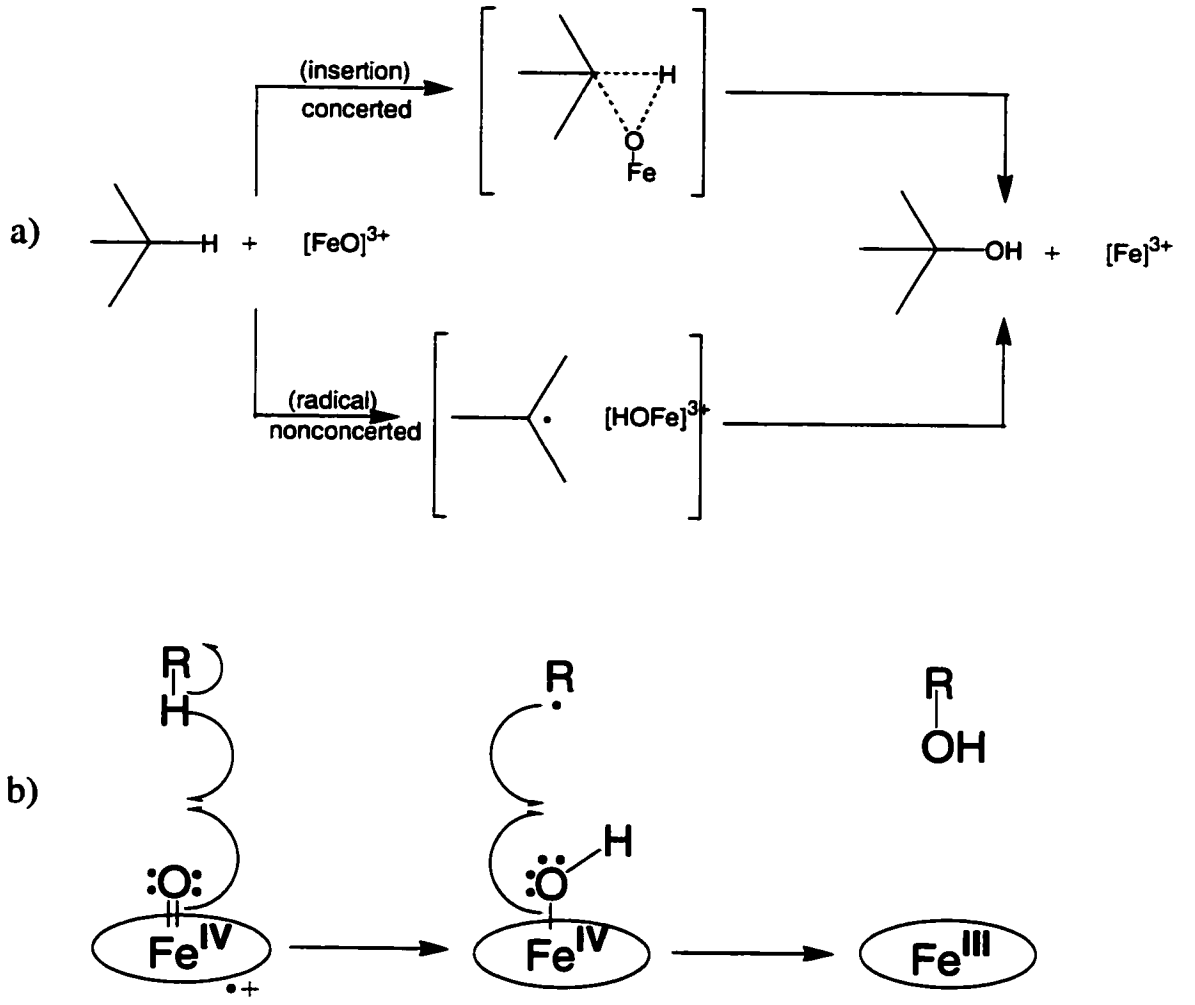

Figure 1.4 a) Schematic diagram of concerted and nonconcerted (radical) mechanisms of hydroxylation by cytochromes P450. b) Concensus P450 oxygen rebound (radical) mechanism of hydroxylation.

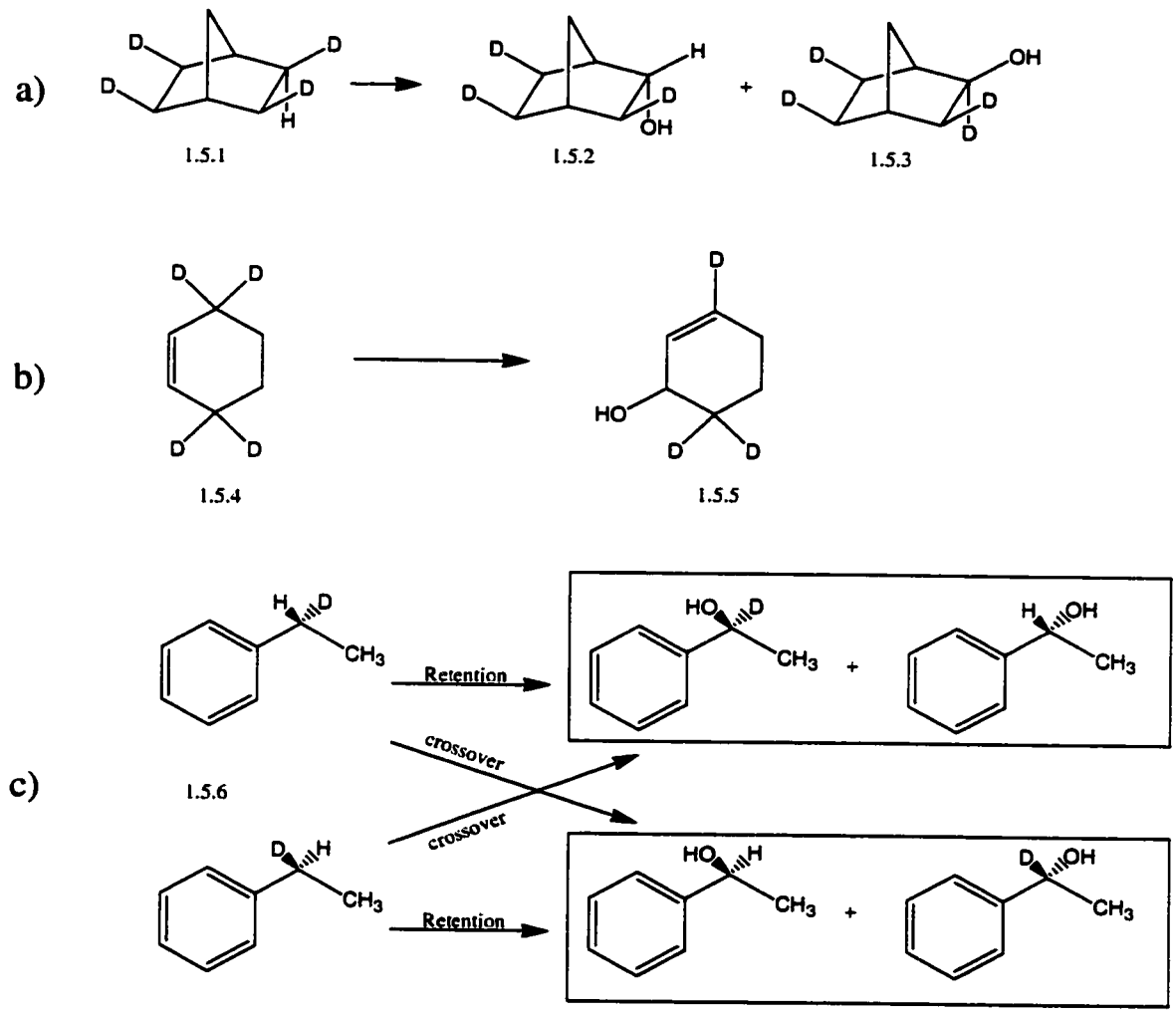

Figure 1.5 Evidence for nonconcerted, stepwise mechanism for aliphatic hydroxylation by cytochromes P450. a) Exo, exo, exo, exo-tetradeutero-norbornane hydroxylation by $P450_{LM2}$ b) tetradeutero-cyclohexene hydroxylation by $P450_{LM2}$ c) 1-d-ethylbenzene hydroxylation by $P450_{LM2}$.

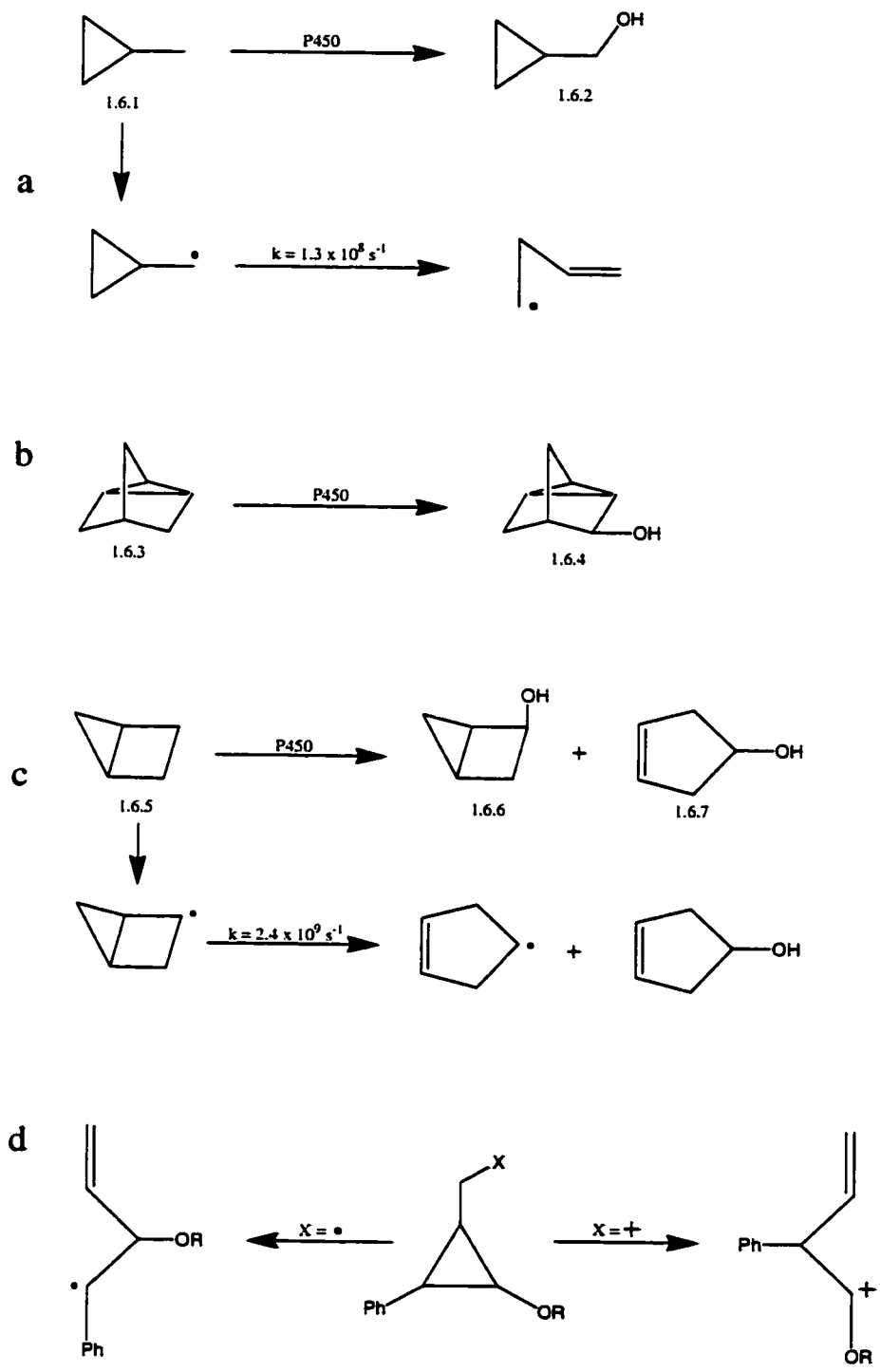

Figure 1.6 Radical clock studies and determination of recombination rate. A) Methylcyclopropane, b) nortricyclane, c) bicyclopentane, d) (2-alkoxy-3-phenylcyclopropyl)methane.

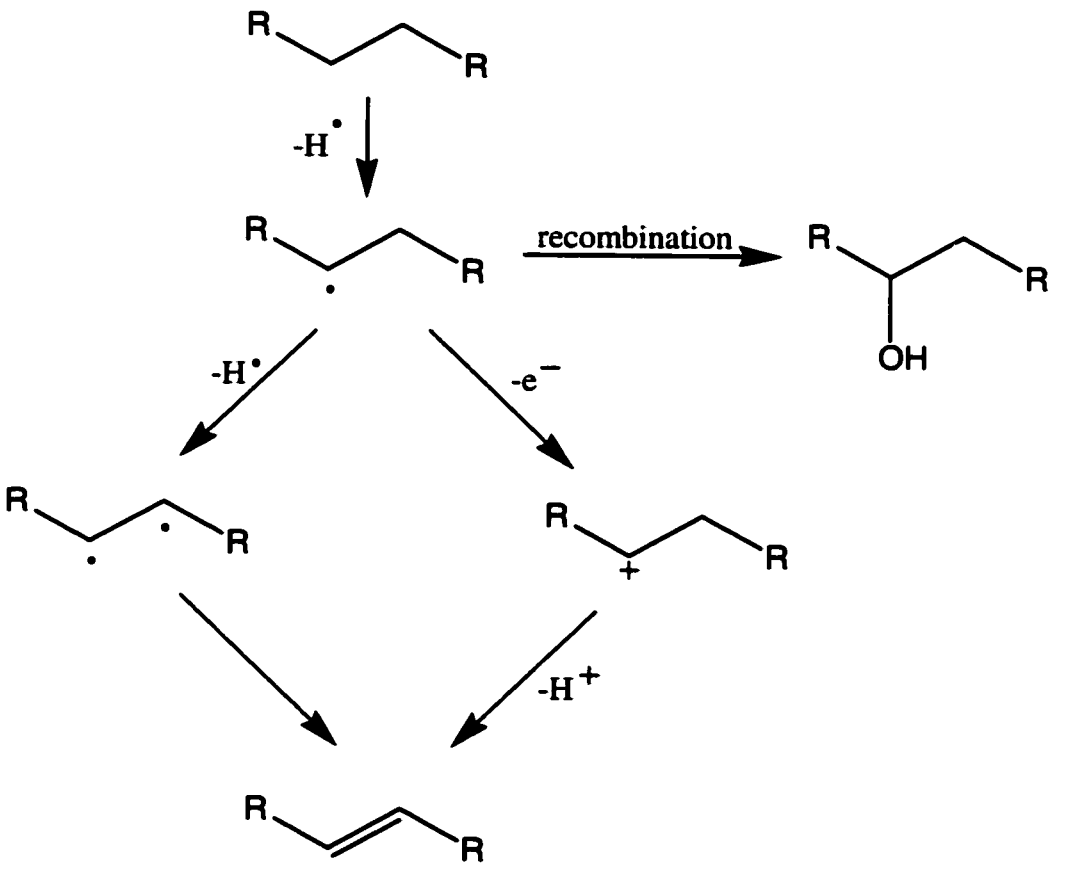

Figure 1.7 Two possible mechanisms of CYP-catalyzed aliphatic desaturation.

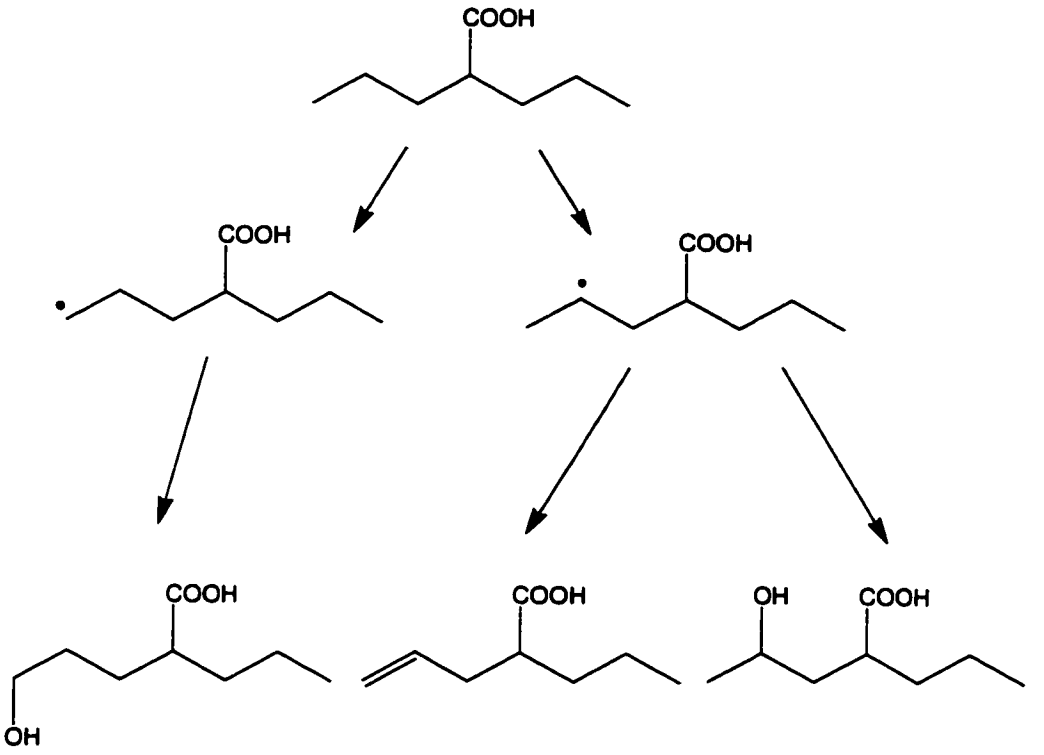

Figure 1.8 Mechanism of $\Delta^{4,5}$-valproic acid formation.

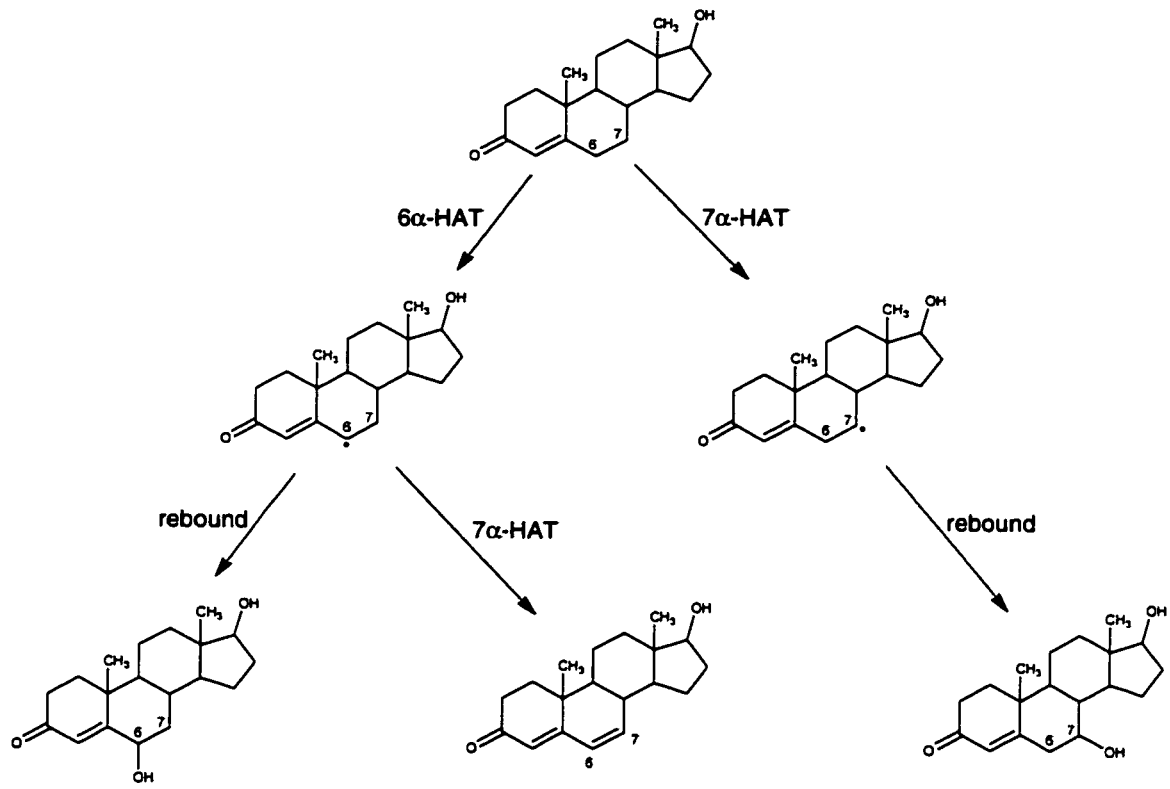

Figure 1.9 Testosterone metabolism by CYP2A1. Desaturation to Δ^6-testosterone only occurs by initial C6-hydrogen atom abstraction.

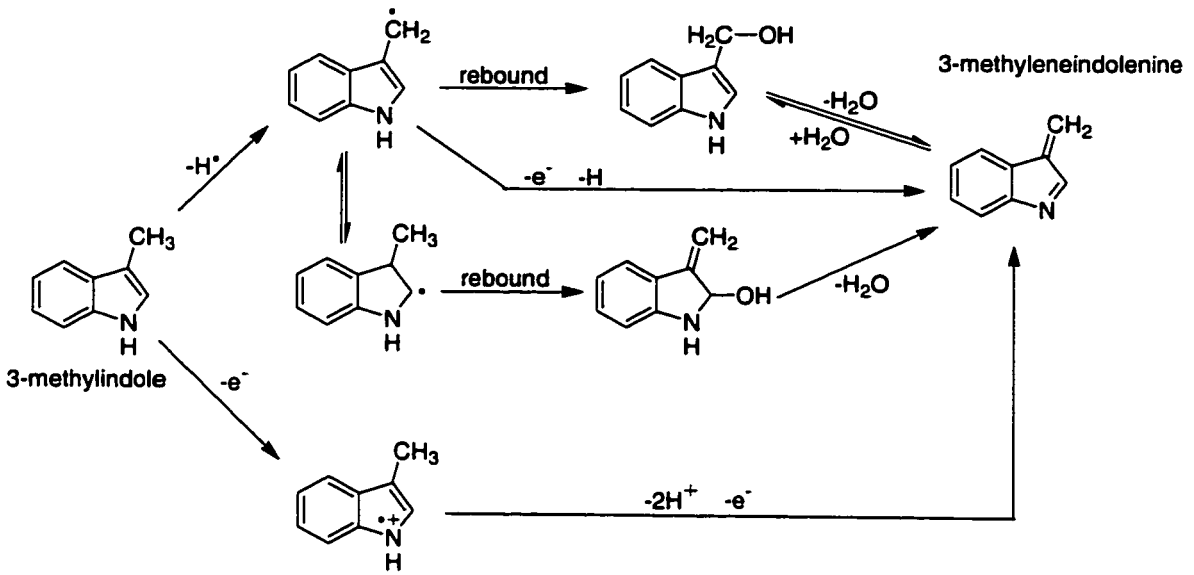

Figure 1.10 Mechanistic scheme for 3-methyleneindolenine formation from 3-methylindole. Nitrogen-containing ring introduces possibility of mixtures of HAT/SET processes leading to desaturation. [a]

[a] Figure taken from (*40*).

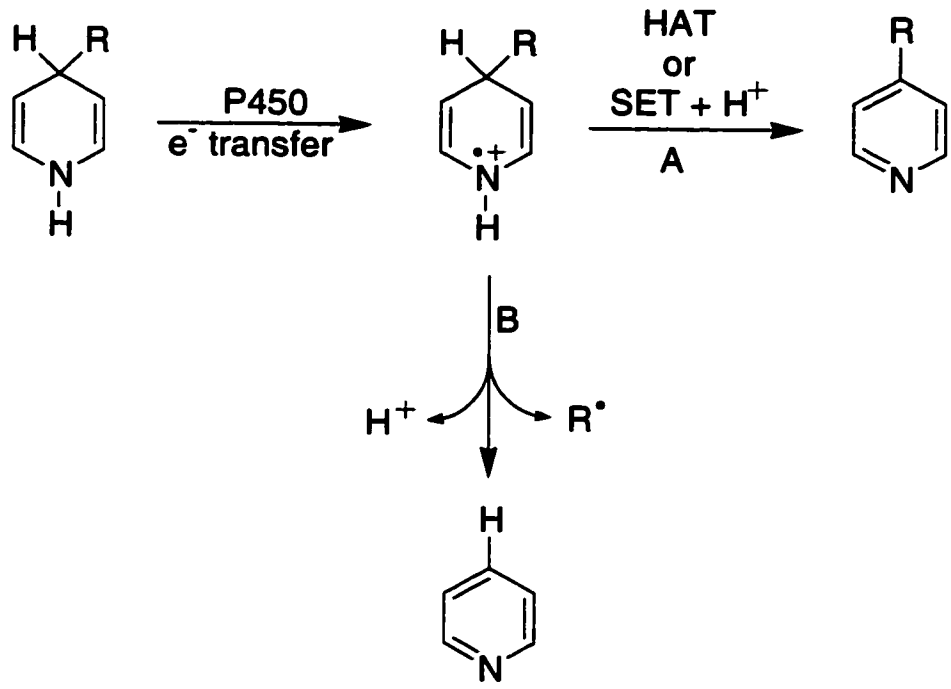

Figure 1.11 Proposed mechanisms for CYP-mediated oxidation of 1,4-dihydropyridines. Electron transfer from the nitrogen initiates desaturation with or without loss of an alkyl radical.

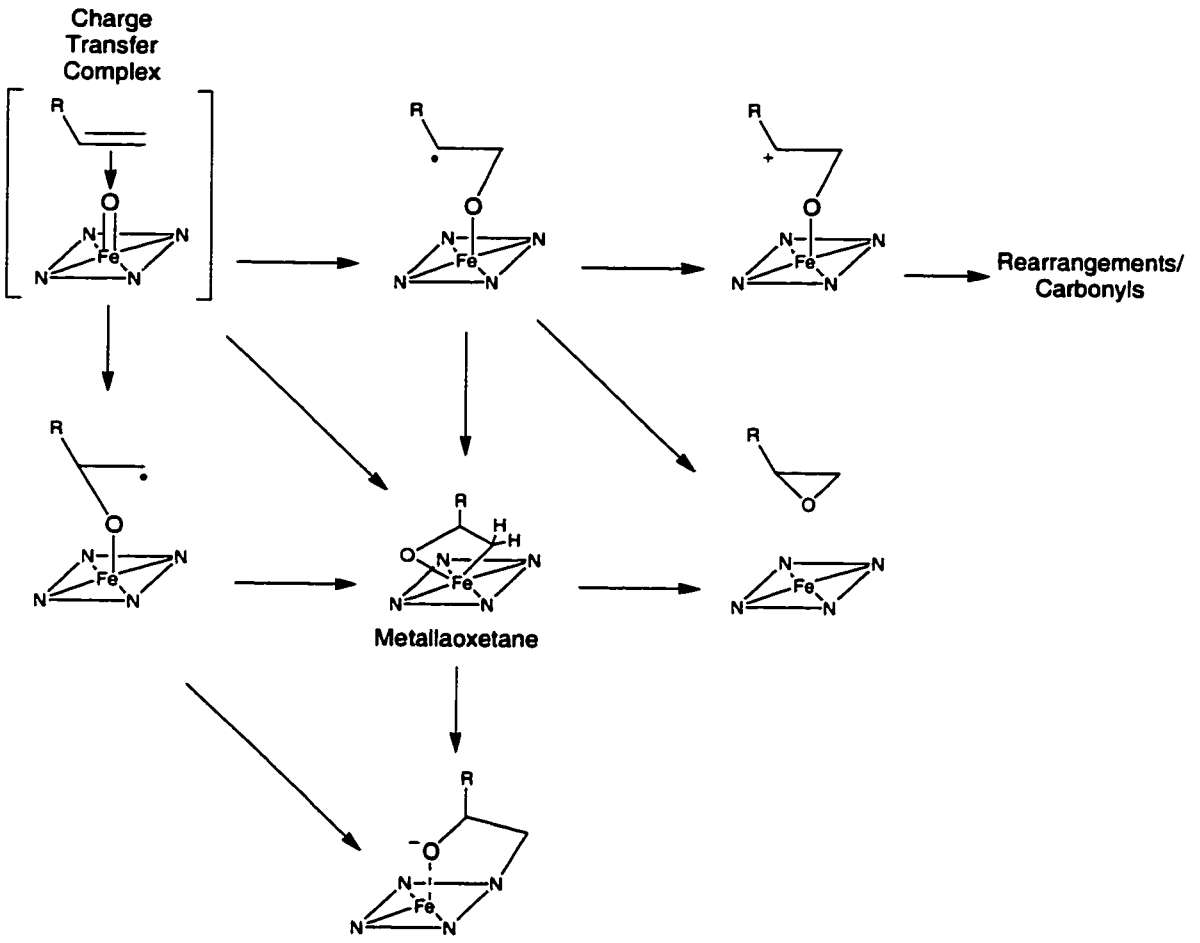

Figure 1.12 Mechanistic alternatives involved in P450-catalyzed epoxidation reactions. [a]

[a] Figure taken from (*5*).

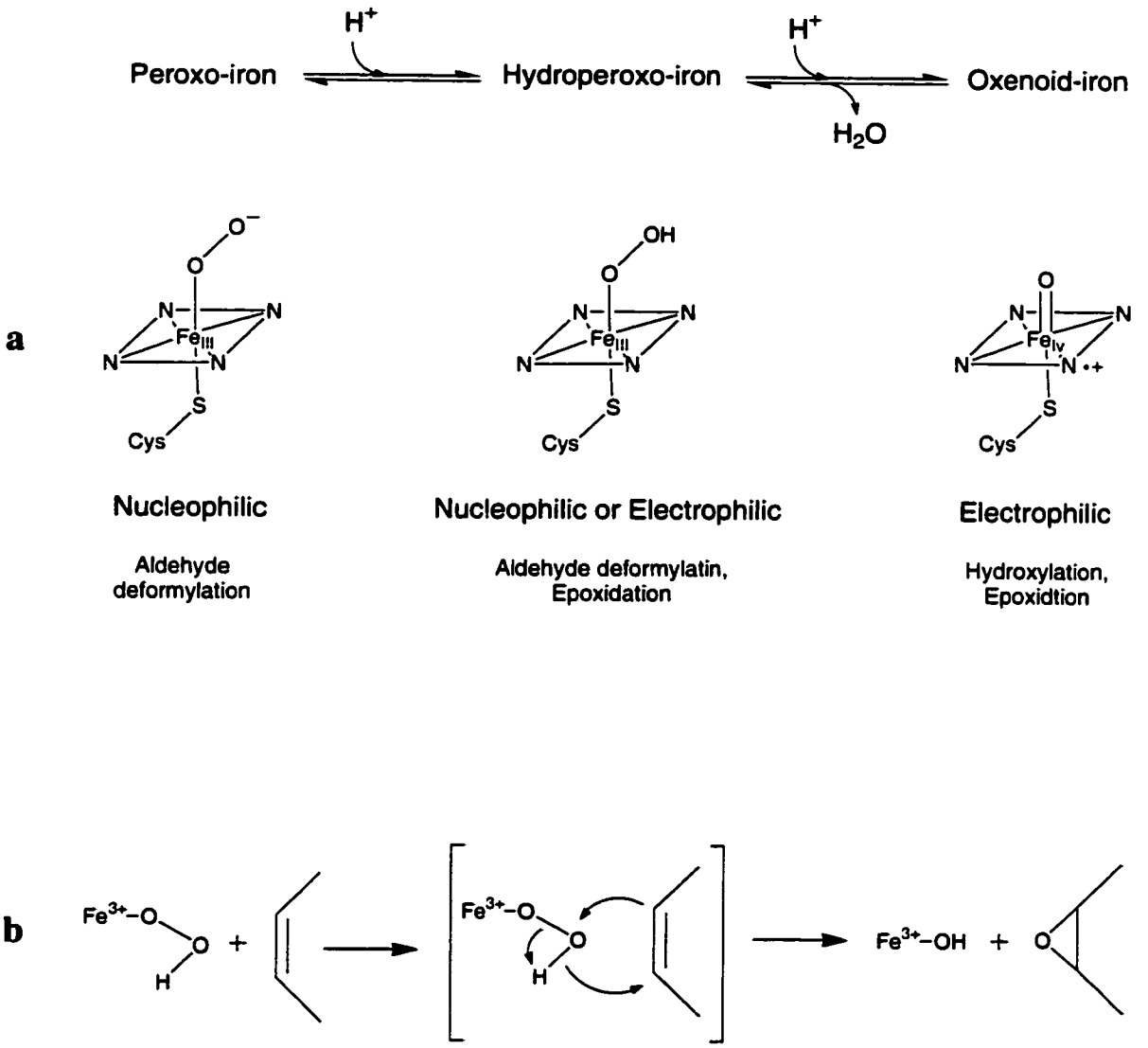

Figure 1.13 a) Proposed versatility of P450 iron-oxygen species. B) Iron-hydroperoxy species mechanism of olefin epoxidation. [a]

[a] Figures taken from (*50*).

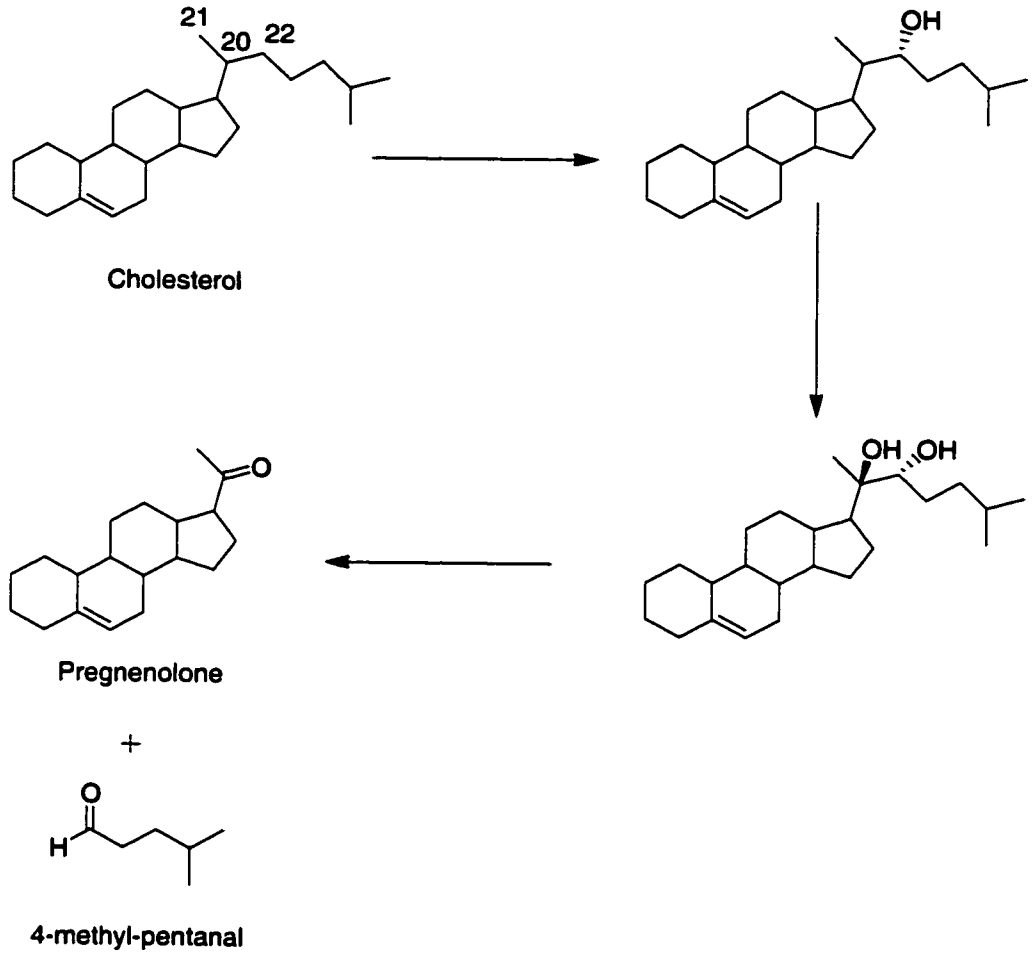

Figure 1.14 Consensus $P450_{SCC}$, cholesterol side-chain cleavage enzyme, reaction sequence.

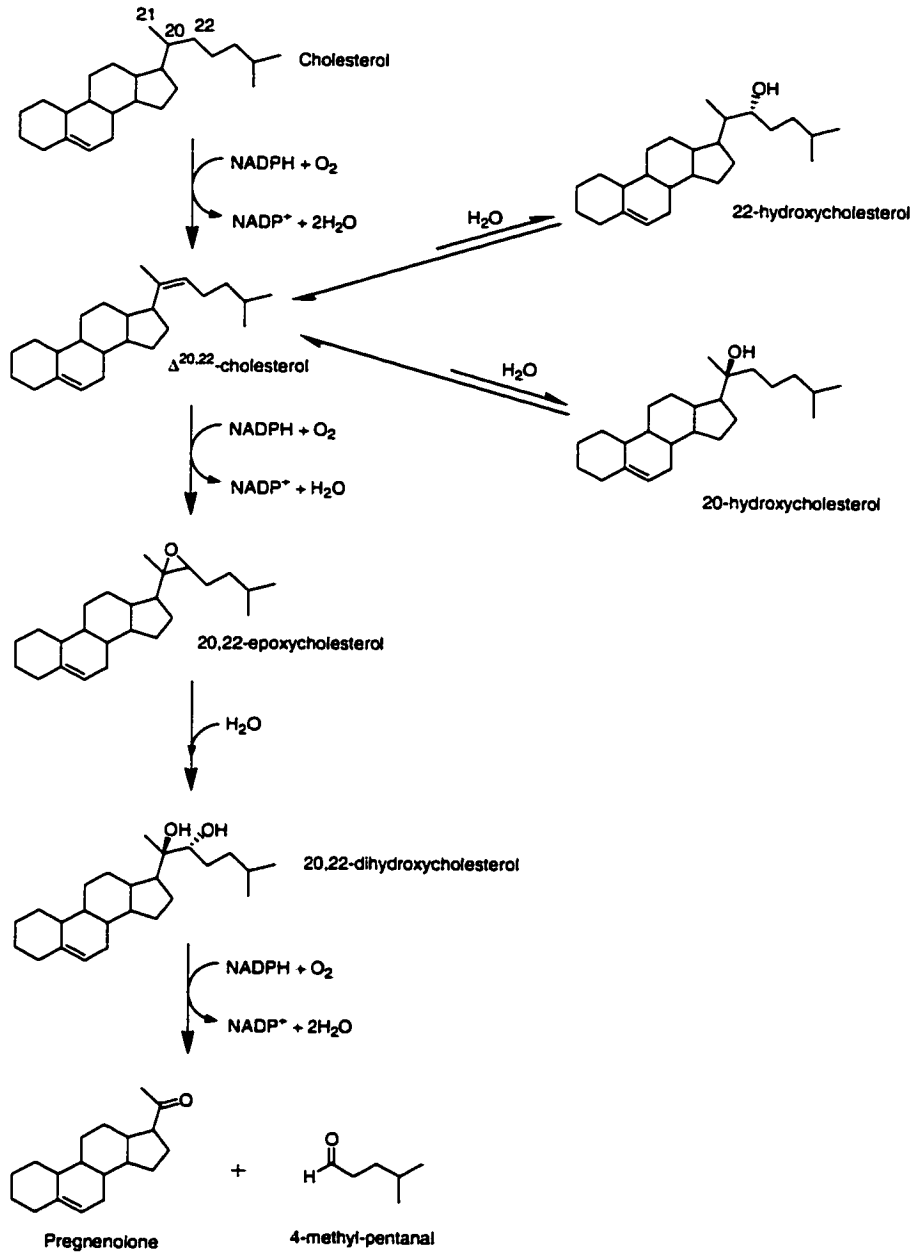

Figure 1.15 Proposed epoxide-diol mechanism of cholesterol conversion to pregnenolone. [a,b]

[a] Figure adapted from (*61*).

[b] At the time of this mechanistic proposal, 20-hydroxycholesterol was considered a viable intermediate.

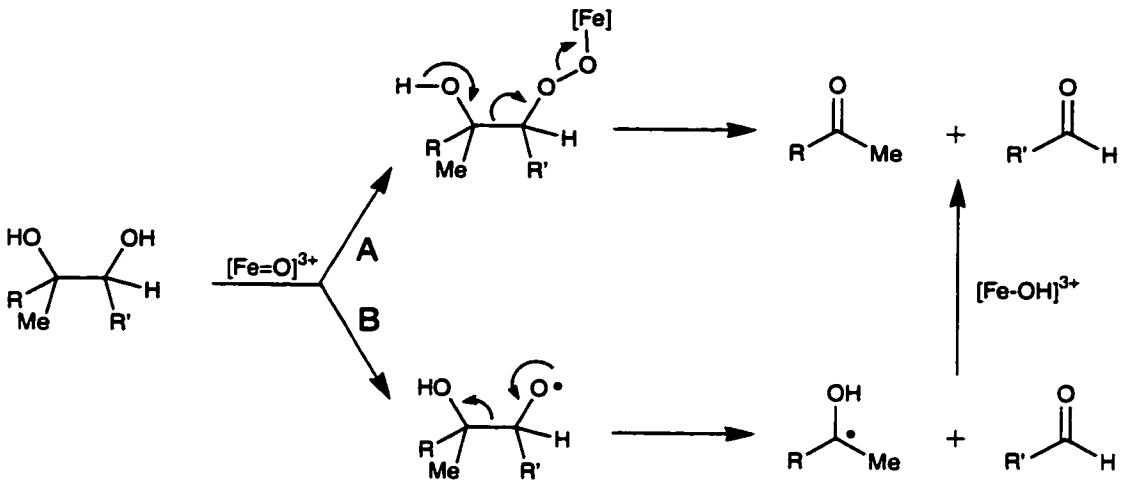

Figure 1.16 Possible mechanisms for $P450_{SCC}$-catalyzed carbon-carbon bond cleavage *in route* to conversion of cholesterol to pregnenolone. [a]

[a] Figure taken from (*5*).

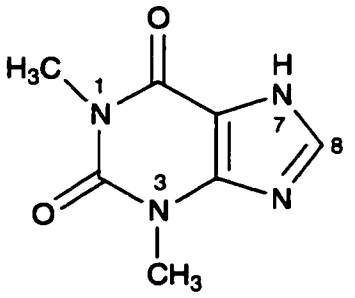

Theophylline

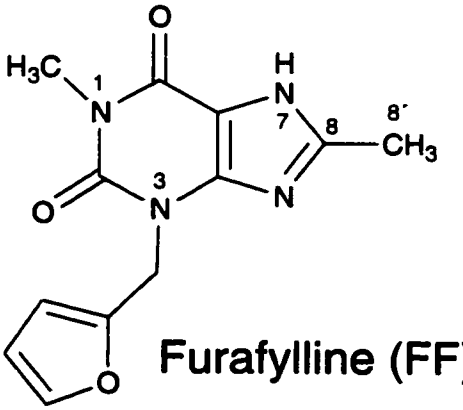

Furafylline (FF)

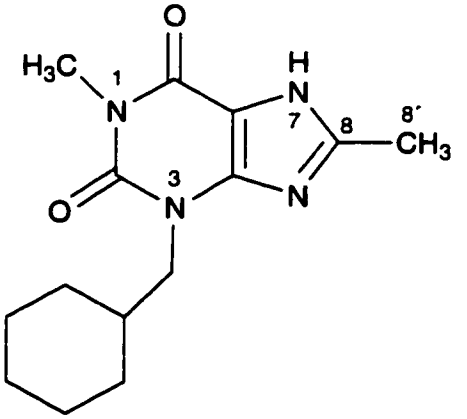

Cyclohexylline (CH)

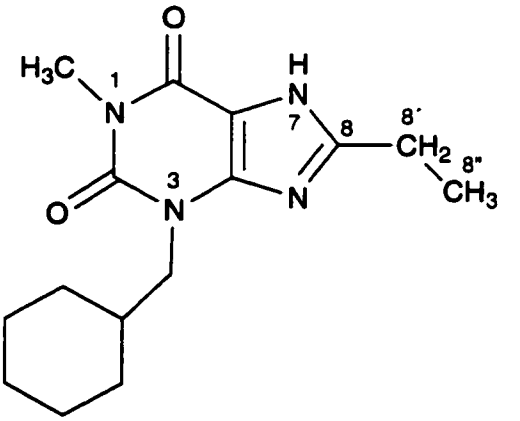

Ethylcyclohexylline (ETC)

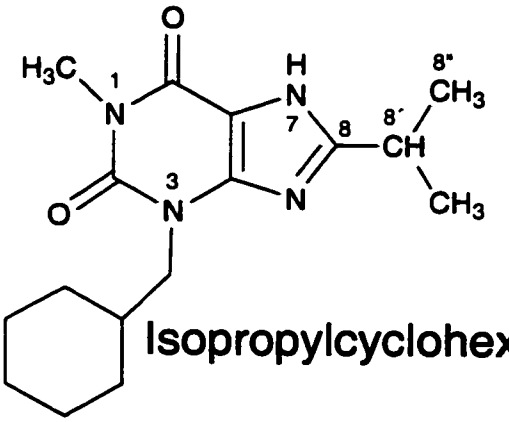

Isopropylcyclohexylline (IPC)

Figure 1.17 Structures of theophylline, furafylline, cyclohexylline, and ethylcyclohexylline.

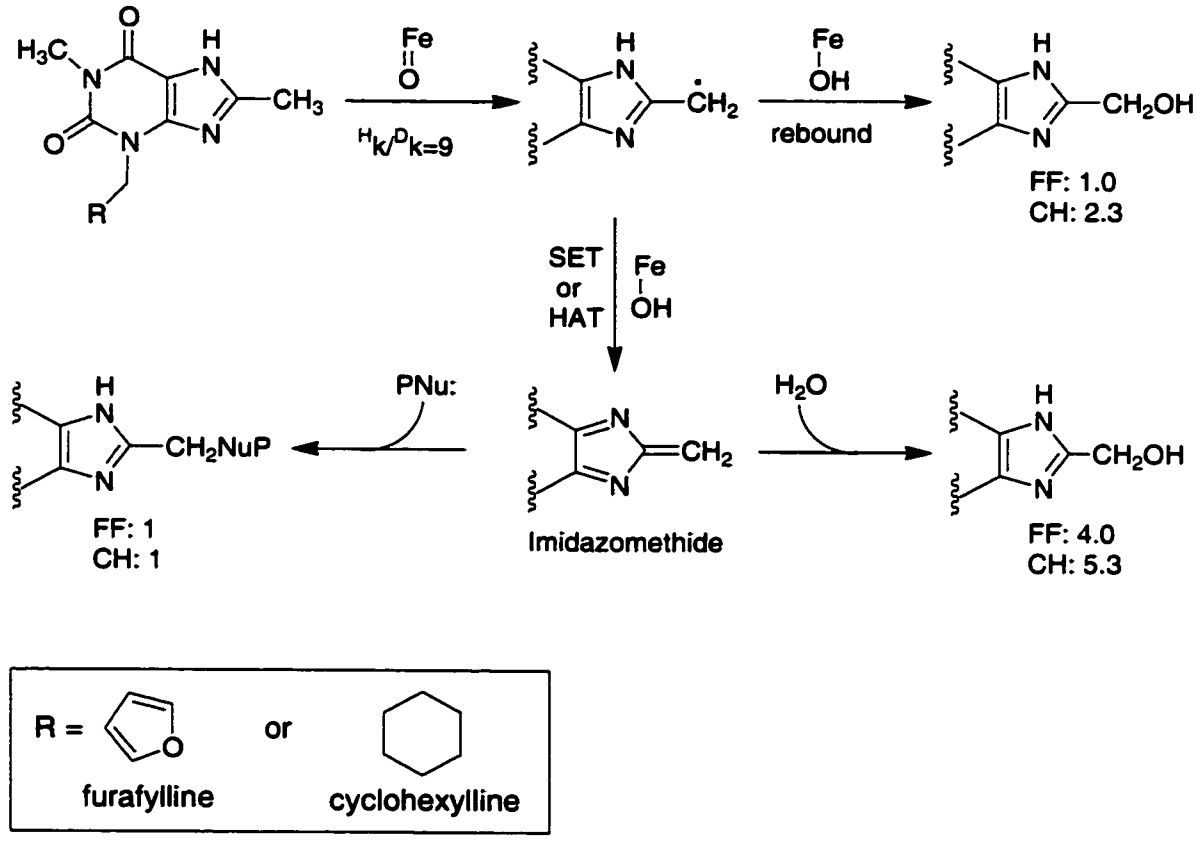

Figure 1.18 Proposed mechanism of furafylline and cyclohexylline metabolism by CYP1A2. [a]

[a] Numbers below the metabolites indicate relative rates of production.

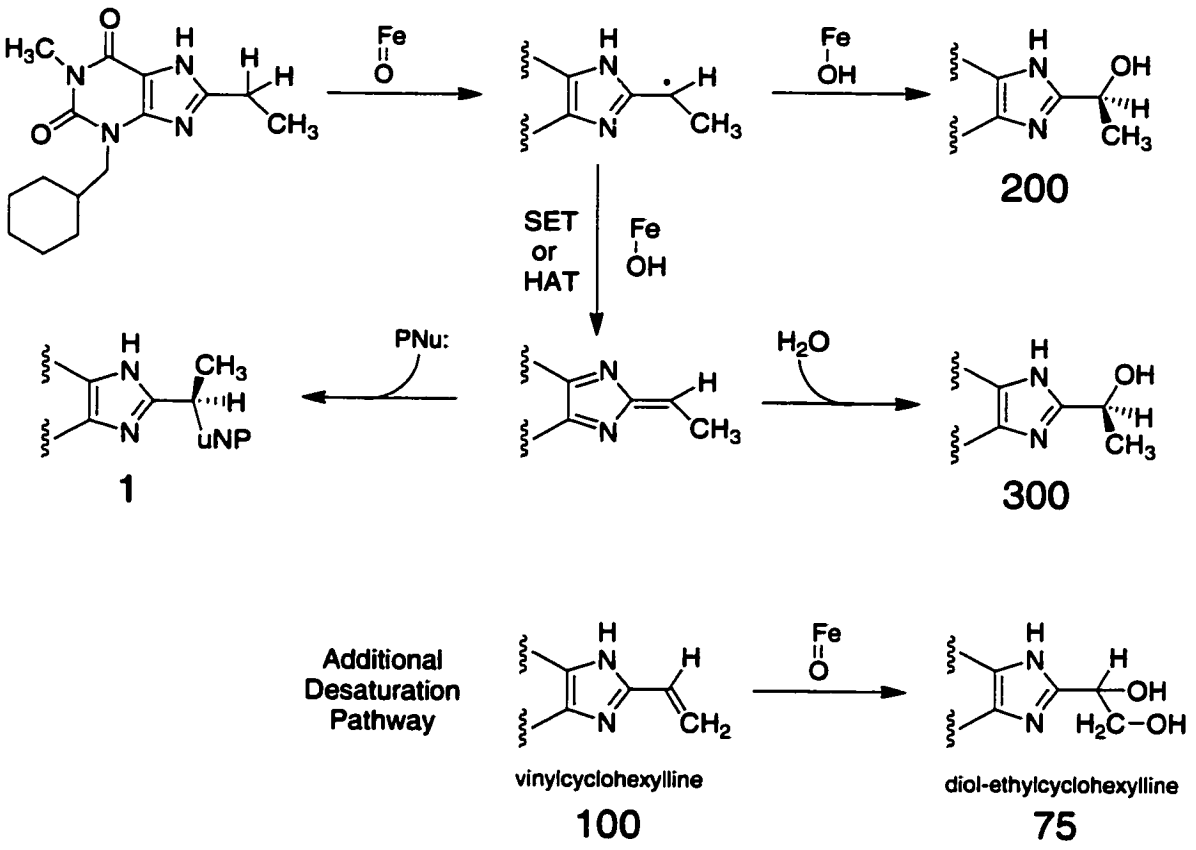

Figure 1.19 Proposed mechanism of ethylcyclohexylline metabolism by CYP1A2. [a,b]

[a] Numbers below the metabolites indicate relative quantities.

[b] The connectivity between the additional desaturation pathway and the core mechanism of metabolism is not yet established.

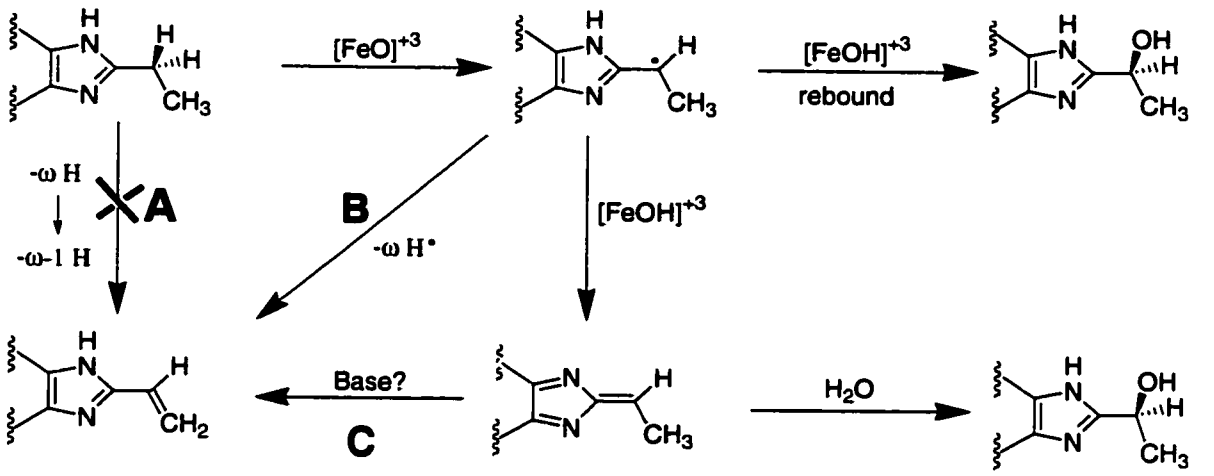

Figure 1.20 Possible mechanisms for CYP1A2-catalyzed olefin formation from ETC. A) dual hydrogen atom transfer initiated at the ω position, B) dual hydrogen atom transfer initiated at the ω-1 position, C) rearrangement of the imidazomethide-type reactive intermediate.

Table 1.1 Competitive ($^{D}V/K$) and non-competitive (^{D}V) deuterium isotope effects for the formation of metabolites from ω D_3-ethylcyclohexylline by CYP1A2.

	8′-OH (total)	8′-OH (H_2O)	8′-OH (O_2)	8″-OH	Olefin	Diol
(^{D}V)	0.76	0.66	1	ND	3.86	3.86
($^{D}V/K$)	0.74	0.64	1	3.26	3.52	3.29

Table 1.2 Competitive ($^{D}V/K$) and non-competitive (^{D}V) deuterium isotope effects for the formation of metabolites from ω D_3- and ω-1 D_2-N^7-methyl-ethylcyclohexylline by CYP1A2. [a]

	COH major	COH minor	8′-OH	Olefin	Total
ω-1 D_2					
(^{D}V)	0.84	0.64	3.44	3.9	1.04
($^{D}V/K$)	0.83	0.5	4.02	5.68	
ω D_3					
(^{D}V)	1.01	1.08	0.92	1.38	0.99
($^{D}V/K$)	1	0.94	0.94	1.53	

[a] COH major and COH minor refer to cyclohexyl-ring hydroxylation products.

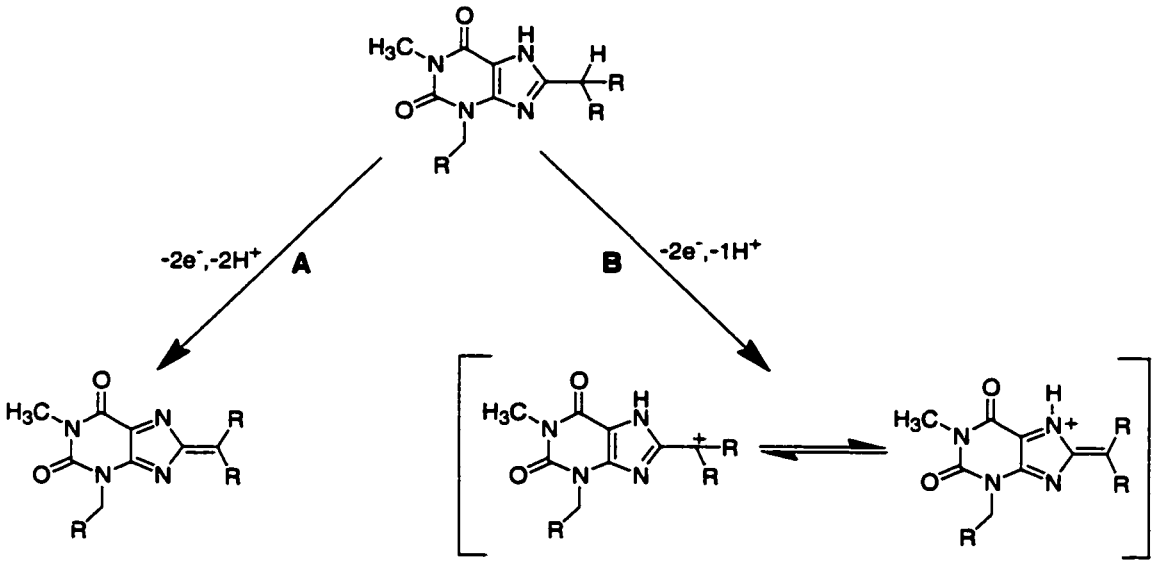

Figure 1.21 Potential mechanisms for oxidation of 8-alkyl xanthines to the desaturated iminium reactive intermediate: A) dual hydrogen atom transfer mechanism B) initial 8′-hydrogen atom transfer followed by a second electron transfer.

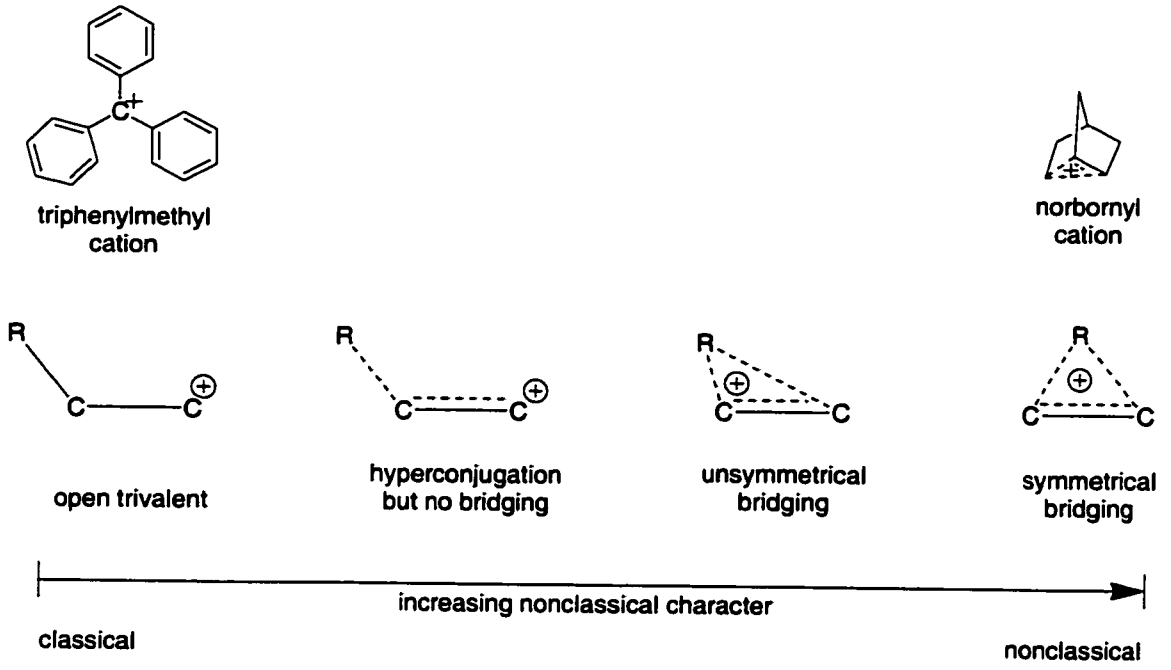

Figure 1.22 Continuum of carbocations, showing the limiting carbenium (classical) and carbonium (nonclassical) classes and species with varying degrees of charge delocalization bridging them. [a]

[a] Portion of figure taken from (*107*).

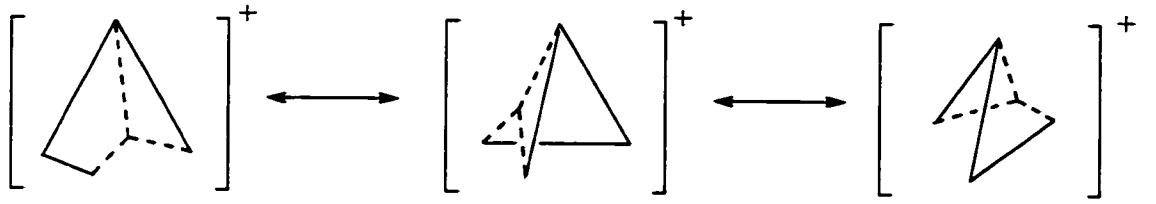

Figure 1.23 Cyclopropylcarbinyl cation nonclassical structure: exists in an equilibrium between 3 nonclassical species (*93*).

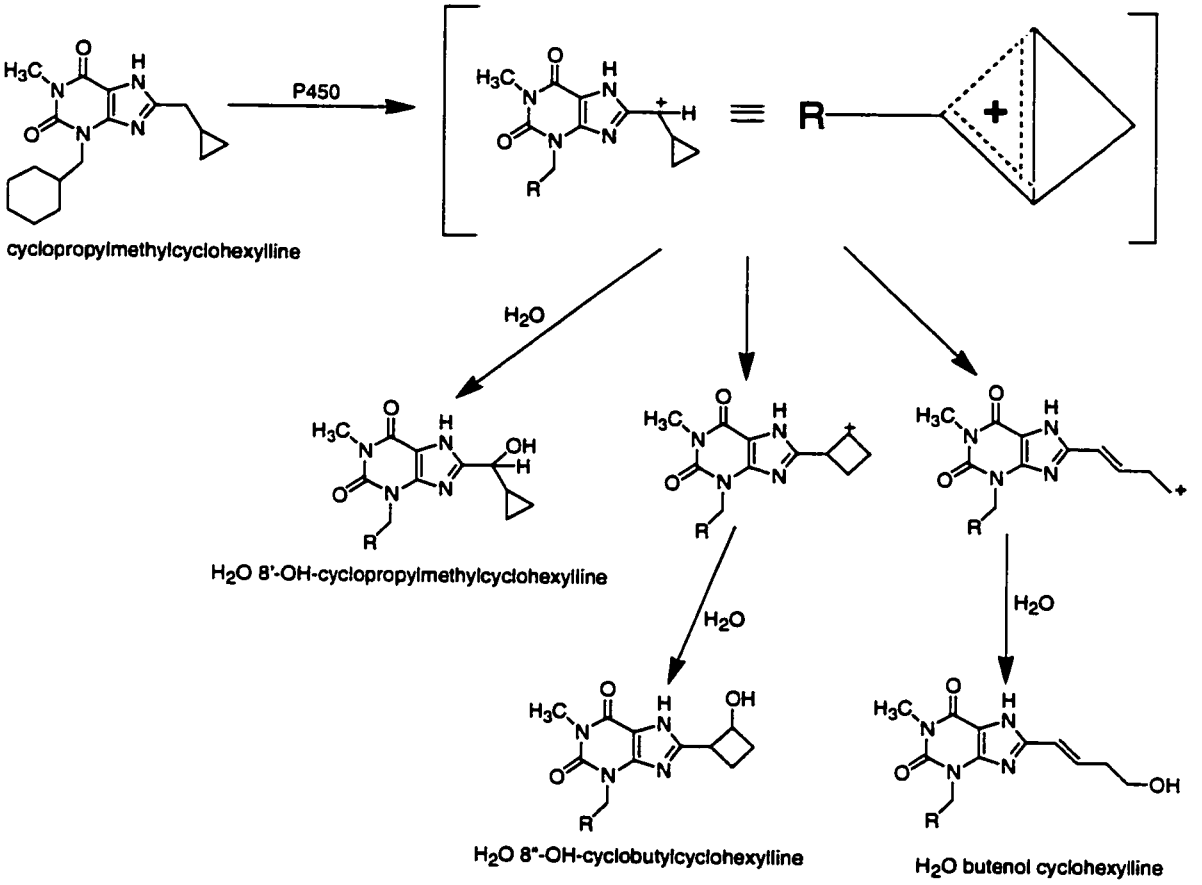

Figure 1.24 Potential outcomes for CYP1A2-catalyzed oxidation of cyclopropylmethylcyclohexylline.

CHAPTER 2

MATERIALS AND METHODS

Chemicals

$H_2{}^{18}O$ (97% and 95%) was obtained from MSD isotopes (Montreal, Canada) and Isotec (Miamisburg, OH), respectively. [$^2H_3{}^{13}C$]iodomethane (^{13}C, 99%; $^2H_3$, 99%) was purchased from Cambridge Isotope Laboratories (Andover, MA). [$^2H_3$]iodomethane ($^2H_3$, 99.5+ %) and [^{13}C]iodomethane (^{13}C, 99%) were purchased from Aldrich Chemical Co. (Milwaukee, WI). Cyclopropyl acetic acid was purchased from Lancaster (Windham, NH). Cyclobutane carboxylic acid, cyclobutanone, cyclopropyl methyl ketone, and sodium bisulfite were obtained from Acros Organics (Morris Plains, NJ). NADPH was purchased from Sigma (St. Louis, MO). All other chemicals were purchased from Aldrich Chemical Co. (Milwaukee, WI). Microsomes prepared from lymphoblastoid cells containing cDNA-expressed human cytochrome P450 1A2 were purchased from Gentest (Woburn, MA). CYP1A2 Supersomes (microsomes prepared from baculovirus infected insect cells co-expressing human cytochrome P450 1A2 and P450 reductase) were also purchased from Gentest.

Instrumentation

^1H NMR spectra were recorded on a Varian VXR300 or a Bruker AM500 instrument. HPLC analyses were performed on a Hewlett-Packard 1100 system (Agilent Technologies, Palo Alto, CA) with UV detection at 280 nm. ESLC-MS analyses were carried out on a Micromass Quattro II tandem quadrupole mass spectrometer with a Micromass Zspray ionization source (Micromass Ltd., Manchester, U.K.) coupled to two Shimadzu LC-10AD HPLC pumps and a Shimadzu SIL-10ADVP auto injector (Shimadzu Scientific Instruments, Inc., Columbia, MD). EIGC-MS analyses were

performed on a Micromass Trio 2000 quadrupole mass spectrometer with a Hewlett-Packard 5890 GC and Hewlett-Packard 7673 autosampler.

Liquid Chromatography–Mass Spectrometry.

N^7-Methyl-isopropylcyclohexylline. Substrate and metabolites were separated using a Hewlett-Packard ODS-Hypersil column (5 μm, 125 x 4 mm) with the following gradient: 44% to 48% solvent B over 12.5 min, 48% to 51% B from 12.5 to 13 min, 51% to 55% B from 13 to 33 min, followed by a 1 min column wash with 95% B and equilibration at the initial conditions for 8 min, where solvent A is H_2O and solvent B is acetonitrile:methanol (1:1). The flow rate was 1 ml/min, with 500μl/min diverted to the mass spectrometer. The instrument settings were: cone voltage 33 kV, probe voltage 3.5 kV, source temperature 150 °C, desolvation temperature 450 °C. Diol-, 8″-OH-, N^7-methyl-diol, 8′-OH-, N^7-methyl-8″-OH-, isopropylcyclohexylline, N^7-methyl-8′-OH-, vinyl-, N^7-methyl-vinyl-, and N^7-methyl-isopropylcyclohexylline eluted at 5.2, 6.9, 8.8, 10.1, 11.2, 17.4, 18.0, 18.8, 27.5, and 29.1 min, respectively.

Isopropylcyclohexylline. Using the same column as above, isopropylcyclohexylline and its metabolites were separated with the following gradient: 25% to 50% solvent B over 20 min, followed by a 3 min column wash with 95% B and equilibration at the initial conditions for 8 min, where solvent A is H_2O and solvent B is acetonitrile. The flow rate was 1 ml/min, with 400μl/min diverted to the mass spectrometer. The instrument settings were: cone voltage 33 kV, probe voltage 3.5 kV, source temperature 150 °C, desolvation

temperature 300 °C. Diol-, 8″-OH-, 8′-OH-isopropylcyclohexylline, methylketone-cyclohexylline, isopropylcyclohexylline, and vinyl-isopropylcyclohexylline eluted at 5.8, 7.4, 9.7, 12.9, 14.9, and 18.3 min, respectively.

Cyclopropylmethylcyclohexylline and Cyclobutylcyclohexylline. Separation and ESLC-MS analysis of these substrates and their metabolites were accomplished using the same column, gradient, and instrument settings as with isopropylcyclohexylline. 8′-OH-cyclopropylmethylcyclohexylline, 8′-OH-cyclobutylcyclohexylline, cyclopropylmethylcyclohexylline, and cyclobutylcyclohexylline eluted at 8.9, 12.2, 14.2, and 16.1 min, respectively.

Gas Chromatography-Mass Spectrometry. Analyte separation for EIGC-MS analysis was accomplished with a J&W (Folsom, CA) DB-5 (30 m x 0.32 mm i.d., 25 μm film thickness) capillary column, with helium as the carrier gas at a head pressure of 5 psi. Injector, interface, and detector temperatures were 250, 200, and 250 °C, respectively. Samples were injected at a column temperature of 120 °C, which was held for 1 min, followed by a linear 12 °C/min ramp to 300 °C, which was held for 4 min.

Semi-Preparatory-Scale HPLC. Specified compounds were purified using a Beckman ODS Ultrasphere column (5 μm, 10 mm x 25 cm) on the Hewlett Packard 1100 HPLC system. The flow rates and solvent proportions that were used for a specific compound are given in the synthesis section.

Syntheses

For convenient reference, chemical structures of synthesized substrates and metabolite standards are shown in figure 2.9.

Note: For unknown reasons, integrations of the cyclohexyl-ring protons ($\delta \approx$ 1.0-1.3 & 1.7-2.0) in ^{1}H-NMR spectra of cyclohexylline derivatives were highly variant and inconsistent with all other structural characterization and purity assessment data, which confirm the compound's identity and the absence of impurities.

5,6-Diamino-1-(cyclohexylmethyl)-3-methyl uracil ***1***. This compound was prepared as described (*88, 89*).

Isopropylcyclohexylline ***2*** *[3,7-Dihydro-8-isopropyl-1-methyl-3-(cyclohexylmethyl)-1H-purine-2,6-dione].* A mixture of 5,6-diamino-1-(cyclohexylmethyl)-3-methyl uracil **1** (0.3 g, 1.2 mmol) and isobutyric anhydride (1 g, 6.3 mmol) was heated for 2 hours at 150 °C. Following the addition of 10% aqueous NaOH (5 ml), the solution was boiled for an additional 1 hour. After pH neutralization with concentrated HCl, the precipitated product was collected by vacuum filtration and recrystallized in acetone. Further purification was by semi-prep HPLC (2.0 ml/min., 25/35/40 (H_2O/acetonitrile/methanol)): mp 174-175 °C; ^{1}H-NMR (300 MHz, $CDCl_3$): δ 4.17 (d, J = 7.3 Hz, 2H, N3-C$\underline{H}_2$), 3.47 (s, 3H, N1-C$\underline{H}_3$), 3.20-3.34 (m, 1H, C8-C$\underline{H}$), 1.9-2.06 (br, 1H, N3-CH_2C$\underline{H}$), 1.60-1.74 (m, 5H), 1.50 (d, J = 6.9 Hz, 6H, C8-CH(C$\underline{H}_3$)$_3$, 1.07-1.24 (m, 5H); ESMS m/z 305 $[M + H]^+$.

D_6-Isopropylcyclohexylline 3 [3,7-Dihydro-8-([dimethyl-$^2H_6$]-isopropyl)-1-methyl-3-(cyclohexylmethyl)-1H-purine-2,6-dione].

($^2H_6$-Dimethyl) isobutyric acid. [$^2H_6$-Dimethyl]-isobutyric acid was prepared according to the method of (*108*). Diethyl malonate (2.25 g, 14 mmol) was added dropwise to a solution of NaH (0.9 g, 37.5 mmol) in dry THF (50 ml). CD_3I (5 g, 34.5mmol) was slowly added, and the solution was stirred at room temperature for 1 hour, followed by refluxing for 90 minutes. H_2O (50 ml) was added, and the solution was extracted with diethyl ether (3 x 100 ml). The ether layers were combined and evaporated. The yellow liquid product was stirred in ethanol (30 ml) and 10% w/v aqueous NaOH (25 ml) for 24 hours at room temperature. The solution was reduced to approximately 30 ml by evaporation, acidified to pH 2 with concentrated H_2SO_4, and extracted with ethyl acetate (3 x 50 ml). The ethyl acetate layers were combined and evaporated. The yellow liquid product was mixed with H_2O (50 ml) and refluxed for 24 hours. The solution was extracted with ethyl acetate (2 x 50 ml), the ethyl acetate layers combined, and the ethyl acetate evaporated to give 2.77g of a yellow liquid with a crystalline precipitate. The crystalline precipitate was recovered by vacuum filtration, dissolved in H_2O (25 ml), and refluxed for 48 hours. The solution was acidified to pH 2 with concentrated H_2SO_4, extracted with ethyl acetate (2 x 50 ml), the ethyl acetate layers combined, and the ethyl acetate evaporated to give 0.35 g (3.7 mmol, 26%) ($^2H_6$-dimethyl) isobutyric acid. ^{1}H-NMR (300 MHz, $CDCl_3$): δ 2.55 (s, 1H).

D_6-Isopropylcyclohexylline 3. As in above synthesis of isopropylcyclohexylline **2**, the title compound was prepared by reaction of the crude [dimethyl-$^2H_6$]-isobutyric acid with 5,6-diamino-1-(cyclohexylmethyl)-3-methyl uracil **1** (0.2 g, 0.8 mmol). The

product was purified by semi-prep HPLC (2.0 ml/min., 25/35/40 (H_2O/acetonitrile/methanol)): mp 173-174; ^{1}H-NMR (300 MHz, $CDCl_3$): δ 4.00 (d, J = 7.3 Hz, 2H, N3-C$\underline{H}_2$), 3.46 (s, 3H, N1-C$\underline{H}_3$), 3.18 (s, 1H, C8-C$\underline{H}$), 1.90-2.07 (br, 1H, N3-$CH_2C\underline{H}$), 1.56-1.80 (m, 8H), 1.05-1.28 (m, 6H); ESMS m/z 311 $[M + H]^+$; 99.2% $^2H_6$, 0.1% $^2H_5$, 0.6% $^2H_0$.

D_1-Isopropylcyclohexylline 4 [3,7-Dihydro-8-([8'-$^2H_1$]-isopropyl)-1-methyl-3-(cyclohexylmethyl)-1H-purine-2,6-dione]. Following the procedure of (*109*), [C_α-$^2H_1$]isobutyric acid was prepared from sodium isobutyrate (10 g, 90 mmol) and sodium metal (0.3 g, 13 mmol) by successive 18 hour treatments with D_2O (5 x 40 ml) in a stainless-steel bomb at 150 °C (4.8 g, 60%). The prepared [C_α-$^2H_1$]isobutyric acid and 5,6-diamino-1-(cyclohexylmethyl)-3-methyl uracil **1** (0.05 g, 0.2 mmol) were combined to synthesize the title compound in a similar manner as in the above syntheses, except 10% NaOD was used in place of 10% NaOH. A portion of the total product (0.047 g, 93%) was purified by semi-prep HPLC (2.0 ml/min., 25/35/40 (H_2O/acetonitrile/methanol)); ^{1}H-NMR (300 MHz, $CDCl_3$): 3.98 (d, J = 7.4 Hz, 2H, N3-C$\underline{H}_2$), 3.46 (s, 3H, N1-C$\underline{H}_3$), 1.90-2.05 (br, 1H, N3-$CH_2C\underline{H}$), 1.54-1.79 (m, 11H), 1.42 (s, 6H, C8-C(D)(C$\underline{H}_3$)$_2$), 1.05-1.30 (m, 6H); ESMS m/z 306 $[M + H]^+$; 99.4% $^2H_1$.

(S)-$^{13}CD_3$-Isopropylcyclohexylline (also called pro-R-$^{13}CD_3$-Isopropylcyclohexylline) ***5*** *[3,7-Dihydro-8-(2-(2S)-[$^2H_3{}^{13}$C-methyl]ethyl)-1-methyl-3-(cyclohexylmethyl)-1H-purine-2,6-dione].*

(4S)-3-Propionyl-4-isopropyl oxazolidinone ***6.*** Following the procedure of Evans, *et al.*(*110*) (Figure 2.1), (4S)-4-isopropyl oxazolidinone (0.775 g, 6 mmol) was dissolved in dry THF (20 ml) in a flame-dried flask, sealed with a rubber septum. The solution, under positive pressure with argon, was cooled to –78 °C in a dry ice/acetone bath, followed by the dropwise addition of n-butyl lithium (10 M in hexanes, 0.6 ml, 6 mmol) with an oven-dried, gas-tight syringe. The reaction was allowed to proceed at –78 °C for 3 hours, under positive pressure with argon. Propionyl chloride (0.521 ml, 0.555 g, 6 mmol) was then added dropwise using an oven-dried, gas-tight syringe, and the reaction kept at –78 °C for an additional 3 hours, followed by gradual warming to room temperature overnight. H_2O (1 ml) was added dropwise, under positive pressure with argon, to quench any remaining n-butyl lithium, and the THF removed *in vacuo*. The residue was brought back up in H_2O, and extracted with CH_2Cl_2 (3 x 50 ml). The CH_2Cl_2 extracts were pooled, dried with $MgSO_4$, filtered, and the CH_2Cl_2 removed *in vacuo* (1.173 g, 6.3 mmol, 106%); ^{1}H-NMR (300 MHz, $CDCl_3$): 4.40 (m, 1H, C4-$\underline{H}$), 4.21 (m, 2H, C5-$\underline{H}_2$), 2.89 (m, 2H, N3-C(=O)C$\underline{H}_2$), 2.36 (m, 1H, C4-C$\underline{H}$), 1.15 (t, J = 7.3 Hz, 3H, N3-C(=O)CH$_2$C$\underline{H}_3$), 0.90 (d, J = 7.3 Hz, 3H, C4-C(H)(C$\underline{H}_3$)$_2$), 0.87 (d, J = 6.8 Hz, 3H, C4-C(H)(C$\underline{H}_3$)$_2$).

(4S)-3-[(2S)-2-($^2H_3{}^{13}$C-methyl)propionyl]-4-isopropyl oxazolidinone ***7.*** The title compound was prepared using a modified procedure of Fletcher, *et al.* (*111*) (Figure 2.1). (4S)-3-Propionyl-4-isopropyl oxazolidinone (1.79 g, 9.66 mmol) was dissolved in dry

THF (32 ml) in a flame-dried flask, sealed with a rubber septum. The flask was evacuated, and the solution sparged with argon (3 x 10 min), followed by cooling to –78 °C in a dry ice/acetone bath. Sodium bis(trimethylsilyl)amide (NaHMDS, 1 M in THF, 1.944 g, 10.6 mmol) was added dropwise with an oven-dried, gas-tight syringe. The reaction, under positive pressure with argon, was allowed to proceed at –78 °C for 3 hours. [$^{2}H_3{}^{13}C$]iodomethane (2.28 g, 15.6 mmol) was then added dropwise using an oven-dried, gas-tight syringe, and the reaction kept at –78 °C for an additional 3 hours, followed by gradual warming to room temperature overnight. H_2O (1 ml) was added dropwise, under positive pressure with argon, to quench any remaining NaHMDS, and the THF removed *in vacuo*. The residue was brought back up in H_2O, and extracted with CH_2Cl_2 (3 x 50 ml). The CH_2Cl_2 extracts were pooled, dried with $MgSO_4$, filtered, and the CH_2Cl_2 removed *in vacuo* (1.757 g, 8.6 mol, 89%). The product was purified by flash chromatography (petroleum ether/ethyl acetate (85/15)) (1.0 g, 4.9 mmol, 51%): S/R = 10, calculated from NMR data by comparison to published results of (*112*); ^{1}H-NMR (500 MHz, $CDCl_3$): 4.40 (m, 1H, C4-$\underline{H}$), 4.23 (t, J = 9.7, 7.7 Hz, 1H, C5-$\underline{H_2}$), 4.16 (dd, J = 3.0, 8.8 Hz, 1H, C5-$\underline{H_2}$), 3.72 (m, 1H, N3-C(=O)C$\underline{H}$), 2.30 (m, 1H, C4-C$\underline{H}$), 1.17 & 1.10 (2 x dd, J = 6.8, 5.5 Hz, 3H, minor and major diastereomer N3-C(=O)C(H)($^{13}CD_3$)C$\underline{H_3}$ respectively, 0.87 (d, J = 7.2 Hz, 3H, C4-C(H)(C$\underline{H_3}$)$_2$), 0.83 (d, J = 6.9 Hz, 3H, C4-C(H)(C$\underline{H_3}$)$_2$).

(2S)-2-($^{2}H_3{}^{13}C$-Methyl)propionic acid 8. Using the procedures of Evans, *et al.* (*113*) and Harding, *et al.* (*114*), (4S)-3-[(2S)-2-($^{2}H_3{}^{13}$C-methyl)Propionyl]-4-isopropyl oxazolidinone from the previous step (1.0 g, 4.9 mmol) yielded the crude carboxylic acid

product (0.3 g, 66%) (Figure 2.1). S/R = 10 is assumed from results of NMR analysis of **7**.

*(S)-$^{13}CD_3$-Isopropylcyclohexylline (also called pro-R-$^{13}CD_3$-Isopropylcyclohexylline) **5**.* As in above synthesis of isopropylcyclohexylline, the prepared (2S)-2-($^2H_3{}^{13}C$-methyl)propionic acid (0.3 g, 3.2 mmol) was reacted with 5,6-diamino-1-(cyclohexylmethyl)-3-methyl uracil **1** (0.05 g, 0.2 mmol). Again, S/R = 10 is assumed from results of NMR analysis of **7**. The product was purified by semi-prep HPLC (2.0 ml/min., 30/30/40 (H_2O/acetonitrile/methanol)); ^{1}H-NMR (500 MHz, $CDCl_3$): δ 3.98 (d, J = 8 Hz, 2H, N3-C$\underline{H}_2$), 3.44 (s, 3H, N1-C$\underline{H}_3$), 3.19 (m, 1H, C8-C$\underline{H}$), 1.96 (br, 1H, N3-$CH_2C\underline{H}$), 1.60-1.82 (m, 9H), 1.41 (dd, J = 4.8, 6.7 Hz, 3H, C8-C(H)($^{13}C^2H_3$)C$\underline{H}_3$, 1.04-1.25 (m, 8H); ESMS m/z 309 $[M + H]^+$; 94.9% $^2H_3{}^{13}C$, 4.5% $^2H_2{}^{13}C$ or $^2H_3{}^{12}C$, 0.2% $^2H_1{}^{13}C$ or $^2H_2{}^{12}C$, 0.4% $^1H_3{}^{12}C$.

*(S)-^{13}C-Isopropylcyclohexylline (also called pro-R-^{13}C-Isopropylcyclohexylline) **9** [3,7-Dihydro-8-(2-(2S)-[^{13}C-methyl]ethyl)-1-methyl-3-(cyclohexylmethyl)-1H-purine-2,6-dione].* This compound was synthesized in the same step-wise manner and purified as in the above synthesis of (S)-$^{13}CD_3$-isopropylcyclohexylline **5**, except [^{13}C]iodomethane was used in the place of [$^2H_3{}^{13}$C]iodomethane (0.02 g, 33%); ^{1}H-NMR (300 MHz, $CDCl_3$): δ 3.99 (d, J = 7.3 Hz, 2H, N3-C$\underline{H}_2$), 3.46 (s, 3H, N1-C$\underline{H}_3$), 3.20 (m, 1H, C8-C$\underline{H}$), 1.98 (br, 1H, N3-$CH_2C\underline{H}$), 1.58-1.75 (m, 9H), 1.41 (dd, J = 6.6, 5.0 Hz, 3H) 1.03-1.27 (m, 9H); ESMS m/z 306 $[M + H]^+$: S/R = 10 calculated from NMR data of (2S)-2-(^{13}C-methyl)propionic acid precursor by comparison to published results of (*112*); [^{1}H-NMR (500 MHz, $CDCl_3$): 1.24 & 1.17 (2 x dd, J = 6.8,128.5 Hz, 3H, major and minor

diastereomer N3-C(=O)C(H)(CH_3)$^{13}C\underline{H}_3$ respectively, 1.24 & 1.17 (2 x dd, J = 6.8, 7.0 Hz, 3H, minor and major diastereomer N3-C(=O)C(H)($^{13}CH_3$)$C\underline{H}_3$ respectively]; 98.6% ^{13}C.

(S)-D_3-Isopropylcyclohexylline (also called pro-S-D_3-isopropylcyclohexylline) ***10*** *[3,7-Dihydro-8-(2-(2S)-[$^2H_3$-methyl]ethyl)-1-methyl-3-(cyclohexylmethyl)-1H-purine-2,6-dione].*

(4S)-3-acetyl-4-isopropyl oxazolidinone ***11.*** This compound was synthesized in the same manner as (4S)-3-Propionyl-4-isopropyl oxazolidinone (see above), except acetyl chloride was used in place of propionyl chloride (*112*) (Figure 2.1). The product was purified by flash chromatography (petroleum ether/ethyl acetate, 85/15) (67% yield); ^{1}H-NMR (200 MHz, $CDCl_3$): 4.39 (m, 1H, C4-$\underline{H}$), 4.24 (t, J = 9.0, 8.5 Hz, 1H, C5-$\underline{H}_2$), 4.19 (dd, J = 3.0, 9.1 Hz, 1H, C5-$\underline{H}_2$), 2.51 (s, 3H, N3-C(=O)C$\underline{H}_3$), 2.36 (m, 1H, C4-C$\underline{H}$), 0.89 (d, J = 7.1 Hz, 3H, C4-C(H)(C$\underline{H}_3$)$_2$), 0.85 (d, J = 6.5 Hz, 3H, C4-C(H)(C$\underline{H}_3$)$_2$).

(4S)-4-Isopropyl-3-[(3,3,3-$^2H_3$)propionyl]oxazolidinone ***12.*** This compound was synthesized using (4S)-3-acetyl-4-isopropyl oxazolidinone (4.45 g, 26 mmol) from the previous step and [$^2H_3$]iodomethane (12 g, 82.8 mmol), following the procedure of Fletcher, *et al.* (*111*) (Figure 2.1), with the critical addition of very thorough and repeated evacuation of the reaction flask and sparging of all solutions with argon. The product was purified by flash chromatography (petroleum ether/ethyl acetate, 85/15) (2.457 g, 13.1 mmol, 50%); ^{1}H-NMR (300 MHz, $CDCl_3$): 4.39 (m, 1H, C4-$\underline{H}$), 4.21 (m, 2H, C5-$\underline{H}_2$), 2.90 (dd, J = 10.7, 18.1 Hz, 2H, N3-C(=O)C$\underline{H}_2$), 2.37 (m, 1H, C4-C$\underline{H}$), 0.89 (d, J = 7.3 Hz, 3H, C4-C(H)(C$\underline{H}_3$)$_2$), 0.85 (d, J = 7.0 Hz, 3H, C4-C(H)(C$\underline{H}_3$)$_2$).

(4S)-4-Isopropyl-3-[(2S)-2-($^2H_3$-methyl)propionyl] oxazolidinone ***13.*** This product was made using (4S)-4-isopropyl-3-[(3,3,3-$^2H_3$)propionyl]oxazolidinone from the previous step, following the procedure outlined above for (4S)-3-[(2S)-2-($^2H_3$ ^{13}C-methyl)propionyl]-4-isopropyl oxazolidinone, except unlabeled iodomethane was used in place of the [$^2H_3$]iodomethane (Figure 2.1). The product was purified by flash chromatography (2.58 g, 12.8 mmol, 76%): S/R = 10, calculated from NMR data by comparison to published results of (*112*); ^{1}H-NMR (500 MHz, $CDCl_3$): 4.37 (m, 1H, C4-H), 4.12 – 4.22 (m, 2H, C5-H_2), 3.68 (q, *J* = 6.9 Hz, 1H, N3-C(=O)CH), 2.26 (m, 1H, C4-CH), 1.13 & 1.06 (2 x d, *J* = 6.8 Hz, 3H, major and minor diastereomer N3-C(=O)C(H)(CD_3)CH_3 respectively, 0.83 (d, *J* = 7.6, Hz, 3H, C4-C(H)(CH_3)$_2$), 0.79 (d, *J* = 7.0, Hz, 3H, C4-C(H)(CH_3)$_2$).

(2S)-2-($^2H_3$-Methyl)propionic acid ***14.*** The carboxylic acid side-chain was cleaved from the chiral auxiliary oxazolidinone (Figure 2.1) using the procedures in (*113, 114*) (0.56 g, 6.1 mmol, 48%). S/R = 10 is assumed from results of NMR analysis of **13**.

(S)-D_3-Isopropylcyclohexylline (also called pro-S-D_3-isopropylcyclohexylline) ***10.*** The prepared (2S)-2-($^2H_3$-methyl)propionic acid (0.3 g, 3.3 mmol) was reacted with 5,6-diamino-1-(cyclohexylmethyl)-3-methyl uracil **1** (0.05 g, 0.2 mmol), as above (0.056 g, 0.2 mmol, 92%). Again, S/R = 10 is assumed from results of NMR analysis of **13**. The product was purified by semi-prep HPLC (2.0 ml/min., 25/35/40 (H_2O/acetonitrile/methanol)); ^{1}H-NMR (500 MHz, $CDCl_3$): δ 3.98 (d, *J* = 7.4 Hz, 2H, N3-CH_2), 3.44 (s, 3H, N1-CH_3), 3.21 (m, 1H, C8-CH), 1.96 (br, 1H, N3-CH_2CH), 1.60-1.73 (m, 7H), 1.41 (d, *J* = 7.3 Hz, 3H, C8-C(H)(C$^2H_3$)CH_3, 1.07-1.27 (m, 7H); ESMS m/z 308 $[M + H]^+$; 6.4% $^2H_6$, 92.5% $^2H_3$, 0.3% $^2H_2$, 0.2% $^2H_1$, 0.6% $^2H_0$.

8′-OH-Isopropylcyclohexylline ***15*** *[3,7-Dihydro-8-(1-hydroxy-1-methylethyl)-1-methyl-3-(cyclohexylmethyl)-1H-purine-2,6-dione].* 5,6-Diamino-1-(cyclohexylmethyl)-3-methyl uracil **1** (0.2 g, 0.8 mmol) and 2-hydroxy isobutyric acid (0.3 g, 2.9 mmol) were mixed for 2 hours at 110 °C. Aqueous NaOH (10%, 5 ml) was added, and the solution was boiled for 1 hour. The pH was neutralized with concentrated HCl and the precipitated product collected by vacuum filtration (0.134 g, 53%). A portion of this product was purified via semi-prep HPLC (2.5 ml/min., 37.5/27.5/35 (H_2O/acetonitrile/methanol)): mp 197-198 °C; ^{1}H-NMR (300 MHz, $CDCl_3$): δ 4.00 (d, J = 7.2 Hz, 2H, N3-C$\underline{H}_2$), 3.45 (s, 3H, N1-C$\underline{H}_3$), 1.90-2.00 (br, 1H, N3-CH_2C$\underline{H}$), 1.6-1.78 (m, 12H), 1.05-1.28 (m, 8H); ESMS m/z 321 $[M + H]^+$ (100%), 303 $[(M + H)^+ - H_2O]$ (52%).

8″-OH-Isopropylcyclohexylline ***16*** *[3,7-Dihydro-8-(2-hydroxy-1-methylethyl)-1-methyl-3-(cyclohexylmethyl)-1H-purine-2,6-dione].* Methyl-(S)-(+)-3-hydroxy-2-methyl propionate (1 g, 8.5 mmol) was hydrolyzed to the corresponding carboxylic acid by refluxing in 10% NaOH (5 ml) for 2 hours. The aqueous solution was acidified with concentrated HCl, and extracted with ethyl acetate (3 x 5 ml). Evaporation of the solvent yielded (S)-(+)-3-hydroxy-2-methylpropionate (0.492 g, 51%). As above, this carboxylic acid product (0.256 g, 2.3 mmol) and 5,6-diamino-1-(cyclohexylmethyl)-3-methyl uracil **1** (0.2 g, 0.8 mmol) were used to make the title compound. A portion of the product was purified by semi-prep HPLC (2.5 ml/min., 50/25/25 (H_2O/acetonitrile/methanol)): mp 187-188 °C; ^{1}H-NMR (300 MHz, $CDCl_3$): δ 3.97 (d, J = 7.2 Hz, 2H, N3-C$\underline{H}_2$), 3.89 (dd, J = 7.3, ≈9 Hz, 2H, C8-CH(CH_3)C$\underline{H}_2$), 3.45 (s, 3H, N1-C$\underline{H}_3$), 3.25-3.37 (m, 1H, C8-C$\underline{H}$),

1.89-2.04 (br, 1H, N3-$CH_2C\underline{H}$), 1.6-1.79 (m, 6H), 1.43 (d, 7.2 Hz, 3H, C8-$CH(CH_2OH)C\underline{H_3}$), 1.00-1.28 (m, 5H); ESMS m/z 321 $[M + H]^+$.

Vinyl-isopropylcyclohexylline ***17*** *[3,7-Dihydro-8-isopropenyl-1-methyl-3-(cyclohexylmethyl)-1H-purine-2,6-dione].* 8'-OH-Isopropylcyclohexylline **15** (1 g, 3 mmol) was refluxed in 20% aqueous sulfuric acid for 2 hours. The precipitated product was collected by vacuum filtration (0.8 g, 87%). A portion of this product was recrystallized in methanol (4x). Additional purification was accomplished by semi-prep HPLC (2.0 ml/min., 20/35/45 (H_2O/acetonitrile/methanol)): mp 233-235; ^{1}H-NMR (300 MHz, $CDCl_3$): δ 6.20 (m, 1H), 5.46 (m, 1H), 4.01 (d, J = 7.3 Hz, 2H, N3-$C\underline{H_2}$), 3.46 (s, 3H, N1-$C\underline{H_3}$), 2.26 (s, 3H, C8-$C(CH_2)C\underline{H_3}$), 1.94-2.04 (br, 1H, N3-$CH_2C\underline{H}$), 1.6-1.82 (m, 9H), 1.04-1.32 (m, 7H); ESMS m/z 303 $[M + H]^+$.

Diol-isopropylcyclohexylline ***18*** *[3,7-Dihydro-8-(1,2-dihydroxy-1-methylethyl)-1-methyl-3-(cyclohexylmethyl)-1H-purine-2,6-dione].* Sodium sulfate was slowly added to a mixture of t-butyl alcohol (100 ml) and 30% HOOH (25 ml) until the solution became biphasic. The upper alcohol layer was removed and dried successively with $MgSO_4$ and $CaSO_4$. To a solution of vinyl-isopropylcyclohexylline **17** (0.152 g, 0.5 mmol) in the t-butyl alcohol/HOOH mixture (8 ml), 140 µl osmium tetroxide solution (2.5 wt % in t-butyl alcohol, 0.0035 g, 0.014 mmol) was added. The solution was stirred overnight at room temperature, followed by removal of the alcohol *in vacuo*. Semi-prep HPLC was used for purification (2.0 ml/min., 50/30/20 (H_2O/acetonitrile/methanol)), yielding pure title compound (10.6 mg, 6.3%): mp 190-191 °C; ^{1}H-NMR (300 MHz, $CDCl_3$): δ 3.95 (d, J = 7.1 Hz, 2H, N3-$C\underline{H_2}$), 3.93 (dd, J = 71.3, 11.3 Hz, 2H, C8-$(CH_3)(OH)C\underline{H_2}$), 3.42

(s, 3H, N1-C$\underline{H}_3$), 1.88-1.99 (br, 1H, N3-$CH_2C\underline{H}$), 1.60-1.78 (m, 10H), 1.00-1.25 (m, 6H); ESMS m/s 337 $[M + H]^+$ (100%), 319 $[(M + H)^+ - H_2O]$ (39%), 301 $[((M + H)^+ - H_2O) - H_2O]$ (1%).

Methylketone-cyclohexylline ***19*** *[3,7-Dihydro-8-acetyl-1-methyl-3-(cyclohexylmethyl)-1H-purine-2,6-dione].* This compound was synthesized by chromic acid oxidation of 8′-OH-ethylcyclohexylline (*90*), following a procedure from Vogel's Textbook of Practical Organic Chemistry (*115*). A portion of the product was purified via semi-prep HPLC (2 ml/min., 40/35/25 (H_2O/ acetonitrile/ methanol)); ^{1}H-NMR (300 MHz, $CDCl_3$): δ 4.00 (d, J = 7.1 Hz, 2H, N3-C$\underline{H}_2$), 3.47 (s, 3H, N1-C$\underline{H}_3$), 2.70 (s, 3H, C8-(C=O)C$\underline{H}_3$), 1.93-2.04 (br, 1H, N3-$CH_2C\underline{H}$), 1.60-1.77 (m, 10H), 1.06-1.27 (m, 8H); ESMS m/z 305 $[M + H]^+$.

N^7-Methylxanthines. The procedure for N^7-methylation of all xanthines studied is as described in (*89*), except D_1-isopropylcyclohexylline **4**, in which [^{13}C]iodomethane was use in place of unlabeled iodomethane.

N^7-Methyl-isopropylcyclohexylline ***20.*** Semi-prep HPLC purification (2 ml/min., 20/35/45 (H_2O/ acetonitrile/ methanol)); ^{1}H-NMR (300 MHz, $CDCl_3$): δ 3.94 (d, J = 7.3 Hz, 2H, N3-C$\underline{H}_2$), 3.91 (s, 3H, N7-C$\underline{H}_3$), 3.39 (s, 3H, N1-C$\underline{H}_3$), 3.05 (m, 1H, C8-C$\underline{H}$), 1.88-2.01 (br, 1H, N3-$CH_2C\underline{H}$), 1.58-1.73 (m, 7H), 1.33 (d, J = 6.9 Hz, 6H, C8-CH(C$\underline{H}_3$)$_2$, 1.03-1.29 (m, 5H); ESMS m/z 319 $[M + H]^+$.

N^7-Methyl-D_6-isopropylcyclohexylline ***21.*** Semi-prep HPLC purification (2 ml/min, 20/35/45 (H_2O/ acetonitrile/ methanol)); ^{1}H-NMR (300 MHz, $CDCl_3$): δ 3.95 (d, J = 7.3 Hz, 2H, N3-C$\underline{H}_2$), 3.92 (s, 3H, N7-C$\underline{H}_3$), 3.39 (s, 3H, N1-C$\underline{H}_3$), 3.01 (s, 1H, C8-C$\underline{H}$),

1.90-2.03 (br, 1H, N3-$CH_2C\underline{H}$), 1.50-1.74 (m, 12H), 1.02-1.29 (m, 13H); ESMS m/z 325 $[M + H]^+$.

N^7-(^{13}C-Methyl)-D_1-isopropylcyclohexylline ***22.*** This compound was prepared from D_1-isopropylcyclohexylline **4** using the general procedure as described in (*89*), except [^{13}C]iodomethane was use in place of unlabeled iodomethane. Semi-prep HPLC purification (2 ml/min, 20/35/45 (H_2O/ acetonitrile/ methanol)); ^{1}H-NMR (300 MHz, $CDCl_3$): 3.94 (d, J = 7.3 Hz, 2H, N3-$C\underline{H}_2$), 3.91 (d, J = 141.1 Hz, N7-$^{13}C\underline{H}_3$), 3.39 (s, 3H, N1-$C\underline{H}_3$), 1.90-2.02 (br, 1H, N3-$CH_2C\underline{H}$), 1.58-1.73 (m, 5H), 1.2 (s, 6H, C8-C(D)($C\underline{H}_3$)$_2$), 1.04-1.27 (m, 5H); ESMS m/z 321 $[M + H]^+$.

N^7-Methyl-(S)-$^{13}CD_3$-isopropylcyclohexylline (also called N-methyl-pro-R-$^{13}CD_3$-isopropylcyclohexylline) ***23.*** Semi-prep HPLC purification (2 ml/min, 20/35/45 (H_2O/ acetonitrile/ methanol)); ^{1}H-NMR (300 MHz, $^2H_6$-Acetone): δ 3.97 (s, 3H, N7-$C\underline{H}_3$), 3.92 (d, J = 7.3 Hz, 2H, N3-$C\underline{H}_2$), 3.30 (s, 3H, N1-$C\underline{H}_3$), 3.24 (m, 1H, C8-C$\underline{H}$), 1.94 (br, 1H, N3-$CH_2C\underline{H}$), 1.60-1.77 (m, 5H), 1.33 (dd, J = 5.2, 6.9 Hz, 3H, C8-C(H)($^{13}C^2H_3$)$C\underline{H}_3$, 1.00-1.26 (m, 5H); ESMS m/z 323 $[M + H]^+$.

N^7-Methyl-(S)-^{13}C-isopropylcyclohexylline (also called N-methyl-pro-R-^{13}C-isopropylcyclohexylline) ***24.*** Semi-prep HPLC purification (2 ml/min, 20/35/45 (H_2O/ acetonitrile/ methanol)); ^{1}H-NMR (300 MHz, $CDCl_3$): 3.94 (d, J = 7.8 Hz, 2H, N3-$C\underline{H}_2$), 3.91 (s, 3H, N7-$C\underline{H}_3$), 3.39 (s, 3H, N1-$C\underline{H}_3$), 3.05 (m, 1H, C8-C$\underline{H}$), 1.94 (br, 1H, N3-$CH_2C\underline{H}$), 1.52-1.75 (m, 10H), 1.33 (dd, J = 6.7, 5.2 Hz, 3H, C8-C(H)($^{13}CH_3$)$C\underline{H}_3$, 0.99-1.28 (m, 10H); ESMS m/z 320 $[M + H]^+$.

N^7-Methyl-(S)-D_3-isopropylcyclohexylline (also called N-methyl-pro-S-D_3-isopropylcyclohexylline) ***25.*** Semi-prep HPLC purification (2 ml/min, 20/35/45 (H_2O/

acetonitrile/ methanol)); ^{1}H-NMR (300 MHz, $^2H_6$-Acetone): 3.93 (s, 3H, N7-C$\underline{H}_3$), δ 3.90 (d, J = 7.3 Hz, 2H, N3-C$\underline{H}_2$), 3.27 (s, 3H, N1-C$\underline{H}_3$), 3.21 (q, J = 6.9 Hz, 1H, C8-C$\underline{H}$), 1.89-2.03 (br, 1H, N3-$CH_2C\underline{H}$), 1.59-1.75 (m, 6H), 1.30 (d, J = 6.8 Hz, 3H, C8-C(H)(C^2H_3)C$\underline{H}_3$, 0.98-1.27 (m, 7H); ESMS m/z 322 $[M + H]^+$.

N^7-Methyl-8′-OH-isopropylcyclohexylline ***26.*** Semi-prep HPLC purification (2.5 ml/min, 27.5/37.5/35 (H_2O/ acetonitrile/ methanol)); ^{1}H-NMR (300 MHz, $CDCl_3$): δ 4.17 (s, 3H, N7-C$\underline{H}_3$), 3.91 (d, J = 7.2 Hz, 2H, N3-C$\underline{H}_2$), 3.40 (s, 3H, N1-C$\underline{H}_3$), 1.85-2.00 (br, 3H, N3-$CH_2C\underline{H}$), 1.59-1.76 (m, 17H), 1.00-1.27 (m, 13H); ESMS m/z 335 $[M + H]^+$ (100%), 317 $[(M + H)^+ - H_2O]$ (64%).

N^7-Methyl-8″-OH-isopropylcyclohexylline ***27.*** Semi-prep HPLC purification (2.5 ml/min, 37.5/35/27.5 (H_2O/ acetonitrile/ methanol)); ^{1}H-NMR (300 MHz, $CDCl_3$): δ 3.98 (dd, J = 7.3, ≈10 Hz, 2H, C8-C(H)(CH_3)C$\underline{H}_2$), 3.93 (s, 3H, N7-C$\underline{H}_3$), 3.90 (d, J = 7.2 Hz, 2H, N3-C$\underline{H}_2$), 3.39 (s, 3H, N1-C$\underline{H}_3$), 3.05-3.13 (m, 1H, C8-C$\underline{H}$), 1.85-1.96 (br, 1H, N3-$CH_2C\underline{H}$), 1.6-1.75 (m, 9H), 1.32 (d, 7.2 Hz, 3H, C8-C(H)(CH_2OH)C$\underline{H}_3$), 1.00-1.30 (m, 18H); ESMS m/z 335 $[M + H]^+$.

N^7-Methyl-vinyl-isopropylcyclohexylline ***28.*** Semi-prep HPLC purification (2 ml/min, 15/35/50 (H_2O/ acetonitrile/ methanol)); ^{1}H-NMR (300 MHz, $CDCl_3$): δ 5.60 (m, J = 1.6 Hz, 1H), 5.38 (m, J = 1 Hz, 1H), 4.00 (s, 3H, N7-C$\underline{H}_3$), 3.93 (d, J = 7.3 Hz, 2H, N3-C$\underline{H}_2$), 3.39 (s, 3H, N1-C$\underline{H}_3$), 2.18 (m, 3H, C8-C(CH_2)C$\underline{H}_3$), 1.91-1.98 (br, 1H, N3-$CH_2C\underline{H}$), 1.57-1.73 (m, 8H), 0.98-1.25 (m, 8H); ESMS m/z 317 $[M + H]^+$.

N^7-Methyl-diol-isopropylcyclohexylline ***29.*** Semi-prep HPLC purification (2 ml/min, 40/30/30 (H_2O/ acetonitrile/ methanol)); ^{1}H-NMR (300 MHz, $^2H_6$-Acetone): δ 4.24 (s,

3H, N7-C$\underline{H}_3$), 3.91 (d, J = 7.2 Hz, 2H, N3-C$\underline{H}_2$), 3.85 (m, 2H, C8-(CH_3)(OH)C$\underline{H}_2$), 3.31 (s, 3H, N1-C$\underline{H}_3$), 1.90-2.02 (br, 1H, N3-CH_2C$\underline{H}$), 1.62-1.80 (m, 10H), 1.03-1.33 (m, 6H); ESMS m/s 351 $[M + H]^+$ (100%), 333 $[(M + H)^+ - H_2O]$ (42%), 319 $[((M + H)^+ - H_2O) - H_2O]$ (1%).

Cyclopropylmethylcyclohexylline ***30*** *[3,7-Dihydro-8-cyclopropylmethyl-1-methyl-3-(cyclohexylmethyl)-1H-purine-2,6-dione].* 5,6-Diamino-1-cyclohexylmethyl-3-methyl uracil **1** (0.05 g, 0.2 mmol) and cyclopropyl acetic acid (0.163 g, 1.6 mmol) were mixed for 2 hours at 130 °C. Aqueous NaOH (10%, 5 ml) was added, and the solution was boiled for an additional 1 hour. The pH was neutralized with concentrated HCl, and the product extracted with ethyl acetate (3 x 7.5 ml) and chloroform (3 x 7.5 ml). The combined extracts were dried over magnesium sulfate, filtered, and the solvent removed *in vacuo*. The product was recrystallized twice in acetone (0.005 g, 8%). ^{1}H-NMR (500 MHz, $CDCl_3$): δ 3.97 (dd, J = 7.4 Hz, 2H, N3-C$\underline{H}_2$), 3.42 (s, 3H, N1-C$\underline{H}_3$), 2.79 (d, J = 7.7 Hz, 2H, C8-C$\underline{H}_2$), 1.95 (m, 1H, N3-CH_2C$\underline{H}$), 1.6-1.8 (m, 7H), 1.05-1.25 (m, 9H), 0.61 (m, 2H), 0.32 (dd, J = 4.9, 10.4 Hz, 2H); ESMS *m/z* 317 $[M + H]^+$ (100%), 221 $[(M + H)^+ - C_7H_{12}]^+$ (5%).

8'-OH-Cyclopropylmethylcyclohexylline ***31*** *[3,7-Dihydro-8-(cyclopropyl-hydroxy-methyl)-1-methyl-3-(cyclohexylmethyl)-1H-purine-2,6-dione].*

Cyclopropane glycolic acid ***32***. Following (*116, 117*) (Figure 2.2), cyclopropylmethyl ketone (12.5 g, 150 mol) was added dropwise to a cold slurry of sodium amide (12 g, 300 mol) in diethyl ether (150 ml). This mixture was gently

refluxed for 0.5 hour, cooled in an ice bath, and diethyl carbonate (36 g, 300 mmol) was added dropwise. This mixture was then gently refluxed for 3 hours, cooled in an ice bath, and ethanol (100 ml) was added to quench remaining sodium amide. The solution was added to ice (250 g), acidified with concentrated HCl, and the organic layer extracted with diethyl ether (3 x 400 ml). The ether extracts were pooled, evaporated to a volume of 750 ml, and washed with water (750 ml), dilute sodium carbonate (750 ml), and again with water (750 ml). The ether layer was then dried over magnesium sulfate, filtered, and the solvent removed. The product was vacuum distilled to give the colorless liquid ethyl cyclopropane-3-oxo propionate **33** (11.8 g, 76 mmol, 51%). This product (4.16 g, 27 mmol), selenium dioxide (3 g, 27 mmol), and dioxane (50 ml) were combined and refluxed for 2.5 hours. After cooling to room temperature, the solution was filtered through a 0.5" bed of alumina, and the product eluted with methylene chloride and ethyl acetate. The solvents were removed *in vacuo* and the product distilled, yielding the yellow liquid ethyl cyclopropane-2,3-dioxo propionate **34** (2.3 g, 13.6 mmol, 51%). To this product, 2 N aqueous NaOH (75 ml) was added dropwise with cooling to keep the solution at approximately room temperature. After 4 hours at room temperature, it was cooled in an ice bath, acidified (pH = 2) with concentrated HCl, saturated with NaCl, and extracted with diethyl ether (3 x 100 ml). The ether extracts were combined and evaporated to give the crystalline solid cyclopropyl tartronic acid **35** (1.72 g, 10.7 mmol, 78.7 %). A mixture of this product (0.750 g, 4.7 mmol), concentrated HCl (15 ml), and barium hydroxide (5 g, 26.4 mmol) was heated to 70 °C for 5 hours, cooled to room temperature, diluted with water (25 ml), saturated with NaCl, and extracted with diethyl

ether (3 x 50 ml). The ether extracts were combined, and the ether evaporated leaving a yellow crystalline solid cyclopropane glycolic acid **32** (0.69 g, 6 mmol, >100%).

*8′-OH-Cyclopropylmethylcyclohexylline **31**.* 5,6-Diamino-1-cyclohexylmethyl-3-methyl uracil **1** (0.05 g, 0.2 mmol) and cyclopropane glycolic acid **32** (0.3 g, 2.6 mmol) were mixed in pyridine (1 ml) and a catalytic amount of concentrated H_2SO_4 for 1 hour at 120 °C. The pyridine was evaporated, 10% aqueous NaOH (5 ml) added, and the solution was boiled for an additional 1 hour. The pH was neutralized with concentrated HCl, and the product extracted with ethyl acetate (3 x 7.5 ml) and chloroform (3 x 7.5 ml). The combined extracts were dried over magnesium sulfate, filtered, and the solvent removed *in vacuo* to give the crude title compound. A portion of this product was purified via semi-prep HPLC (2.5 ml/min., 37.5/27.5/35 (H_2O/acetonitrile/methanol)). ^{1}H-NMR (500 MHz, $CDCl_3$): δ 4.46 (d, J = 7.4 Hz, 1H, C8-C<u>H</u>), 3.96 (ddd, J = 13, 7.4, 7.4 Hz, 2H, N3-C<u>H</u>$_2$), 3.69 (br, 1H, C8-C(H)-O<u>H</u>), 3.43 (s, 3H, N1-C<u>H</u>$_3$), 1.95 (m, 1H, N3-CH$_2$C<u>H</u>), 1.71-1.56 (m, 9H), 1.35-1.29 (m, 1H, C8-C(OH)(H)-C<u>H</u>), 1.26-1.03 (m, 6H), 0.54-0.67 (m, 4H, C8-C(OH)(H)(CH)-(C<u>H</u>$_2$)$_2$); ESMS *m/z* 333 $[M + H]^+$ (83%), 315 $[(M + H)^+ - H_2O]$ (100%), 219 $[((M + H)^+ - H_2O) - C_7H_{12}]^+$ (96%).

*Trans-butenol-cyclohexylline **36** [3,7-Dihydro-8-[(1E)-4-hydroxy-but-1-enyl]-1-methyl-3-(cyclohexylmethyl)-1H-purine-2,6-dione].* 8′-OH-Cyclopropylmethylcyclohexylline **31** (5 mg) was heated at 100 °C in 10% aqueous sulfuric acid for 12 hours. The products of this reaction (trans isomer **36**, unrearranged 8′-OH-cyclopropylmethylcyclohexylline **31**, and cis isomer **37**) were separated and purified by semi-prep HPLC (2.0 ml/min.,

45/20/35 (H_2O/acetonitrile/methanol), Rt = 18.3, 19.8, and 20.7 min, respectively); ^{1}H-NMR (500 MHz, $CDCl_3$): δ 6.95 (dt, *J* = 16.1, 7.4 Hz, 1H, C8-CH=C<u>H</u>), 6.48 (dt, *J* = 16.1, 1.2-1.9 Hz, 1H, C8-C<u>H</u>), 3.92 (d, *J* = 7.4 Hz, 2H, N3-C<u>H</u>$_2$), 3.72 (t, *J* = 6.5 Hz, 2H, C8-CH=CHCH$_2$C<u>H</u>$_2$), 3.29 (s, 3H, N1-C<u>H</u>$_3$), 2.50 (qd, J = 6.8, 1.2-1.9 Hz, 2H, C8-CH=CHC<u>H</u>$_2$), 1.91-2.05 (br, 1H, N3-CH$_2$C<u>H</u>), 1.56-1.74 (m, 5H), 1.04-1.24 (m, 6H); ESMS m/z 333 $[M + H]^+$ (100%), 237 $[(M + H)^+ - C_7H_{12}]^+$ (9%).

Cis-butenol-cyclohexylline 37 [3,7-Dihydro-8-[(1Z)-4-hydroxy-but-1-enyl]-1-methyl-3-(cyclohexylmethyl)-1H-purine-2,6-dione]. This product was generated in the same reaction as above; ^{1}H-NMR (500 MHz, $CDCl_3$): δ 6.46 (dt, *J* = 11.1, 1.2-1.9 Hz, 1H, C8-C<u>H</u>), 6.25 (dt, *J* = 11.7, 8 Hz, 1H, C8-CH=C<u>H</u>), 3.93 (d, *J* = 6.8 Hz, 2H, N3-C<u>H</u>$_2$), 3.79 (t, *J* = 6.2 Hz, 2H, C8-CH=CHCH$_2$C<u>H</u>$_2$), 2.97 (dtd, *J* = 7.4, 6.2, 1.2-1.9 Hz, 2H, C8-CH=CHC<u>H</u>$_2$), 1.63-1.73 (m, 5H), 1.07-1.23 (m, 6H); ESMS m/z 333 $[M + H]^+$ (100%), 315 $[(M + H)^+ - H_2O]$ (18%), 237 $[(M + H)^+ - C_7H_{12}]^+$ (3%), 219 $[((M + H)^+ - H_2O) - C_7H_{12}]^+$ (19%).

Cyclobutylcyclohexylline 38 [3,7-Dihydro-8-cyclobutyl-1-methyl-3-(cyclohexylmethyl)-1H-purine-2,6-dione]. 5,6-diamino-1-cyclohexylmethyl-3-methyl uracil **1** (0.05 g, 0.2 mmol) and cyclobutane carboxylic acid (0.314 g, 3.1 mmol) were mixed for 2 hours at 130 °C. 10% aqueous NaOH (5 ml) added, and the solution was boiled for an additional 1 hour. The pH was neutralized with concentrated HCl, and the product extracted with ethyl acetate (3 x 7.5 ml) and chloroform (3 x 7.5 ml). The combined extracts were dried over magnesium sulfate, filtered, and the solvent removed *en vacuo*. The product was

recrystallized twice in acetone (0.009 g, 14%). ^{1}H-NMR (500 MHz, $CDCl_3$): δ 3.97 (dd, J = 7.4 Hz, 2H, N3-C$\underline{H}_2$), 3.71 (m, 1H, C8-C$\underline{H}$), 3.46 (s, 3H, N1-C$\underline{H}_3$), 2.37-2.54 (m, 4H, C8-CH(C$\underline{H}_2$)$_2$), 2.03-2.16 (m, 1H), 1.93-2.02 (m, 2H), 1.64-1.74 (m, 9H), 1.04-1.27 (m, 6H); ESMS *m/z* 317 $[M + H]^+$ (100%).

8'-OH-Cyclobutylcyclohexylline ***39*** *[3,7-Dihydro-8-(1-hydroxy-cyclobutyl)-1-methyl-3-(cyclohexylmethyl)-1H-purine-2,6-dione].*

1-hydroxy-cyclobutane carboxylic acid. Following (*118*), sodium bisulfite (0.720 g, 6.9 mmol) dissolved in water (1 ml) was added drop wise to a mixture of cyclobutanone (0.450 g, 6.42 mmol), potassium cyanide (0.442 g, 6.79 mmol), and water (1.12 ml), while maintaining approximately room temperature with a cold water bath. The reaction was stirred overnight, yielding two phases. The organic layer was extracted with diethyl ether (3 x 7.5 ml) and chloroform (3 x 7.5 ml). The combined extracts were dried over magnesium sulfate, filtered, and the solvent evaporated to give 0.715 g (7.4 mmol, >100%) crude 1-hydroxy-cyclobutane carbonitrile. This yellow oil product was mixed with concentrated HCl (7.5 ml) and heated at 120 °C for 6 hours. The HCl was removed *en vacuo*, and the black oil residue was triturated in pet ether (3 x 10 ml) with heating. The pet ether portions were combined and the solvent evaporated, yielding crude 1-hydroxy-cyclobutanone (0.285 g, 2.45 mmol, 38%).

8'-OH-Cyclobutylcyclohexylline ***39.*** 5,6-diamino-1-cyclohexylmethyl-3-methyl uracil **1** (0.05 g, 0.2 mmol) and 1-hydroxy-cyclobutane carboxylic acid (0.124 g, 1.1 mmol) were mixed with stirring and heated at 120 °C for 1 hour. After adding 10%

aqueous NaOH (5 ml), the solution was boiled for an additional 1 hour. The pH was neutralized with concentrated HCl, and the product extracted with ethyl acetate (3 x 7.5 ml) and chloroform (3 x 7.5 ml). The combined extracts were dried over magnesium sulfate, filtered, and the solvent removed *en vacuo* to give 0.085 g (2.6 mmol, >100%) crude title compound. A portion of this product was purified via semi-prep HPLC (2 ml/min., 10/25/65 H_2O/ acetonitrile/ methanol); ^{1}H-NMR (500 MHz, $CDCl_3$): δ 4.52 (br, 1H, C8-CO<u>H</u>), 4.00 (d, *J* = 7.4 Hz, 2H, N3-C<u>H</u>$_2$), 3.45 (s, 3H, N1-C<u>H</u>$_3$), 2.73 (m, 2H), 2.45 (m, 2H), 2.13 (m, 1H), 2.07 (m, 1H), 1.97 (m, 1H, N3-CH$_2$C<u>H</u>), 1.59-1.73 (m, 11H), 1.08-1.25 (m, 6H); ESMS *m/z* 333 $[M + H]^+$ (100%), 315 $[(M + H)^+ - H_2O]$ (72%), 219 $[((M + H)^+ - H_2O) - C_7H_{12}]^+$ (25%).

<u>Metabolic Studies</u>

All incubations, unless otherwise noted, contained 0.375 μM CYP1A2 (human lymphoblastoid CYP1A2 microsomes) in 200 μl total volume. Standard incubation buffer was 100 mM potassium phosphate, 1mM EDTA, pH 7.4. Saturating xanthine substrate concentrations (60 μM) were preincubated with the CYP1A2 for 3 min at 37 °C, and the incubations initiated with the addition of NADPH (final concentration, 1.0 mM). Incubations were terminated at 30 min by the addition of 40 ul cold 40% aqueous trifluoroacetic acid (TFA). The samples were then centrifuged at 14000 RPM for 10 min in an Eppendorf 5415C centrifuge. The supernatants were analyzed by LC, ESLC-MS, or EIGC-MS.

$H_2{}^{18}O$ Incorporation Experiments

Incubations to determine incorporation of oxygen from the medium into the carbinol metabolites were conducted using the same incubation procedure as above, with the only difference being the concentration of potassium phosphate buffer and EDTA, due to the addition of 20% - 40% (v/v) $H_2{}^{18}O$. Calculations were performed following the procedure of Racha, *et al.* (*89*), with full propagation of error.

$^{18}O_2$ Incorporation Experiments

Incubations of isopropylcyclohexylline in the presence of $^{18}O_2$ were conducted following the procedure of Racha, *et al.* (*89*). $^{18}O_2$ content of carbinols was standardized to that calculated for cyclohexyl-ring hydroxylation products, which are expected to contain 100% molecular oxygen, via the P450 oxygen-rebound mechanism.

Stereoselectively Labeled Substrates and Prochiral Oxidation

Stereoselectively labeled isobutyric acids were synthesized following literature procedures (*110-114*). As shown in Figure 2.1, the stepwise synthesis for incorporation of a label into both enantiomeric positions uses the same chiral auxiliary starting material, (4S)-3-propionyl oxazolidinone. The orientation of label incorporation is dependent upon the point at which it is inserted into the sequence of steps.

Also shown in Figure 2.1 is the interesting nomenclature problem associated with generation of one stereoselectively labeled acid containing $^{13}CD_3$, while the other has $^{12}CD_3$. As a result of the different isotopic composition of the incorporated labels, both acids and their corresponding isopropylcyclohexylline products have the same (S)

stereochemical designation (Cahn-Ingold-Prelog system of ranking substituents on an asymmetric carbon), even though they have different spatial orientations of the deuterated methyl group. This presents a major obstacle to coherent discussion of the deuterium isotope effects observed with these substrates. To compensate, the stereoselectively labeled substrates will be referred to by the prochiral position of label incorporation (i.e. (S)-$^{13}CD_3$-IPC **5** is pro-R-$^{13}CD_3$-IPC, (S)-^{13}C-IPC **9** is pro-R-^{13}C-IPC, and (S)-D_3-IPC **10** is pro-S-D_3-IPC). Figure 2.3 illustrates the nomenclature and relationship between the prochiral stereochemistry of labeling and the pro-stereochemistry of oxidation.

Prochiral Stereoselectivity Studies

Thorough investigation of intramolecular deuterium isotope effects on the metabolism of a prochiral substrate necessitates consideration of the enzyme's predisposition for oxidation of that substrate in either of two distinct diastereomeric orientations within the enzyme active site (*119*). The 8′-carbon of isopropylcyclohexylline **2** and N^7-methyl-isopropylcyclohexylline **20** is prochiral, and therefore any isotope effects observed with stereoselectively per-deuterated substrates will be a composite of both the isotope effect and a stereoselectivity factor. From this and drawing upon the methods of Sugiyama and Trager (*119*), we assessed the prochiral stereoselectivity ($^{R/S}P_S$) of CYP1A2-catalyzed oxidation of IPC **2** to vinyl-IPC **17** and of N-methy-IPC **20** to N-methyl-vinyl-IPC **28** by EIGC-MS analysis of incubations with the stereoselectively-^{13}C-labeled substrates (**9** and **24**, respectively).

The electron impact mass spectrum of the bis-trimethylsilyl derivative of N-methyl-diol-isopropylcyclohexylline **29** is shown in Figure 2.4. The predominant

fragment is due to the loss of -CH_2-O-TMS to generate the ion at m/z 391. Because the diol is a secondary oxidation product derived from the vinyl metabolite, this fragmentation process, in conjunction with stereoselectively labeled ^{13}C-substrate, provides a convenient means to determine the prochiral stereoselectivity involved in CYP1A2 desaturation of N-methyl-IPC **20** and IPC **2** to their respective vinyl metabolites (**24** and **9**). As shown in Figure 2.5, the relative abundance of the ions at m/z 391 and m/z 392 in the electron impact mass spectrum of the diol formed from pro-R-^{13}C-isopropylcyclohexylline **9** and N^7-methyl-pro-R-^{13}C-isopropylcyclohexylline **24** provides a measure of olefin formation via oxidation of the pro-R-methyl and the pro-S-methyl group, respectively.

Following (*119*), the method for determining the prochiral stereoselectivity of IPC **2** and N-methyl-IPC **20** oxidation by CYP1A2 is shown in figure 2.6. $^{R/S}P_S$ is defined as the ratio of products obtained from oxidation of the pro-R methyl group vs. the pro-S methyl group; however, because the ^{13}C-labeled substrates are not enantiomerically pure, the measured m/z 392/391 ion ratios must be corrected for the products formed from the contaminating enantiomer. Figure 2.6 shows that the ratio of ions at m/z 392 and 391 is equal to:

$$\frac{392}{391} = \frac{b+c}{a+d} = \frac{F_{1-x}\alpha + F_x(1-\alpha)}{F_x\alpha + F_{1-x}(1-\alpha)}$$

Where F_x is the fraction of products from oxidation of the pro-R methyl group, F_{1-x} is the fraction of products from oxidation of the pro-S methyl group, and α is the fraction pro-R-^{13}C-label incorporation in the substrate (α = 0.9). Because $^{R/S}P_S$ equals F_x/F_{1-x}, dividing the top and bottom by F_{1-x} gives:

$$\frac{392}{391} = \frac{\alpha + {}^{R/S}P_S(1-\alpha)}{{}^{R/S}P_S\alpha + (1-\alpha)}$$

Simplifying this equation for $^{R/S}P_S$ gives,

$${}^{R/S}P_S = \frac{\alpha + {}^{392}/_{391} * \alpha - {}^{392}/_{391}}{{}^{392}/_{391} * \alpha + \alpha - 1}$$

Observed 392/391 ion ratios were manually corrected for natural isotope contribution, determined from unlabeled diol metabolite standard, before using in this formula. The contaminating 1% of unlabeled substrate is not considered in this analysis. All calculations were performed with full propagation of error.

Incubations of pro-R-^{13}C-IPC **9** and N-methyl-pro-R-^{13}C-IPC **24** with CYP1A2 were analyzed by EIGC-MS. Because the N-methyl-diol metabolite generated in incubations with the N-methyl substrate could not be efficiently extracted, all incubations were terminated with cold 40% aqueous TFA, centrifuged, and the supernatants evaporated at room temperature with a stream of nitrogen. To distinguish between N-desmethyl- and N-methyl-diol, incubation residues from N-methyl-pro-R-^{13}C-IPC **24** incubations were treated with n-propyl iodide overnight (*89*), whereby the N-desmethyl metabolites were converted to N-propyl compounds. In contrast, pro-(R)-^{13}C-IPC **9** incubations were derivatized with methyl iodide. In this way, the analyte of interest from incubations with either substrate is N-methyl-diol-IPC. After derivatization the solutions were filtered and evaporated with a stream of nitrogen. The residues were treated with 50 μL of 20% (v/v) BSTFA in acetonitrile at room temperature for 1 h prior to analysis.

Isotope Effect Studies

Intermolecular. Competitive intermolecular deuterium isotope effects ($^{D}V/K$) on N-methyl-IPC and IPC metabolite formation were determined by ESLC-MS-SIM analysis of incubations with 1:1 mixtures of deuterated and unlabeled substrate. Ratios of integrated peak areas of the ions indicative of metabolites derived from deutero- vs. protio-substrate were corrected for incomplete deuteration of the substrate and for natural isotope contribution, determined from authentic standards or from separate incubations with non-deuterated substrate.

Intramolecular. Intramolecular deuterium isotope effects (^{D}V) were determined from ESLC-MS-SIM analysis of incubations with pro-R-$^{13}CD_3$- or pro-S-D_3-labeled isopropylcyclohexylline (**5** and **10**, respectively) and N^7-methyl-isopropylcyclohexylline (**23** and **25**, respectively). The observed D_3/D_2 metabolite ion peak area ratios were manually corrected for natural isotope contribution and incomplete deuteration of the substrates. Following the procedure of Sugiyama and Trager (*119*), figures 2.7 and 2.8 illustrate the method for calculating the expected isotope effect for oxidation of a particular prochiral methyl group ($^{D}V_{exp,pro\text{-}R}$ and $^{D}V_{exp,pro\text{-}S}$, respectively) from the observed D_3/D_2 ratio by correcting for the stereoselectivity of label incorporation and for the equilibrium between catalytically susceptible pro-R or pro-S methyl group orientation. All calculations were made with full propagation of error.

Carbocation Detection Studies

Incubations of CYP1A2 with cyclopropylmethylcyclohexylline **30** (with and without $H_2{}^{18}O$ (40% v/v)) and cyclobutylcyclohexylline **38** were terminated at 30 min by the addition of and extraction with ethyl acetate (3 x 1 ml). The extracts were pooled, dried with magnesium sulfate, filtered, and the ethyl acetate evaporated under a stream of nitrogen at room temperature. The extraction residue was brought back up in 50 µl methanol for HPLC and ESLC-MS analysis.

Solvolysis of synthetic 8′-OH-CPMC **31** was performed by incubation in 10% H_2SO_4 at 100 °C for 12 hours. Products generated by this method were purified by semi-prep HPLC and characterized by ESLC-MS and NMR (see synthesis section of Materials and Methods for details).

Sequential Metabolism Studies

Parallel incubations (400 ul) of Gentest lymphoblast expressed human CYP1A2 (40 pmole, 0.36 mg protein) and Gentest CYP1A2 Supersomes (10 pmole, 0.046 mg protein) with ^{15}N-IPC (100 µM), ^{15}N-IPC + vinyl-IPC **17**, and ^{15}N-IPC + diol-IPC **18** were performed (see Table 2.1). P450 activities in incubations with the two different enzyme sources were normalized to a rough approximation. Vinyl **17** and diol **18** concentrations in co-incubations with ^{15}N-IPC were meant to meet or exceed total concentrations of those metabolites produced over the course of normal 30 min incubations. Aliquots (200 µl) were removed at 5 and 30 min, killed by the addition of 40 ul cold 40% aqueous trifluoroacetic acid (TFA), centrifuged, and analyzed by ESLC-

MS-SIM. An external standard curve was used to quantify labeled and unlabeled metabolites from their integrated ion peak areas. Correction for natural isotope contribution to ^{15}N-metabolite peak areas from corresponding unlabeled metabolites was performed manually using experimentally determined natural isotope abundance values from the standard curve.

K_m and k_{cat} Determinations

The K_m and k_{cat} determinations for IPC **2**, vinyl-IPC **17**, and diol-IPC **18** metabolism by both Gentest lymphoblast expressed human CYP1A2 (40 pmole, 0.36 mg protein) and Gentest CYP1A2 Supersomes (10 pmole, 0.046 mg protein) were performed by incubation (400 μl) of each 'substrate' separately. Standard incubation procedures were used except that IPC **2** and vinyl-IPC **17** incubations were only 5 min to minimize substrate depletion, while diol-IPC **18** incubations were 30 min due to low turnover.

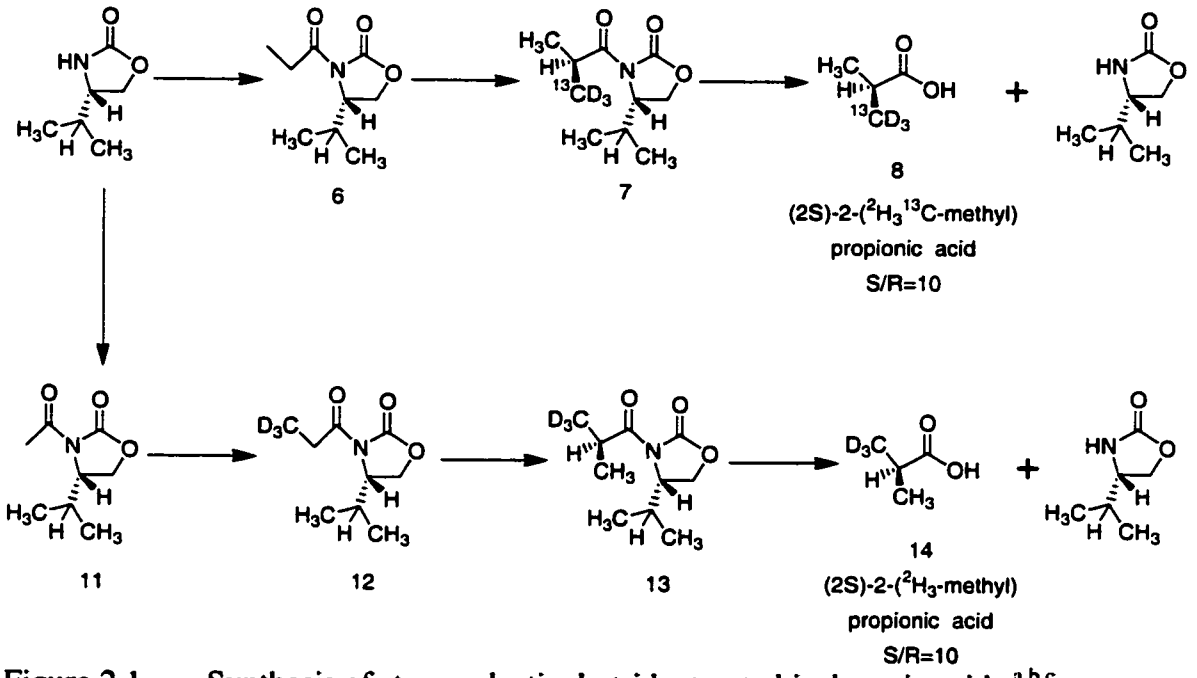

Figure 2.1 Synthesis of stereoselectively trideuterated isobutyric acids.[a,b,c]

[a] Conditions and reagents for each step are given in the synthesis section of Materials and Methods.
[b] Methylpropionic acid is also known as isobutyric acid.
[c] Figure shown is adapted from (*112*).

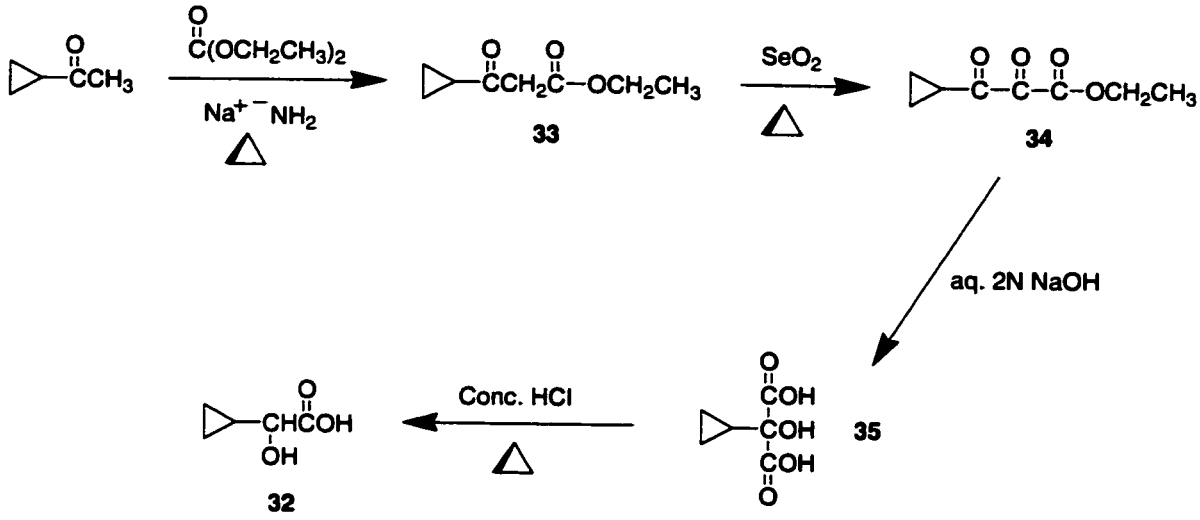

Figure 2.2 Synthesis of cyclopropane glycolic acid **32**.

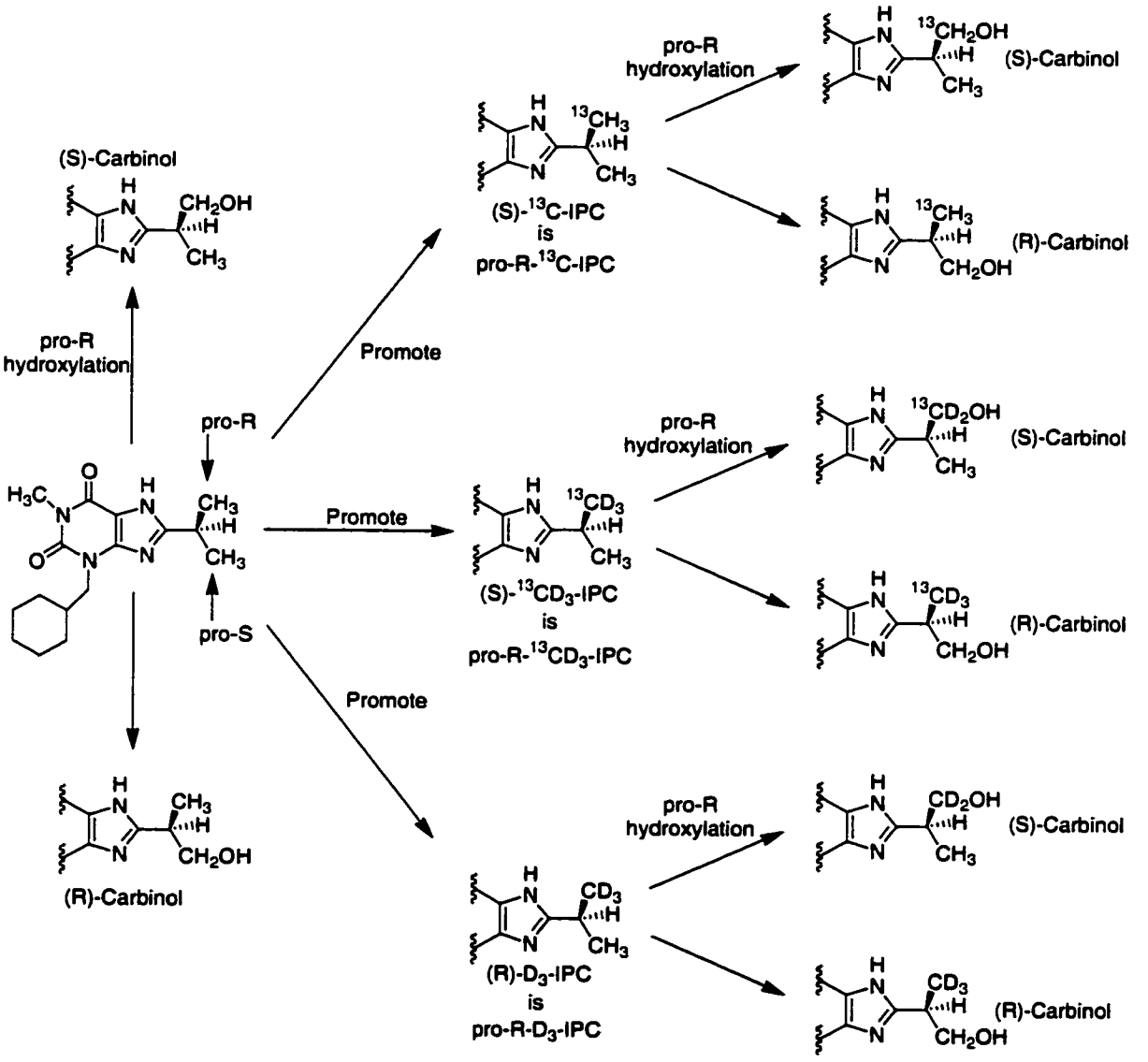

Figure 2.3 Absolute stereochemistry and pro-stereochemistry of isopropylcyclohexylline substrates. The unlabeled isopropyl group contains pro-R and pro-S methyl groups. Promotion of one methyl group in stereochemical priority by isotopic substitution or hydroxylation results in a chiral compound that has a known stereochemical designation (eg. (S)-^{13}CD$_3$-IPC), while being labeled in a particular prochiral position in reference to the original unlabeled substrate (i.e. (S)-^{13}CD$_3$-IPC is labeled in the pro-R position). In the end, regardless of the stereochemistry of label incorporation, pro-R- and pro-S-hydroxylation always results in (S)- and (R)-carbinol formation, respectively.

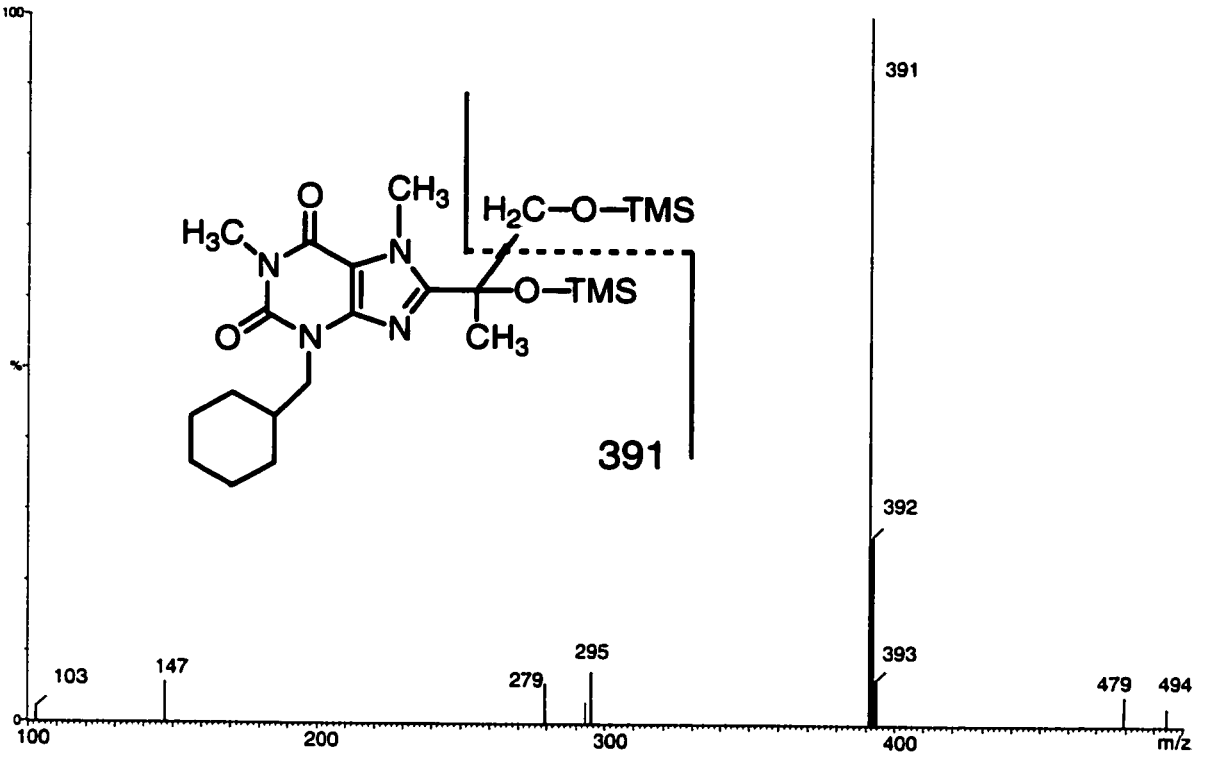

Figure 2.4 Electron impact mass spectrum of the bis-trimethylsilyl derivative of N-methyl-diol-isopropylcyclohexylline **29**. The predominant fragment of the parent ion (m/z = 494) is the ion m/z 391 due to loss of $-CH_2$-O-TMS.

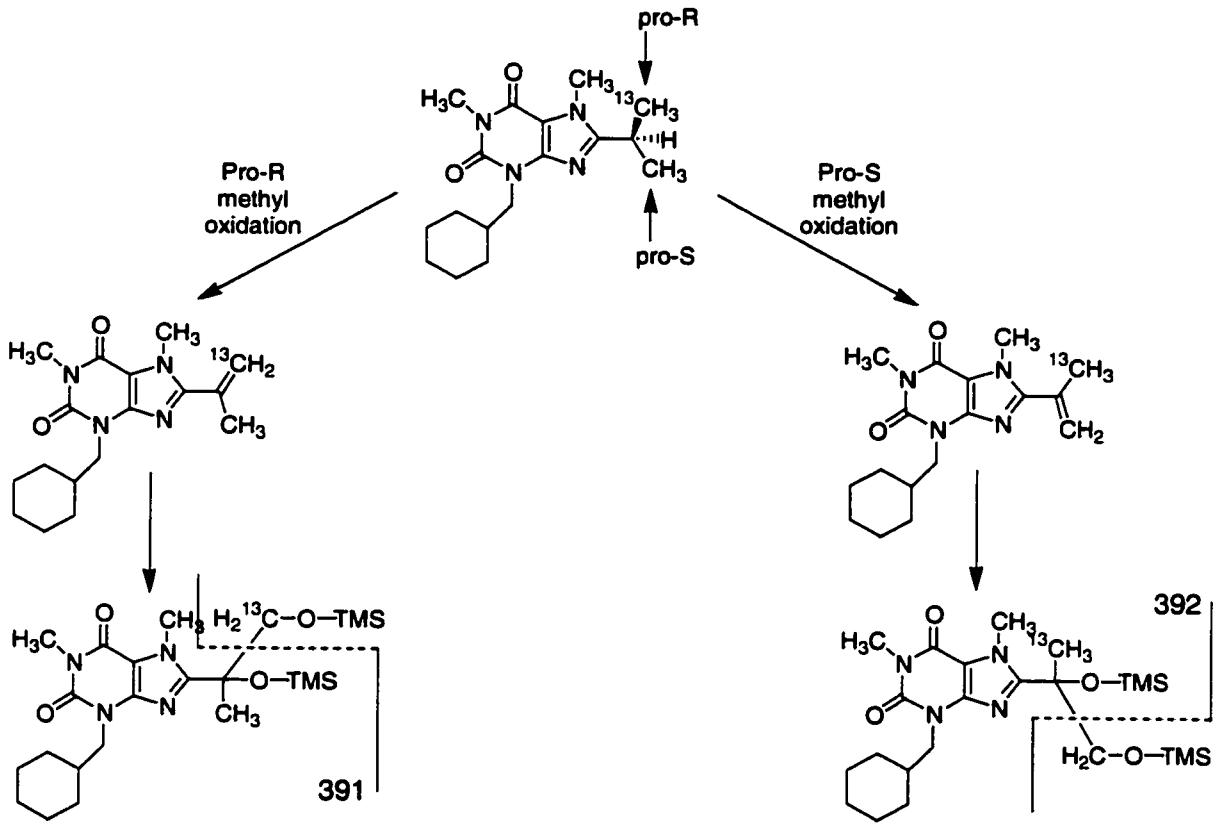

Figure 2.5 Fragmentation of N-methyl-diol-isopropylcyclohexylline arising from incubations with pro-R-^{13}C-IPC **9**. Pro-R-methyl group oxidation gives an ion at m/z 391, whereas pro-S-methyl group oxidation gives an ion at m/z 392.

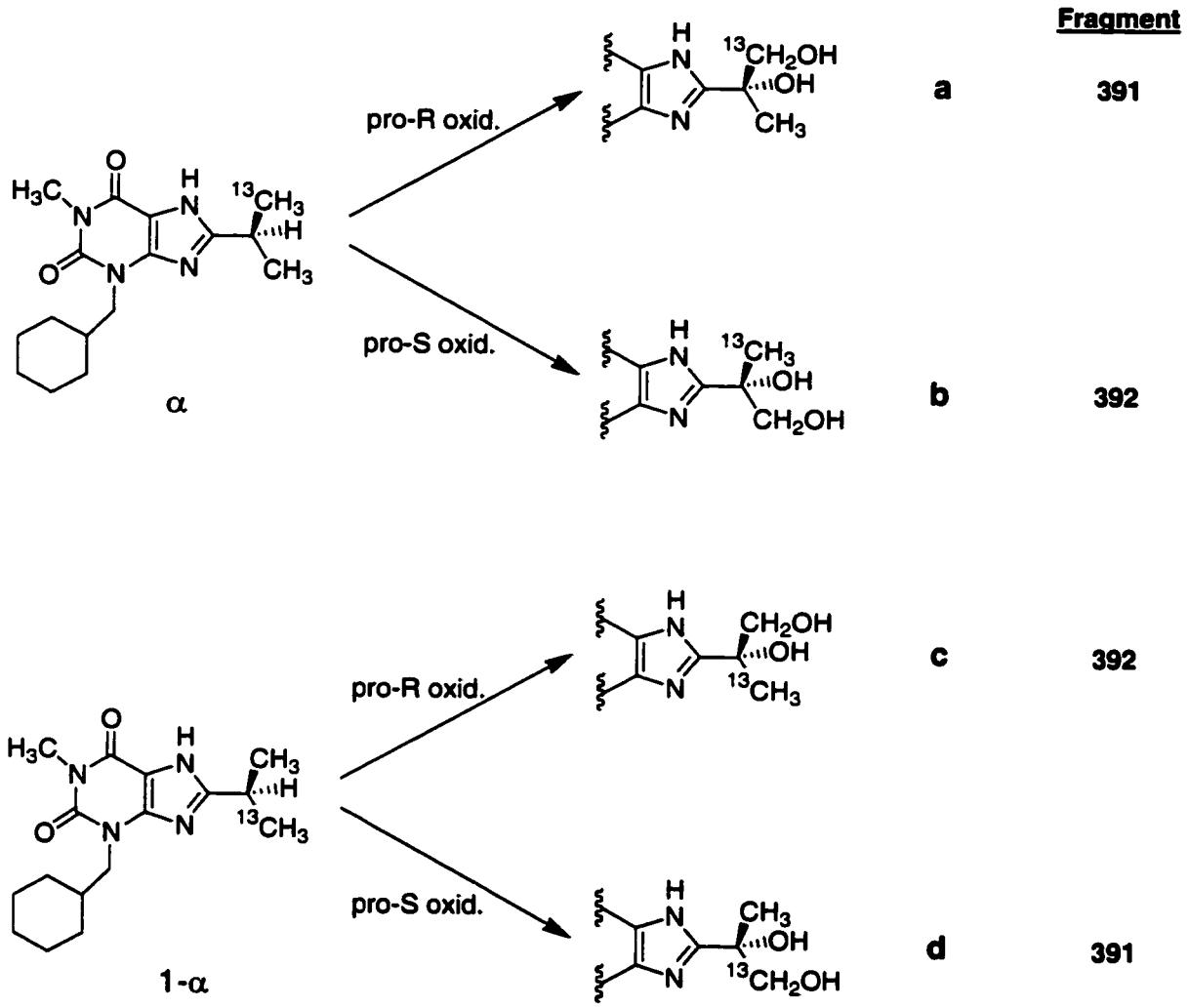

Figure 2.6 Determination of prochiral stereoselectivity ($^{R/S}P_S$) of vinyl formation from IPC and N-methyl-IPC using pro-R-^{13}C-IPC **9** and N-methyl-pro-R-^{13}C-IPC **24**, respectively: α is the fraction pro-R-label in synthesized substrate.[a,b]

[a] $^{R/S}P_S$ is the ratio of products obtained from oxidation of the pro-R methyl group to that of the pro-S methyl group.
[b] Figure is adapted from (*119*).

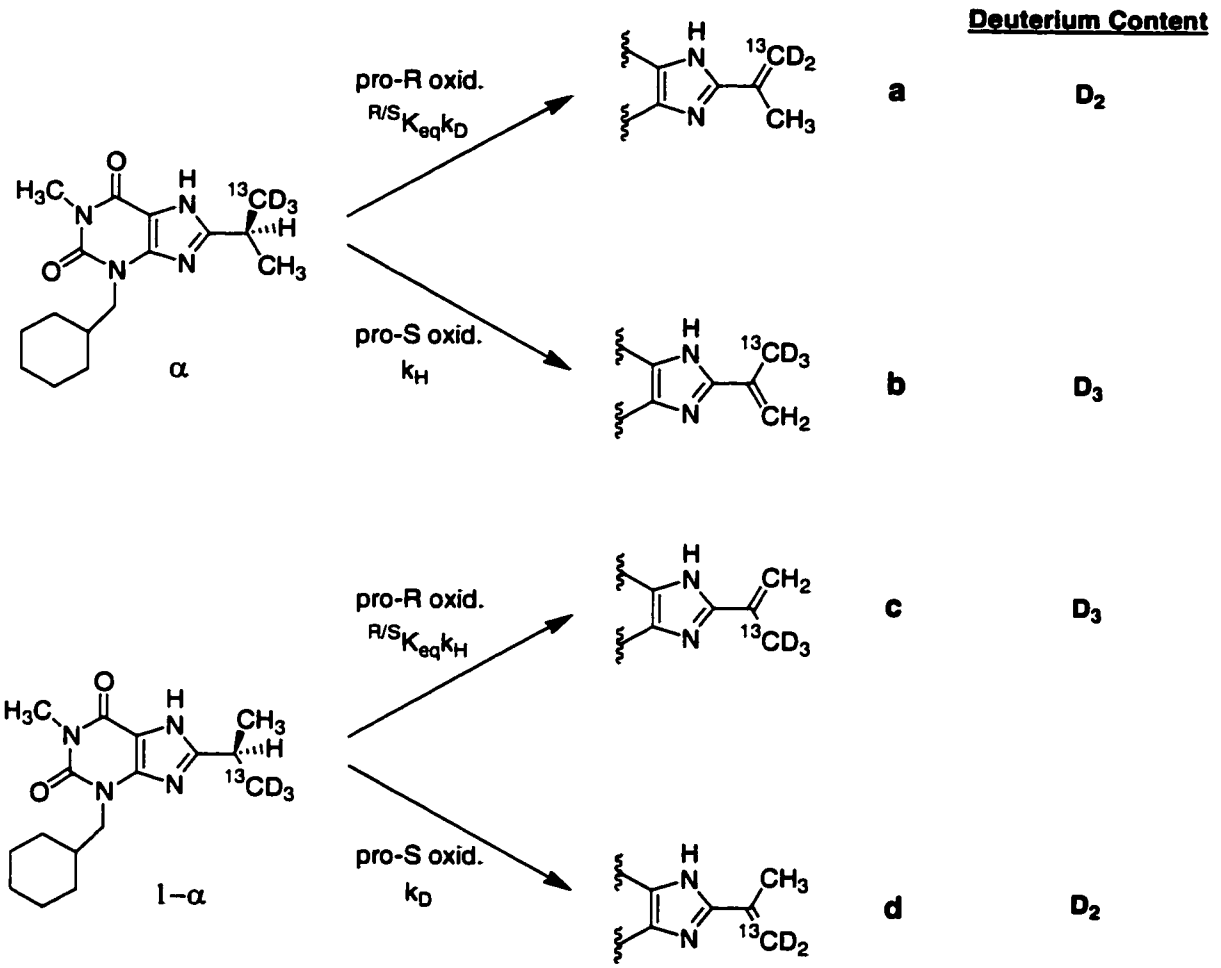

Figure 2.7 Method for determining the deuterium isotope effect on pro-R-methyl group desaturation to the vinyl metabolite of IPC and N-methyl-IPC using pro-R-$^{13}CD_3$-IPC **5** and N-methyl-pro-R-$^{13}CD_3$-IPC **23**, respectively: α is the fraction pro-R-label incorporation in the substrate, $^{R/S}K_{eq}$ is the equilibrium constant for catalytically susceptible orientation of the pro-R vs. pro-S methyl groups, k_H & k_D are the rate constants for removal of a hydrogen or deuterium, respectively.[a]

$$\frac{D_3}{D_2}=\frac{b+c}{a+d}=\frac{\alpha * k_H+(1-\alpha)^{R/S}K_{eq}k_H}{\alpha^{R/S}K_{eq}k_D+(1-\alpha)k_D}=\left(\frac{k_H}{k_D}\right)\left(\frac{\alpha+(1-\alpha)^{R/S}K_{eq}}{\alpha^{R/S}K_{eq}+(1-\alpha)}\right)$$

Where $^{R/S}K_{eq} = {}^{R/S}P_S$, assuming rapid equilibration of methyl groups at the active site and no difference in the energy of activation for oxidation of the two methyl groups. Therefore,

$${}^{D}V_{exp.pro-R}=\frac{k_H}{k_D}=\left(\frac{D_3}{D_2}\right)\Big/\left(\frac{\alpha+(1-\alpha)^{R/S}P_S}{\alpha^{R/S}P_S+(1-\alpha)}\right)$$

[a] Figure and equations adapted from (*119*).

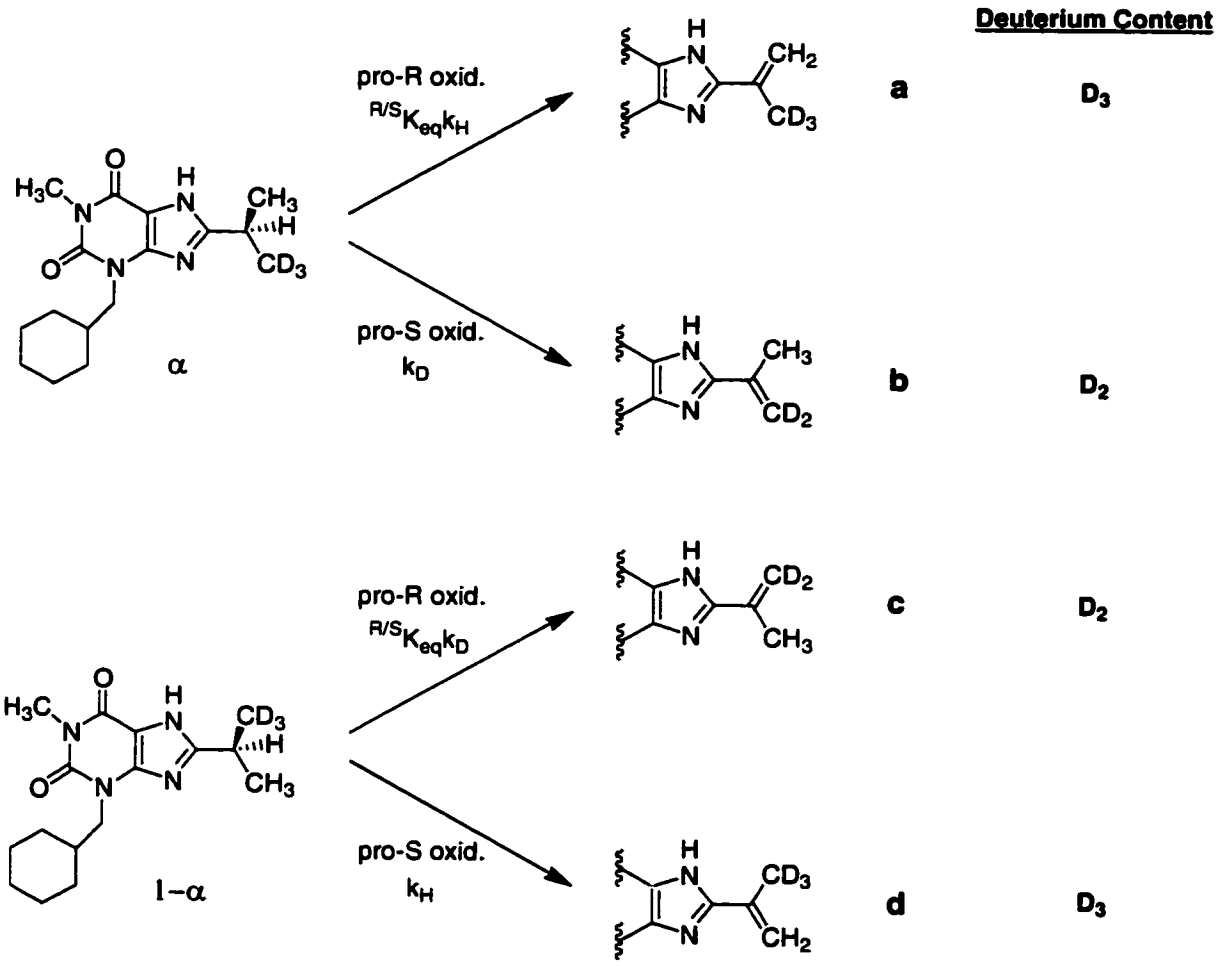

Figure 2.8 Method for determining the deuterium isotope effect on pro-S-methyl group desaturation to the vinyl metabolite of IPC and N-methyl-IPC using pro-S-D_3-IPC **10** and N-methyl-pro-S-D_3-IPC **25**, respectively: α is the fraction pro-S-label incorporation in the substrate, $^{R/S}K_{eq}$ is the equilibrium constant for catalytically susceptible orientation of the pro-R vs. pro-S methyl groups, k_H & k_D are the rate constants for removal of a hydrogen or deuterium, respectively.[a]

$$\frac{D_3}{D_2}=\frac{b+c}{a+d}=\frac{\alpha^{R/S}K_{eq}k_H+(1-\alpha)k_H}{\alpha^{*}k_D+(1-\alpha)^{R/S}K_{eq}k_D}=\left(\frac{k_H}{k_D}\right)\left(\frac{\alpha^{R/S}K_{eq}+(1-\alpha)}{\alpha+(1-\alpha)^{R/S}K_{eq}}\right)$$

Where $^{R/S}K_{eq} = {}^{R/S}P_S$, assuming rapid equilibration of methyl groups at the active site and no difference in the energy of activation for oxidation of the two methyl groups. Therefore,

$$^{D}V_{exp.pro-S}=\frac{k_H}{k_D}=\left(\frac{D_3}{D_2}\right)\Big/\left(\frac{\alpha^{R/S}P_S+(1-\alpha)}{\alpha+(1-\alpha)^{R/S}P_S}\right)$$

[a] Figure and equations adapted from (*119*).

Table 2.1 Incubations Performed in Studies of CYP1A2-catalyzed Sequential Metabolism of Isopropylcyclohexylline **2**. [a]

	Substrate Concentrations (μM)		
Enzyme Source	^{15}N-IPC	Unlabeled 8-Vinyl-IPC [d]	Unlabeled 8-Diol-IPC [d]
LB [b]	100	3.2	2.7
SS [c]	100	3.5	2

[a] 400 μl total incubation volume.
[b] Gentest lymphoblast expressed human CYP1A2 (40 pmole, 0.36 mg protein).
[c] Gentest CYP1A2 Supersomes (10 pmole, 0.046 mg protein).
[d] Incubation also contained 100 μM ^{15}N-IPC.

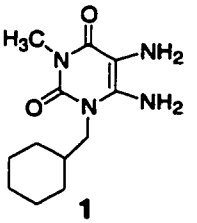

1
5,6-Diamino-1-(cyclohexylmethyl)-3-methyl uracil

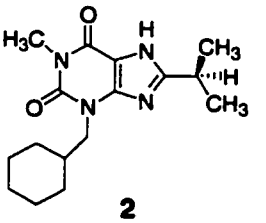

2
isopropylcyclohexylline (IPC)

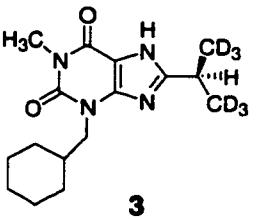

3
D_6-isopropylcyclohexylline (D_6-IPC)

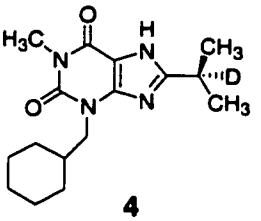

4
D_1-isopropylcyclohexylline (D_1-IPC)

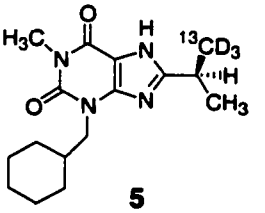

5
pro-R-$^{13}CD_3$-isopropylcyclohexylline (pro-R-$^{13}CD_3$-IPC)

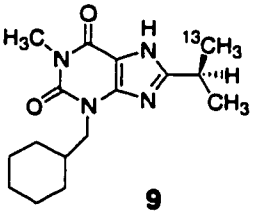

9
pro-R-^{13}C-isopropylcyclohexylline (pro-R-^{13}C-IPC)

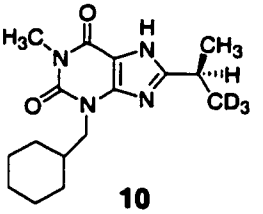

10
pro-S-D_3-isopropylcyclohexylline (pro-S-D_3-IPC)

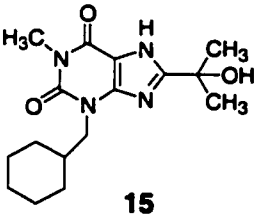

15
8'-OH-isopropylcyclohexylline (8'-OH-IPC)

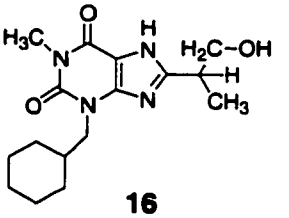

16
8"-OH-isopropylcyclohexylline (8"-OH-IPC)

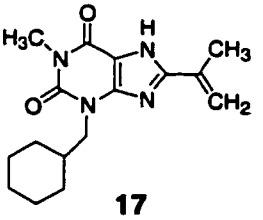

17
vinyl-isopropylcyclohexylline (vinyl-IPC)

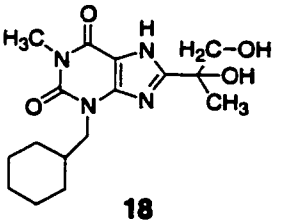

18
diol-isopropylcyclohexylline (diol-IPC)

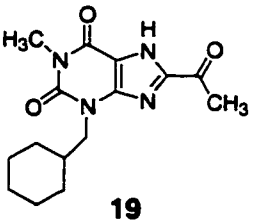

19
methylketone-cyclohexylline

Figure 2.9 Structures of synthetic compounds.

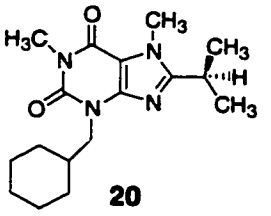

20

N^7-methyl-isopropylcyclohexylline

(N-Methyl-IPC)

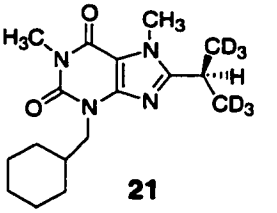

21

N^7-methyl-D_6-isopropylcyclohexylline

(N-Methyl-D_6-IPC)

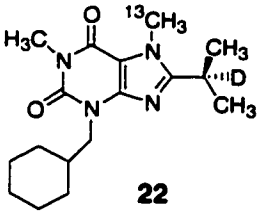

22

N^7-(^{13}C-methyl)-D_1-isopropylcyclohexylline

[N-(^{13}C-Methyl)-D_1-IPC]

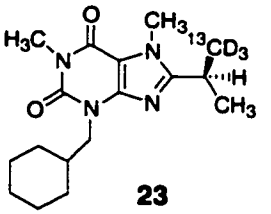

23

N^7-methyl-pro-R-$^{13}CD_3$-isopropylcyclohexylline

(N-methyl-pro-R-$^{13}CD_3$-IPC)

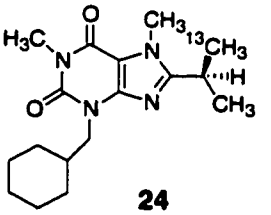

24

N^7-methyl-pro-R-^{13}C-isopropylcyclohexylline

(N-methyl-pro-R-^{13}C-IPC)

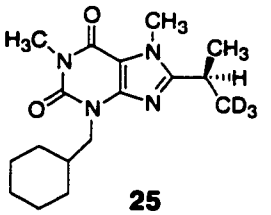

25

N^7-methyl-pro-S-D_3-isopropylcyclohexylline

(N-methyl-pro-S-D_3-IPC)

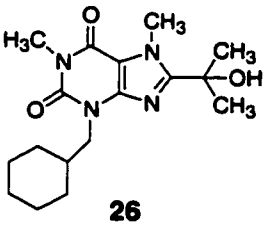

26

N^7-methyl-8'-OH-isopropylcyclohexylline

(N-methyl-8'-OH-IPC)

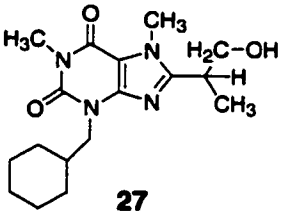

27

N^7-methyl-8"-OH-isopropylcyclohexylline

(N-methyl-8"-OH-IPC)

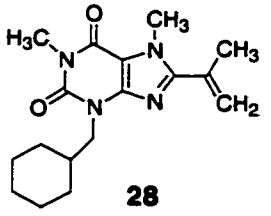

28

N^7-methyl-vinyl-isopropylcyclohexylline

(N-methyl-vinyl-IPC)

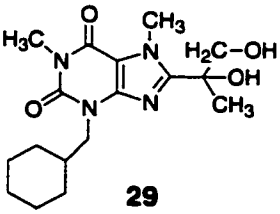

29

N^7-methyl-diol-isopropylcyclohexylline

(N-methyl-diol-IPC)

Figure 2.9 (continued)

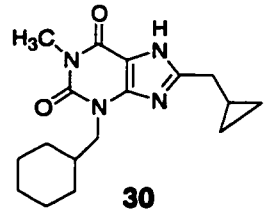

30
cyclopropylmethylcyclohexylline
(CPMC)

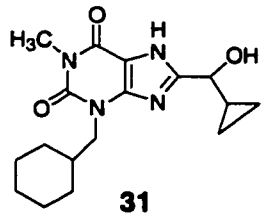

31
8'-OH-cyclopropylmethylcyclohexylline
(8'-OH-CPMC)

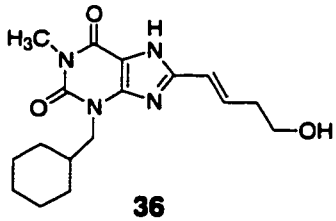

36
trans-butenol-cyclohexylline

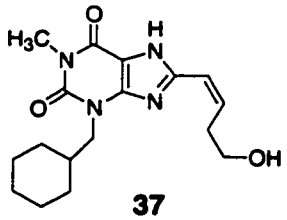

37
cis-butenol-cyclohexylline

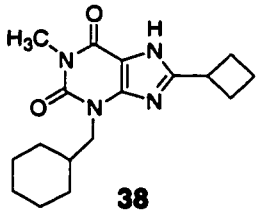

38
cyclobutylcyclohexylline
(CBC)

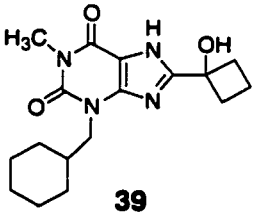

39
8'-OH-cyclobutylcyclohexylline
(8'-OH-CBC)

Figure 2.9 (continued)

CHAPTER 3

RESULTS

3.1 N^7-METHYL-ISOPROPYLCYCLOHEXYLLINE

Identification of Metabolites

Incubations of N^7-methyl-isopropylcyclohexylline **20** (60 μM) with CYP1A2 (75 pmol Gentest lymphoblast expressed) were analyzed by ESLC-MS-SIM (Figure 3.1). When available, authentic standards were used to confirm the identity of the metabolites, based on retention time and mass. Metabolites a, b, c, and d have the mass of mono-hydroxylation products, and are presumed to be cyclohexane ring hydroxylation metabolites, by comparison to previously reported results with cyclohexylline (*89*). Metabolites e, f, g, and h were identified as N^7-methyl-diol-isopropylcyclohexylline **29**, N^7-methyl-8″-OH-isopropylcyclohexylline **27**, N^7-methyl-8′-OH-isopropylcyclohexylline **26**, and N^7-methyl-vinyl-isopropylcyclohexylline **28**, respectively (see Figure 2.9 for chemical structures). The N^7-desmethyl metabolites, diol-isopropylcyclohexylline **18**, 8″-OH-isopropylcyclohexylline **16**, and isopropylcyclohexylline **2** were also produced in incubations, however they are minor metabolites and neither visible nor labeled in Figure 3.1. The predominant products, aside from the cyclohexyl ring carbinols, are N-methyl-diol-IPC **29**, N-methyl-8′-OH-IPC **26**, and N-methyl-vinyl-IPC **28**, in that order (912, 717, and 153 pmol, respectively, produced in a typical 30 min incubation with 75 pmol enzyme). Accurate quantitation of the cyclohexyl ring hydroxylation products is not possible without synthetic metabolite standards, however approximation of their quantities, based on the standard curve of **27**, indicates that they constitute roughly 40-50% of the observed turnover.

Incubation of N-methyl-vinyl-IPC **28** with CYP1A2 (results not shown) indicated that N-methyl-diol-IPC **29** constitutes the vast majority of metabolic turnover of the olefin, presumably through a putative epoxide intermediate. Minor amounts of cyclohexyl ring hydroxyl product, N-methyl-8″-OH-IPC **27**, N-methyl-8′-OH-IPC **26**, diol-IPC **18**, and 8″-OH-IPC **16** were also observed. Because 1) N-methyl-diol-IPC **29**, diol-IPC **18**, and 8″-OH-IPC **16** formation require a minimum of two oxidations of **20**, 2) N-methyl-diol-IPC **29** is formed directly from N-methyl-vinyl-IPC **28** via hydrolysis of a putative epoxide intermediate, and 3) N-methyl-diol-IPC **29** is the most abundant metabolite of **20** and is produced in quantities 6 fold greater than N-methyl-vinyl-IPC **28**, metabolism of N-methyl-IPC **20** by CYP1A2, unlike that of N-methyl-ethylcyclohexylline, involves a substantial amount of sequential metabolism, be it dissociative or non-dissociative (*56*).

<u>$H_2{}^{18}O$ Incorporation into Carbinol Metabolites</u>

The results of CYP1A2 incubations with N^7-methyl-isopropylcyclohexylline **20** (60μM) in the presence of $H_2{}^{18}O$ (40% v/v) are shown in Table 3.1. Only the N-methyl-diol **29** and N-desmethyl-diol **18** metabolites contained oxygen from the medium (68% and 96% containing one atom of ^{18}O, respectively). The oxygen of all other carbinol products presumably comes solely from molecular oxygen, as has been found in previous studies of N^7-methyl xanthines (*89*). The lack of $H_2{}^{18}O$ incorporation into mono-hydroxylation products is consistent with their formation by the consensus P450 oxygen-rebound mechanism of hydroxylation. Interpretation of the results for the diol

metabolites is less clear. Diol formation is thought to involve hydrolysis of the putative epoxide of the olefin metabolites. However, if this were the case, one equivalent of oxygen in the diol products should be sourced entirely to the medium, as has been found in the diol metabolite of ethylcyclohexylline (unpublished results). The results with the N-desmethyl-diol-IPC metabolite **18** are consistent with this hypothesis, but the less than 1 equivalent of ^{18}O incorporation into N-methyl-diol-IPC **29** suggests a different or additional process is contributing to its formation. ESLC-MS-SIM and ESLC-MS/MS analysis of N-methyl-diol-IPC **29** and diol-IPC **18** from co-incubations of N-methyl-vinyl-IPC **28** and vinyl-IPC **17** with CYP1A2 confirmed that less than one equivalent of oxygen from the medium is incorporated into N-methyl-diol-IPC **29** (69 ± 1 %), and that water incorporation is almost exclusively in the 8′-position (94.5 ± 0.2 %), as would be expected from hydrolysis of the putative epoxide intermediate.

Prochiral Stereoselectivity of Olefin Formation

The prochiral stereoselectivity ($^{R/S}P_S$) of CYP1A2-catalyzed desaturation of N-methyl-IPC **20** to form the olefin metabolite **28** was determined to be 2.78 ± 0.12. This indicates a clear preference for desaturation of the pro-R methyl group (73.5% pro-R-oxidation).

Deuterium Isotope Effects

Competitive Intermolecular. Competitive intermolecular deuterium isotope effects ($^{D}V/K$) for the formation of metabolites from N-(^{13}C-methyl)-D_1-IPC **22** and N-methyl-D_6-IPC **21** are given in Table 3.2. The incorporation of a ^{13}C-stable label into the N^7-

methyl group of the D_1-substrate was necessary for mass separation of N-methyl metabolites in order to distinguish between products derived from the deutero vs. protio substrates in the incubation, as many of the observed metabolites are devoid of the ω-1 hydrogen atom. Figure 3.2 illustrates the proposed mechanism of N-methyl-IPC **20** metabolism based on these isotope effects.

Large and equivalent normal isotope effects were observed for formation of N-methyl-vinyl-IPC **28**, N-methyl-diol-IPC **29**, and N-methyl-8′-OH-IPC **26** from the ω-1 D_1-substrate **22**, suggesting that all are initiated by ω-1 hydrogen atom abstraction. N-methyl-8″-OH-IPC **27** and N-desmethyl-IPC **2** formation had large and equivalent inverse isotope effects, demonstrating isotopically sensitive branching from the deuterated 8′-position to these unlabeled sites of oxidation. As described in the introduction, when isotopically sensitive branching is evident, the ratio of the observed isotope effects provides an estimate of the intrinsic isotope effect. In this case, the lower limit of the intrinsic isotope effect on ω-1 hydrogen atom removal is 12.2 (2.94/0.24). While consistent with hydrogen atom abstraction in the consensus P450-catalyzed hydroxylation mechanism, this isotope effect is significantly higher than that observed for the similar process in N-methyl-ethylcyclohexylline (5.4 (^{D}V) and 8 ($^{D}V/K$), see table 1.2).

N-methyl-vinyl-IPC **28** formation from the ω-D_6-substrate **21** shows a negligible isotope effect, while N-methyl-8′-OH-IPC **26**, N-desmethyl-substrate **2**, and N-methyl-diol-IPC **29** formation displayed slightly inverse isotope effects (Table 3.2). The metabolic switching observed between desaturation to form the olefin **28** and

recombination to form the 8′-carbinol **26** (see figure 3.2) indicates a low and normal isotope effect ($^{D}V/K$ = 1.02/0.84 = 1.2) for the second hydrogen atom transfer of the desaturation process. This magnitude of this isotope effect is consistent with literature results (*32, 35, 38*) and with those from N-methyl-ethylcyclohexylline desaturation (1.5 (^{D}V) and 1.6 ($^{D}V/K$), see table 1.2). The large and normal isotope effect observed for N-methyl-8″-OH-IPC **27** formation (11.57) is made even larger (lower limit of 13.9) upon accounting for the isotopically sensitive branching between paths A and B in figure 3.2 (11.57/0.83=13.9). While extremely high for a deuterium isotope effect, this value is consistent with the consensus hydrogen atom abstraction mechanism of hydroxylation, and is similar in magnitude to that seen for ω-1 hydroxylation with the ω-1 D_1-substrate **22**. The difference in isotope effects for ω-hydroxylation between the ω-1 D_1 and ω D_6 substrates presumably lies in the contribution of secondary isotope effects in the case of the D_6 substrate. Finally, the minor inverse isotope effect on N-methyl-diol-IPC **29** formation (0.91) from **21** is consistent with literature results on the epoxidation of olefins (*47*), and hydrolysis of the epoxide is not expected to be isotopically sensitive. Therefore, these results are consistent with formation and hydrolysis of the putative epoxide intermediate to form the diol. In addition, the results argue against the participation of a second mechanism of diol formation involving a second hydroxylation of the mono-hydroxylated products, **26** and **27**, as this mechanism would be expected to contribute a large normal isotope effect to the observed isotope effects on diol formation with the ω D_6 substrate.

Recent studies with Ezlopitant (*91, 120, 121*), which displays similar metabolism on a benzylic isopropyl group, have shown that cytochromes P450 are capable of converting an alkene metabolite to its corresponding primary alcohol (*91*). The proposed mechanism of this transformation (Figure 3.3) involves initial epoxidation of the olefin, followed by conversion of the epoxide to an aldehyde intermediate by an NIH shift-type mechanism. The primary alcohol then forms from the aldehyde after the addition of a hydride from NADPH (*91*). While the large normal isotope effects on primary alcohol **27** formation from N-methyl-IPC **20** are consistent with direct ω-hydroxylation, it is possible that N-methyl-8″-OH-IPC **27** is formed by an 'alkene hydration' mechanism, like that of Ezlopitant. However, ESLC-MS-SIM analysis (results not shown) of N-methyl-vinyl-IPC **28** incubation with CYP1A2 indicate that only minute amounts of N-methyl-8″-OH-IPC **27** are formed directly from the olefin. The N-methyl-diol/N-methyl-8″-OH integrated ion peak area ratio was 308 ± 21, while this same ratio in N-methyl-IPC **20** incubations was 10.2 ± 0.5. If the principal mechanism of primary alcohol **27** formation were alkene hydration, the N-methyl-diol/N-methyl-8″-OH ratio would be expected to be similar in both cases, because the epoxide intermediate would be expected to show similar partitioning between hydrolysis and primary alcohol formation in either case. Therefore, these results, in addition to the isotope effect analysis results, indicate that the principal means of primary alcohol formation from N-methyl-IPC **20** is direct ω hydroxylation via the consensus P450 oxygen rebound mechanism. Additional evidence against the participation of the alkene hydration mechanism lies in the $H_2{}^{18}O$ incorporation results. While essentially no oxygen from water is incorporated into N-

methyl-8″-OH-IPC **27**, the primary alcohol of Ezlopitant possesses only oxygen from the medium, due to exchange of the aldehyde oxygen (*91*). Finally, in incubations with N-(^{13}C-methyl)-D_1-IPC **22**, the fraction D_0 N-methyl-8″-OH-IPC of total N-methyl-8″-OH-IPC (D_0 and D_1) provides a measure of the fraction of N-methyl-8″-OH-IPC **27** formed via N-methyl-vinyl-IPC **28** vs. direct ω-hydroxylation, due to the requisite loss of the ω-1 deuterium of N-(^{13}C-methyl)-D_1-IPC **22** when forming the olefin. Because a kinetic deuterium isotope effect and corresponding metabolic switching between the 8′- and 8″-positions are expected to participate in the metabolism of N-(^{13}C-methyl)-D_1-IPC **22**, the experimentally determined fraction D_0 N-methyl-8″-OH-IPC (0.019 ± 0.001) is a lower limit of the fraction of N-methyl-8″-OH-IPC **27** formed from N-methyl-vinyl-IPC **28**. Thus, incubations with N-(^{13}C-methyl)-D_1-IPC **22** also support the hypothesis that the vast majority of N-methyl-8″-OH-IPC **27** formation is via direct ω-hydroxylation.

Intramolecular. Results from N-methyl-ETC (unpublished results), N-methyl-CH, and N-methyl–FF (*89*) suggest that N-methyl-xanthine metabolism follows normal P450-metabolism paradigms. The metabolic processes active on both prochiral methyl groups of N-methyl-IPC are then expected to be identical, as has been seen in other similar systems [Obach, 2001 #34; Sugiyama, 1986 #19]. Accordingly, the isotope effects for oxidation of either methyl group should be similar, if not identical. Intramolecular isotope effect (^{D}V) studies with pro-S-D_3-IPC **25** and pro-R-$^{13}CD_3$-IPC **23** were performed to test this hypothesis.

Observed D_3/D_2 ion ratios of N-methyl-vinyl-IPC **28**, N-methyl-diol-IPC **29**, and N-methyl-8″-OH-IPC **27** formed in incubations with the stereoselectively per-deuterated substrates are shown in Table 3.3. These results however, do not convey much meaning until the stereoselectivity of label incorporation and $^{R/S}K_{eq}$ is taken into account. Table 3.4 shows the expected isotope effects for pro-R and pro-S methyl oxidation ($^{D}V_{exp,pro\text{-}R}$ and $^{D}V_{exp,pro\text{-}S}$, respectively) to the vinyl **28** and diol **29** metabolites. The low and equivalent isotope effects are consistent with desaturation of both methyl groups via dual hydrogen atom abstraction (ω-1 followed by ω hydrogen atom removal).

Because N-methyl-8″-OH-IPC **27** is evidently formed by direct ω-hydroxylation (see above), a separate metabolic pathway from N-methyl-vinyl-IPC **28** and N-methyl-diol-IPC **29** formation, the experimentally determined $^{R/S}P_S$ for desaturation (initial ω-1 hydrogen atom removal) is not applicable in the analysis of **27**. Unfortunately, an experimentally determined $^{R/S}P_S$ is not currently available for ω-hydroxylation. However, as discussed by Sugiyama and Trager (*119*), if we assume 1) that there is rapid equilibration of the methyl groups at the active site and 2) that there is no difference in the energy of activation for hydroxylation of the two prochiral methyl groups, then we are able to calculate an estimate of $^{R/S}K_{eq}$ based on observed D_3/D_2 N-methyl-8″-OH ion ratios in incubations with the stereoselectively trideuterated substrates (Table 3.5). The results show that the prochiral stereoselectivity of ω-hydroxylation (0.36) is exactly opposite that of desaturation (2.78). This calculated equilibrium constant may then be used to estimate the intrinsic isotope effect for pro-R and pro-S ω-hydroxylation in the same manner as an experimentally determined $^{R/S}P_S$ value would be used (Table 3.5).

While the expected isotope effects calculated in this manner are estimates based on the initial assumption of equality of the intrinsic isotope effects for oxidation of each methyl group, the values in both cases are nonetheless large, normal, and consistent with literature results (*119*), albeit different than the observed intermolecular isotope effects for ω-hydroxylation (12.2-13.9), for unknown reasons. Ideally, the $^{R/S}P_S$ for ω hydroxylation would be experimentally determined. In this way, the true isotope effects could be accurately determined and the assumptions made in this analysis tested.

Figure 3.4 shows the proposed N-methyl-IPC **20** metabolic mechanism, including isotope effects on the individual prochiral methyl groups.

3.2 ISOPROPYLCYCLOHEXYLLINE

Identification of Metabolites

Figure 3.5 is a representative chromatogram of ESLC-MS-SIM analysis of CYP1A2 (75 pmol Gentest lymphoblast expressed) incubations with saturating concentrations (60μM) of isopropylcyclohexylline **2**. When available, authentic standards were used to confirm the identity of the metabolites, based on retention time and mass. Metabolites a, b, d, e, and g were identified as diol- **18**, 8″-OH- **16**, 8′-OH-isopropylcyclohexylline **15**, methylketone-cyclohexylline **19**, and vinyl-isopropylcyclohexylline **17**, respectively (see Figure 2.9 for chemical structures). Metabolite c is an unidentified product ($[M + H]^+$ 319), possibly 8-allylic alcohol (unreported data). The fragmentation of an additional unidentified metabolite ($[M + H]^+$ 319, 10.7 min) produced in trace quantities is consistent with an 8″-aldehyde product. In

contrast to the results with N-methyl-IPC **20**, very little cyclohexyl ring hydroxylation is observed in CYP1A2 metabolism of IPC **2**. This is consistent however, with the results of CYP1A2 metabolism of N^7-methyl and N^7-protio analogs of FF, CH, and ETC (*89*). Product formation from **2** was linear and product ratios reasonably constant over the course of a 30 minute incubation, indicating that, unlike ETC, FF, and CH, isopropylcyclohexylline **2** metabolism does not result in detectable enzyme inactivation. On the other hand, the quantities and ratios of products in incubations with IPC varied considerably with protein content and incubation volume. In a typical 30 min, 200 µl incubation with 75 pmol of Gentest lymphoblast expressed human CYP1A2, quantities of metabolites are as follows: diol-IPC **18**, 1368 pmol; vinyl-IPC **17**, 435 pmol; 8′-OH-IPC **15**, 351 pmol; methylketone-cyclohexylline **19**, 83 pmol; and 8″-OH-IPC **16**, 9 pmol. These results show that the metabolic profile of IPC **2** is similar to that of N-methyl-IPC **20** and ETC; in all cases, the predominant metabolites are diol, olefin, and 8′-OH. IPC metabolism also results in substantial amounts of methylketone-cyclohexylline **19** formation, which requires that CYP1A2 catalyze a carbon-carbon bond cleavage reaction.

Separate incubations of CYP1A2 with vinyl-IPC **17** and diol-IPC **18** (results not shown) indicate that the ketone metabolite **19** is a primary metabolite of diol-IPC **18**, and diol-IPC **18** is formed directly from vinyl-IPC **17** through a putative epoxide intermediate. Methylketone-cyclohexylline **19**, therefore, is a tertiary-metabolite of IPC **2**, requiring at least three successive oxidative steps, much like the series of reactions catalyzed by $P450_{SCC}$ (Figures 1.14 - 1.16). The disregarded epoxide-diol mechanism of $P450_{SCC}$-catalyzed oxidation of cholesterol (Figure1.15) is of particular interest, as it is

possible that CYP1A2 catalyzes a similar series of reactions on IPC **2**. Unfortunately, efforts to synthesize or identify the putative epoxide intermediate in incubations have been unsuccessful.

Incubations of CYP1A2 with high concentrations (60 μM) of 8′-OH-IPC **15** and 8″-OH-IPC **16** (results not shown) result in relatively minor amounts of diol-IPC **18** formation in comparison to incubations with vinyl-IPC **17**, suggesting that these mono-hydroxylated metabolites do not participate to any significant extent in the reaction sequence leading to diol **18** formation.

Lastly, in addition to substantial amounts of diol-IPC **18**, metabolite c, methylketone **19**, and possible aldehyde, incubations of vinyl-IPC **17** with CYP1A2 are shown to produce relatively large quantities 8″-OH-IPC **16** (results not shown). The diol-IPC/8″-OH-IPC ratio in CYP1A2 incubations with IPC **2** and vinyl-IPC **17** are 35 and 28, respectively. This indicates that the 8″-OH-IPC **16** observed in IPC **2** incubations may be due to an alkene hydration mechanism like that proposed for ezlopitant (Figure 3.3) (*91*), as the partitioning between hydrolysis or rearrangement of the putative epoxide intermediate is nearly the same for either substrate. In incubations with D_1-IPC **4**, the fraction D_0 8″-OH-IPC of total 8″-OH-IPC (D_0 and D_1) provides a measure of the fraction of 8″-OH-IPC **16** formed via vinyl-IPC **17** vs. direct ω-hydroxylation, due to the requisite loss of the ω-1 deuterium of D_1-IPC **4** when forming the olefin. Because a kinetic deuterium isotope effect and corresponding metabolic switching between the 8′- and 8″-positions are expected to participate in the metabolism of D_1-IPC **4**, the experimentally determined fraction D0 8″-OH-IPC (0.745 ± 0.004) is a lower limit of the

fraction of 8″-OH-IPC **16** formed from vinyl-IPC **17**. Thus, incubations with D_1-IPC **4** support the hypothesis that the majority of 8″-OH-IPC **16** formation is through an alkene hydration mechanism, like Ezlopitant.

$H_2{}^{18}O$ and $^{18}O_2$ Incorporation into Carbinol Metabolites

Tables 3.6 and 3.7 show the results of CYP1A2 incubations with IPC **2** in the presence of $H_2{}^{18}O$ and $^{18}O_2$, respectively. The 8′-OH metabolite **15** contains mixed sources of oxygen, with 43% coming from water and the balance from molecular oxygen. This indicates that at least 43% of 8′-OH-IPC **15** formation is not attributable to normal P450 oxygen rebound, and is presumably via hydration of a desaturated iminium reactive intermediate like that proposed for furafylline, cyclohexylline, and ethylcyclohexylline (*89, 90*). Both atoms of oxygen in the diol are accounted for between the two experiments, with one equivalent sourced entirely to H_2O and the other to O_2. This is consistent with diol formation via hydrolysis of the putative epoxide intermediate. ESLC-MS-SIM and ESLC-MS/MS analysis of diol-IPC **18** and N-methyl-diol-IPC **29** from co-incubations of vinyl-IPC **17** and N-methyl-vinyl-IPC **28** with CYP1A2 again showed the incorporation of one equivalent of oxygen from the medium into diol-IPC **18** (97 ± 3 %); in addition, this analysis indicated that water incorporation is almost exclusively in the 8′-position (96.9 ± 0.2 %), as would be expected from hydrolysis of the putative epoxide intermediate. The oxygen in 8″-OH-IPC **16** and unidentified metabolite c is sourced almost exclusively to molecular oxygen, consistent with hydroxylation via the consensus P450 oxygen rebound mechanism. This result for 8″-OH-IPC **16** is

inconsistent with its formation from the olefin **17** by a similar mechanism as Ezlopitant, in which one would expect exclusive oxygen incorporation from water (Figure 3.3) (*91*). Finally, the results with the ketone **19** are less clear, as oxygen incorporation assessment is inconsistent between the two experiments ($H_2{}^{18}O$ and $^{18}O_2$). A possible explanation for this result lies in the different means of incubation termination; incubations with $H_2{}^{18}O$ were terminated with aqueous TFA, while those with $^{18}O_2$ were terminated by extraction with ethyl acetate and brought back up in methanol. The acidic conditions of the $H_2{}^{18}O$ experiments could lead to exchange of the carbonyl oxygen with the medium, and therefore overestimation of $H_2{}^{18}O$ incorporation. Partial support for this, lies in the results from $H_2{}^{18}O$ experiments in which half of the incubation was terminated with TFA and the other half by extraction; the ketone metabolite showed 92 ± 1 % $H_2{}^{18}O$ incorporation under acidic conditions and 5 ± 2 % by extraction.

Figure 3.6 illustrates the metabolic scheme for IPC **2** using the information presented to this point. Because the data from ETC suggest that the only route of olefin formation is via rearrangement of the iminium reactive intermediate, this pathway is included in figure 3.6 as a possibility with IPC **2**.

Prochiral Stereoselectivity of Olefin Formation

The prochiral stereoselectivity ($^{R/S}P_S$) in the desaturation of isopropylcyclohexylline **2** was determined to be 0.70 ± 0.03. This value indicates that CYP1A2 has a slight preference for desaturation of the pro-S methyl group (58.8% pro-S-oxidation) of IPC **2**.

Deuterium Isotope Effects

Competitive Intermolecular. Competitive intermolecular deuterium isotope effects ($^{D}V/K$) for formation of metabolites from D_6-isopropylcyclohexylline **3** are shown in Table 3.8. Vinyl-IPC **17**, diol-IPC **18**, 8″-OH-IPC **16**, and methylketone-cyclohexylline **19** formation all had small, normal, and nearly equivalent isotope effects. The similarity in isotope effects for formation of these metabolites suggests that all are formed through a single metabolic pathway, as shown in figure 3.6. The slightly larger isotope effect for 8″-OH-IPC **16** indicates that direct ω-hydroxylation by the consensus P450 oxygen-rebound mechanism, as was seen for N-methyl-8″-OH-IPC **27**, may contribute to its formation, in agreement with the deuterium retention data from studies with D_1-IPC **4**. 8′-OH-IPC **15** formation from both water and molecular oxygen incorporation displayed large, but different, inverse isotope effects (0.27 and 0.34, respectively). These results indicate that CYP1A2 is able to switch from the isotopically sensitive desaturation pathway (forming vinyl- **17**, diol- **18**, 8″-OH-IPC **16**, and methylketone-cyclohexylline **19**) to non-isotopically sensitive 8′-OH-IPC **15** formation from either source of oxygen. Taking into account the metabolic switching to the 8′-carbinol from H_2O or from O_2, the lower limit for the isotope effect on ω hydrogen atom removal in vinyl formation is 4.3 or 5.4, respectively (1.45/0.34 or 1.45/0.27). These isotope effects are much larger than expected for the second hydrogen atom transfer in a desaturation reaction via dual hydrogen atom abstraction, but are consistent with the isotope effects on vinyl-ETC formation (^{D}V and $^{D}V/K$ = 5-6, see table 1.1). Evidence suggests that vinyl-ETC is formed exclusively by rearrangement of the iminium reactive intermediate (Path C,

Figure 1.20). In light of these results, Figure 3.7 shows the possible mechanisms for vinyl-IPC **17** formation. While desaturation by dual hydrogen atom abstraction, initiated with ω hydrogen atom removal, would account for the high isotope effects for desaturation, it is excluded as a mechanistic possibility based on the minor quantities of 8″-OH-IPC **16** produced in an incubation with IPC **2** and evidence that the majority of 8″-OH-IPC **16** is produced from vinyl-IPC **17**. If desaturation were initiated by ω-hydrogen atom transfer, one would expect to see substantial quantities of 8″-OH-IPC **16**, especially when considering the predominance of the desaturation pathway. Chemical dehydration of 8′-OH-IPC **15** is another mechanistic possibility of major concern, as synthetic vinyl-IPC **17** is made by this very method. Control incubations of 8′-OH-IPC **15** indicate that vinyl-IPC **17** is formed by dehydration of 8′-OH-IPC **15** under typical incubation and workup conditions, but the quantity of **17** formed in this manner would be expected to contribute only a minor portion (less than 1%) of total observed vinyl-IPC **17** (results not shown). Therefore, this mechanism was also ruled out. The only two reasonable mechanisms remaining are both initiated by ω-1 hydrogen atom transfer. Removal of a second hydrogen atom from the ω-position would form the olefin **17** directly by dual hydrogen atom transfer (Path A, Figure 3.7), whereas second hydrogen atom transfer or second electron transfer from the N^7-position would form the iminium reactive intermediate which could then be rearranged to the olefin **17** (Path B, Figure 3.7). The magnitudes of the observed isotope effects (Table 3.8) are more consistent with the latter, while the fact that both 8′-OH-IPC **15** from water and molecular oxygen have inverse and different isotope effects suggests that both the 8′-carbon radical and the

iminium reactive intermediate are isotopically sensitive branching points, and therefore both mechanisms of olefin formation are active (see introduction p. 26-29). The possibility of erroneous results because of our acidic conditions for termination of the incubation is ruled out by finding that the observed isotope effects and $H_2{}^{18}O$ incorporation are similar (virtually identical) when incubations are split, with half killed by TFA, while the other half is extracted with ethyl acetate (except for the ketone, which is expected to exchange (TFA = 85% $H_2{}^{18}O$; extract = 7% $H_2{}^{18}O$)) (results not shown).

Non-competitive Intermolecular. Non-competitive intermolecular deuterium isotope effects (^{D}V) for formation of metabolites from D_1-isopropylcyclohexylline **4** are shown in Table 3.9. All metabolites, save 8″-OH-IPC **16**, display small normal isotope effects. The significant inverse isotope effect on 8″-OH-IPC **16** indicates metabolic switching between ω hydroxylation and all other metabolic pathways, which are initiated with ω-1 HAT. These results indicate a normal isotope effect of 3.0 (≈ 1.3/0.43) associated with removal of the 8′ hydrogen atom.

Intermolecular isotope effect experiments do not allow us to distinguish between the isotope effects of desaturation on the prochiral methyl groups of IPC **2**. As shown in Figure 3.8, after initial 8′-hydrogen atom transfer, the resulting 8′-carbon radical is expected to adopt a planar, sp^2-hybridized structure. The significant barrier of rotation (≈ 15 kcal/mol) may create a situation in which each individual prochiral methyl group is in a fixed position; this is supported by results with ETC, which show that no inversion of

configuration or rotation about the C^8-$C^{8'}$ bond occurs after initial ω-1 hydrogen atom transfer. From this, it is conceivable that the two prochiral methyl groups of the 8′-carbon radical intermediate of IPC **2** are positioned such that they experience different desaturation processes; one is closer to the Fe^{IV}-OH species and therefore is more susceptible to desaturation via dual hydrogen atom transfer, while the other is removed enough from the reactive oxygen species to avoid dual HAT, but is close to an active site base, facilitating ω proton removal and subsequent reactive intermediate rearrangement. These two desaturation processes are expected to display different isotope effects (low for dual HAT and high for base-catalyzed intermediate rearrangement). Intramolecular isotope effect studies were used to determine the isotope effects for desaturation of the individual prochiral methyl groups.

Intramolecular. D_3/D_2 ion ratios of the vinyl **17**, diol **18**, 8″-carbinol **16**, and ketone **19** metabolites in incubations with the stereoselectively tri-deuterated substrates are given in Table 3.10. Table 3.11 shows the expected isotope effects for formation of these same metabolites by oxidation of the pro-R or pro-S methyl groups, after all appropriate corrections. The vinyl metabolite is known to be the precursor to the diol, ketone, and the majority of the 8″-OH, therefore we are able to apply the same corrections to all of their observed D_3/D_2 ion ratios (i.e. use the experimentally determined $^{R/S}P_S$ of desaturation). It should be noted that in order to apply these corrections for prochiral stereoselectivity to all of the above metabolites based on the experimentally determined $^{R/S}P_S$ for desaturation, we have to assume that there is no preference for diol, ketone, or

8″-OH formation from cis or trans isomers of the desaturation pathway. Lending credence to this assumption is the observation that ketone **19** formation shows the same $^{12}C/^{13}C$ methyl group oxidation ratio (1.32 ± 0.01) in incubations with pro-R-^{13}C-IPC **9** as was found for the diol **18** (1.28 ± 0.02). Accordingly, the isotope effects for formation of all of these metabolites via oxidation of either of the prochiral methyl groups are found to be large and inconsistent with the dual hydrogen atom abstraction mechanism of desaturation (^{D}V = 4.2-5.4). These results indicate that the predominant desaturation process acting on both methyl groups is the same and is some process other than dual hydrogen atom abstraction, possibly base-catalyzed rearrangement of the reactive intermediate.

3.3 CYCLOPROPYLMETHYLCYCLOHEXYLLINE

Identification of Metabolites

Incubations with cyclopropylmethylcyclohexylline **30** were performed as a probe of 8′-carbocationic character *in route* to or as the reactive intermediate formed in CYP1A2 incubations with 8-alkyl xanthines. Figure 3.9 shows a representative chromatogram of ESLC-MS-SIM analysis of a CYP1A2 (75 pmole Gentest lymphoblast expressed) incubation (30 min) with CPMC **30** (60 μM). 8′-OH-CPMC **31** (peak b) was identified by comparison to a synthetic standard. No other mono-hydroxylation products were observed. In incubations of CPMC **30** in the presence of $H_2{}^{18}O$ (40% v/v), 64 ± 8% of the oxygen in 8′-OH-CPMC **31** was sourced to the medium. Thus, even though reactive intermediate formation is evident because of water incorporation into the 8′-

carbinol **31**, rearrangement or ring-opening of CPMC **30** does not occur in incubations with CYP1A2. These results suggest the lack of 8′-carbocationic character in the generated reactive intermediate.

Solvolysis of 8′-OH-Cyclopropylmethylcyclohexylline

To investigate whether cationic ring-opening or rearrangement of CPMC **30** is probable, solvolysis reactions of 8′-OH-CPMC **31** were conducted. Solvolysis of synthetic 8′-OH-CPMC **31** in 10% H_2SO_4 at 100 °C generated two products, trans- and cis-8′-butenol-cyclohexylline (**36** and **37**, respectively), in a constant ratio (4/1) over the course of the 12 hour reaction (Figure 3.10). These same ring-opened products were generated in a solvolysis reaction conducted in incubation buffer (100 mM potassium phosphate, 1 mM EDTA, pH 7.4) at 100 °C, albeit at approximately $1/10^{th}$ the rate (results not shown). These results indicate that ring-opening of CPMC **30** via cyclopropylcarbinyl cation formation is possible, and therefore we could expect to see ring-opened products in CYP1A2 incubations with CPMC **30**, if an 8′-carbocation is generated. Because the only metabolite produced in CYP1A2 incubations with CPMC **30** is 8′-OH-CPMC **31** from mixed oxygen sources, these solvolysis studies suggest that the reactive intermediate of 8-alkyl xanthines in incubations with CYP1A2 does not possess carbocationic character in the 8′-position. However, the possibility exists that the equilibrium of cyclopropyl, cyclobutyl, and homoallyl carbonium ions varies with temperature; under experimental conditions, the cyclopropyl species may be greatly favored. Also, the carbonium ions may differ in their reactivity toward nucleophilic

attack by a water molecule, particularly when in the confines of enzyme active site. Thus, solvolysis studies at elevated temperatures in bulk medium may not provide the best assessment of carbocationic rearrangement under experimental conditions.

Cyclobutylcyclohexylline

To test for the possibility that cyclopropylcarbinyl cationic rearrangement of CPMC **30** produces unstable cyclobutyl alcohols that then rearrange to form 8′-OH-CPMC **31**, cyclobutylcyclohexylline **38** (60 μM) was incubated with CYP1A2 (75 pmole Gentest lymphoblast expressed). ESLC-MS analysis showed that while several metabolites are produced (Figure 3.11), one of which was identified as 8′-OH-CBC **39** using a synthetic standard, no 8′-OH-CPMC **31** was observed (Figure 3.12). Additionally, 8′-OH-CBC **39** proved to be exceedingly stable in solvolysis reactions, eventually producing an unidentified mix of degradation products (results not shown). These results indicate that cyclobutyl carbinol metabolites are stable and do not rearrange to the 8′-OH-CPMC **31**.

Conclusion

Unambiguous assignment of cationic character to the reactive intermediate is not possible with the results from studies with CPMC **30**. The cumulative evidence argues against the formation of an 8′-carbocation, however we cannot unequivocally rule out its existence.

3.4 SEQUENTIAL METABOLISM

Figure 3.13 illustrates the metabolic events and expected equilibria in CYP1A2 incubations with IPC **2**. In addition to its unbound state, the enzyme can exist any of several substrate/intermediate-bound states. Table 3.12 shows the results of kinetic studies with IPC **2**, vinyl-IPC **17**, and diol-IPC **18** in incubations with either Gentest CYP1A2 Supersomes or Gentest lymphoblast expressed CYP1A2. Gentest CYP1A2 Supersomes contain co-expressed NADPH P450 reductase, while Gentest lymphoblast expressed CYP1A2 is dependent on the constitutive NADPH P450 reductase present in the lymphoblast cell line. As a result, CYP1A2 Supersomes possess significantly greater reductase activity. These results allow calculation of the fraction of the enzyme existing in bound complexes with IPC **2**, vinyl-IPC **17**, and diol-IPC **18** (Table 3.13). The observed differences between the two systems are presumed to be due to the different levels of reductase present, and hence the rates of electron transfer.

Following the methods of Sugiyama, *et al.*, isotope tracing experiments were performed to determine the extent of non-dissociative sequential metabolism of IPC **2** occurring in incubations with lymphoblast expressed CYP1A2 and CYP1A2 Supersomes (Tables 3.14 and 3.15, respectively) (*56*). This method requires the measurement of the rates of metabolite formation from a labeled substrate and an unlabeled primary metabolite, in the same incubation. In this way, the amount of released primary metabolite that recombines with the enzyme to form the secondary metabolite can be corrected for.

The results of these experiments allow the determination of factors A and B, which are fully defined and derived in the reference (*56*). Factor A is the fraction of the

sum of the labeled primary and secondary metabolites that is present as the labeled primary metabolite at the end of the incubation, and factor B corrects for the fraction of the labeled, released primary metabolite that is converted to the labeled secondary metabolite. Because the metabolism of IPC **2** involves two metabolic steps in which non-dissociative sequential metabolism may be operative (vinyl-IPC **17** to diol-IPC **18**, and diol-IPC **18** to methylketone-cyclohexylline **19**), incubations of ^{15}N-labeled IPC with unlabeled vinyl-IPC **17** or diol-IPC **18** were performed separately. In these cases, factors A and B are defined as follows:

For incubations of ^{15}N-IPC with unlabeled vinyl-IPC:

$$A = \frac{^{15}Nvinyl}{(^{15}Nvinyl + ^{15}Ndiol + ^{15}Nketone)} \qquad B = \frac{(diol + ketone)/vinyl}{\left(1 - e^{-((diol+ketone)/vinyl)}\right)}$$

For incubations of ^{15}N-IPC with unlabeled diol-IPC:

$$A = \frac{^{15}Ndiol}{(^{15}Ndiol + ^{15}Nketone)} \qquad B = \frac{ketone/diol}{\left(1 - e^{-(ketone/diol)}\right)}$$

The calculated A and B factors for the lymphoblast and Supersomes systems are given in Tables 3.14 and 3.15, respectively, along with the measured amounts of metabolites. The ratio of the primary metabolite formed (vinyl or diol) and further converted to the downstream metabolite (diol or ketone, respectively) to the amount of primary metabolite released to the medium (k_{cat}/k_{off}, see Figure 3.13) is given by the calculation (1-A*B/A*B) (Tables 3.14 and 3.15). The normalized branching ratios for the two systems, as well as the overall increase in the efficiency of transmission of the olefin to ketone that is observed with Supersomes, are shown in Figure 3.14. Like the

overall 5-fold increase in the rate of IPC **2** metabolism with CYP1A2 Supersomes vs. lymphoblast expressed CYP1A2 (see Table 3.12), the ratio of rate constants for vinyl-IPC **17** continuation to diol-IPC **18** vs. release also increases 4.9 ± 0.3 fold, while the ratio of rate constants for diol-IPC **18** continuation to methylketone-cyclohexylline **19** vs. release increases 11.5 ± 1.1 fold. Another remarkable finding was the 17-fold increase in the overall transmission of metabolites through the non-dissociative sequential metabolism pathway. These results indicate that the improved efficiency of intermediate transmission along the non-dissociative path may be magnified relative to total product formation rates. In addition, these results suggest that electron transfer rate increases are not the same for all rate constants, and that k_{off} rate constants are important contributors to the proportion of intermediates retained in the enzyme active site for a second catalytic cycle (as was found by (*74*)).

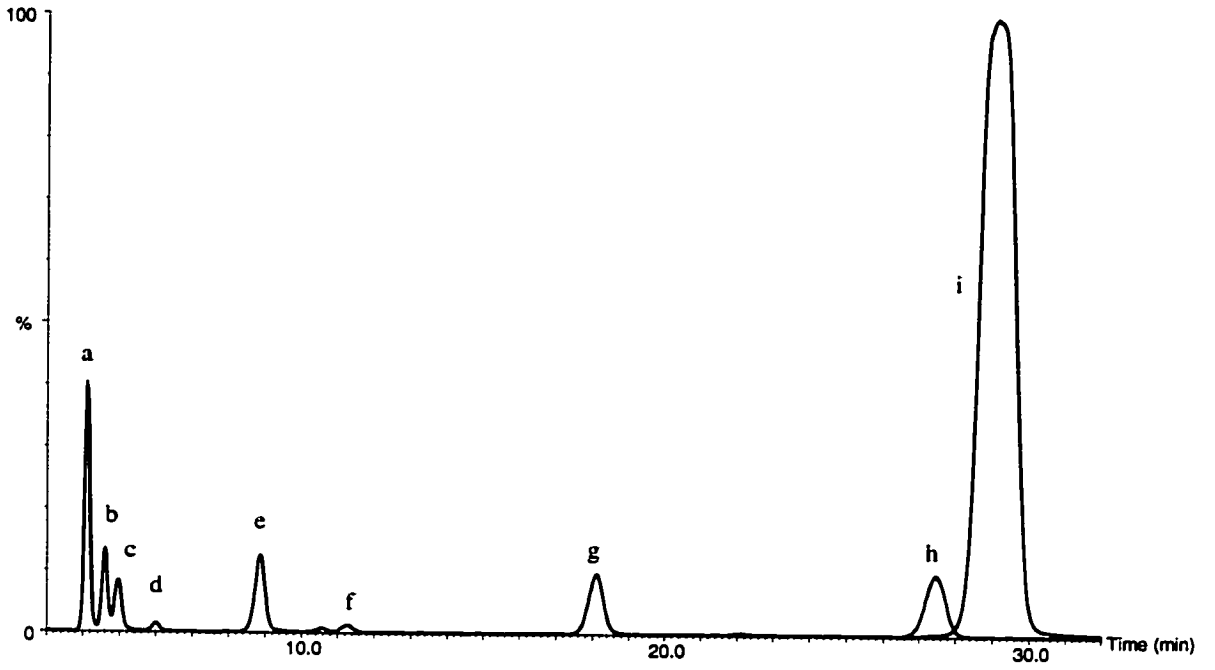

Figure 3.1 ESLC-MS-SIM chromatogram of CYP1A2 incubation (75 pmol Gentest lymphoblast expressed, 200 µl, 30 min) with N^7-methyl-isopropylcyclohexylline **20** (60 µM). Ion channels shown are those of the protonated parent ions: $[M + H]^+$ 335 (2 - 7 min), 351 (7 - 10.65 min), 335 (9.25 - 20.75 min), 317 & 319 (20 - 32 min). Amounts of identified metabolites provided were determined using an external standard curve and are corrected back to the original incubation mixture. (a, b, c, d) unknown mono-hydroxylation metabolites (4.1, 4.6, 4.9, 6.0 min, respectively), (e) N^7-methyl-diol-isopropylcyclohexylline **29** (8.8 min, 912 pmol), (f) N^7-methyl-8″-OH-isopropylcyclohexylline **27** (11.2 min, 31 pmol), (g) N^7-methyl-8′-OH-isopropylcyclohexylline **26** (18.0 min, 717 pmol), (h) N^7-methyl-vinyl-isopropylcyclohexylline **28** (27.5 min, 153 pmol), (i) N^7-methyl-isopropylcyclohexylline **20** (29.1 min), (not shown) diol-isopropylcyclohexylline **18** (5.3 min), (not shown) 8″-OH-isopropylcyclohexylline **16** (6.9 min), (not shown) isopropylcyclohexylline **2** (17.4 min, 7 pmol).

Table 3.1 Incorporation of $H_2{}^{18}O$ into carbinol metabolites of N^7-methyl-isopropylcyclohexylline **20** by CYP1A2.

Metabolite	% oxygen from H_2O [a]
N^7-methyl-8′-OH-IPC **26**	0.3 ± 0.7
N^7-methyl-8″-OH-IPC **27**	0.7 ± 1.7
N^7-methyl-diol-IPC **29** [b]	68 ± 1
N^7-methyl-3′-(cyclohexyl-OH) #1	0.1 ± 0.1
N^7-methyl-3′-(cyclohexyl-OH) #2	0.0 ± 0.4
N^7-methyl-3′-(cyclohexyl-OH) #3	-0.7 ± 1.0
8″-OH-IPC **16**	-0.9 ± 1.5
N^7-desmethyl-diol-IPC **18** [b]	96 ± 15

[a] Values expressed as percent $H_2{}^{18}O$ incorporation into total of each carbinol.

[b] Incorporation of 2 equivalents of oxygen from the medium into the diol metabolites (**29** and **18**) is possible, but no evidence for incorporation of a second atom is seen. Therefore, the oxygen incorporation values for **29** and **18** are given as percent of one equivalent of $H_2{}^{18}O$ incorporation.

Table 3.2 Competitive intermolecular deuterium isotope effects ($^{D}V/K$) for formation of N^7-methyl-isopropylcyclohexylline metabolites by CYP1A2.

Metabolite	N^7-([^{13}C]methyl)-D_1-isopropylcyclohexylline **22** $^{D1}V/K$	N^7-methyl-D_6-isopropylcyclohexylline **21** $^{D6}V/K$
N^7-methyl-vinyl-IPC **28**	2.94 ± 0.02	1.02 ± 0.02
N^7-methyl-diol-IPC **29**	3.03 ± 0.03	0.91 ± 0.01
N^7-methyl-8′-OH-IPC **26**	2.96 ± 0.02	0.84 ± 0.01
N^7-methyl-8″-OH-IPC **27**	0.24 ± 0.005	11.57 ± 0.20
N^7-desmethyl-IPC **2**	0.24 ± 0.003	0.83 ± 0.01

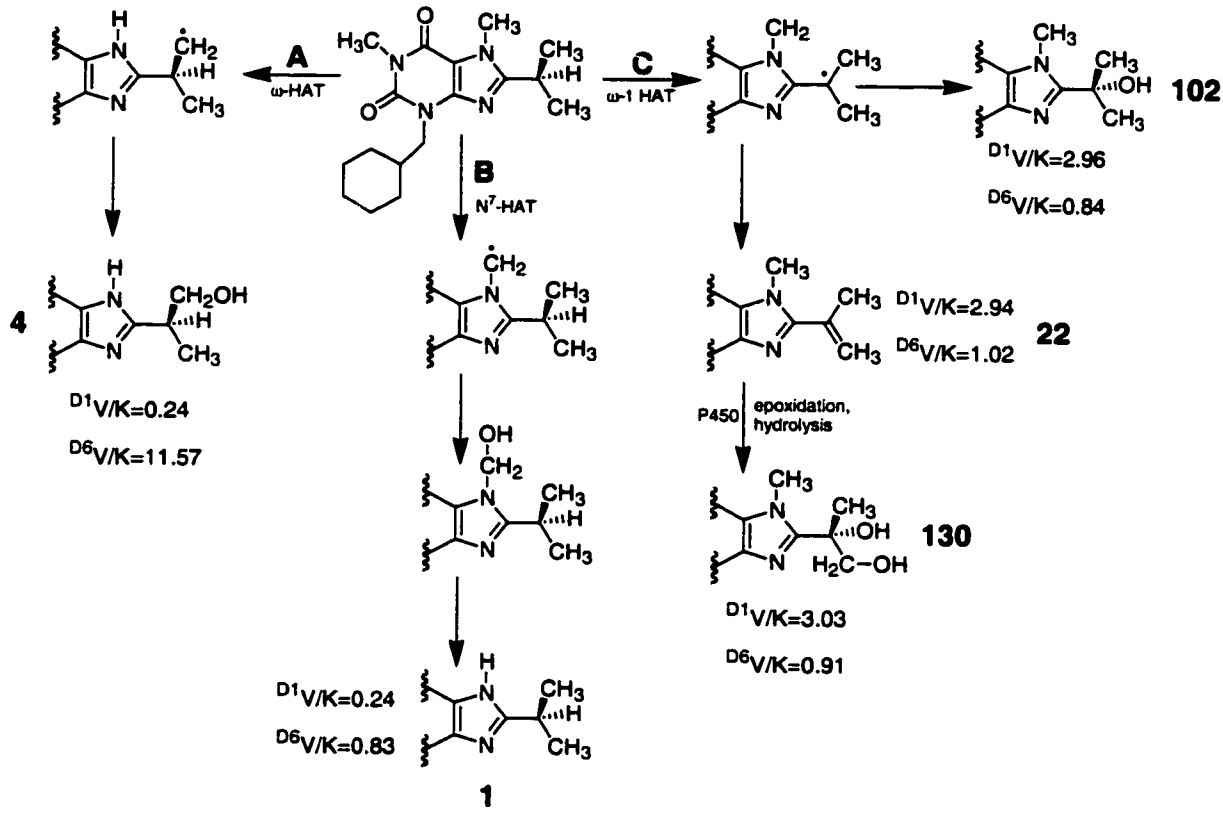

Figure 3.2 Competitive intermolecular isotope effect derived N^7-methyl-isopropylcyclohexylline **20** metabolic scheme. A) consensus P450 oxygen-rebound hydroxylation of ω-position, B) N-demethylation, and C) ω-1 hydrogen atom abstraction and partitioning of resultant 8′-carbon radical between consensus P450 oxygen-rebound hydroxylation of ω-1 position vs. desaturation via abstraction of a second hydrogen atom from either ω-methyl group. [a]

[a] Numbers in bold by observed metabolites are relative quantities of each produced in a typical incubation.

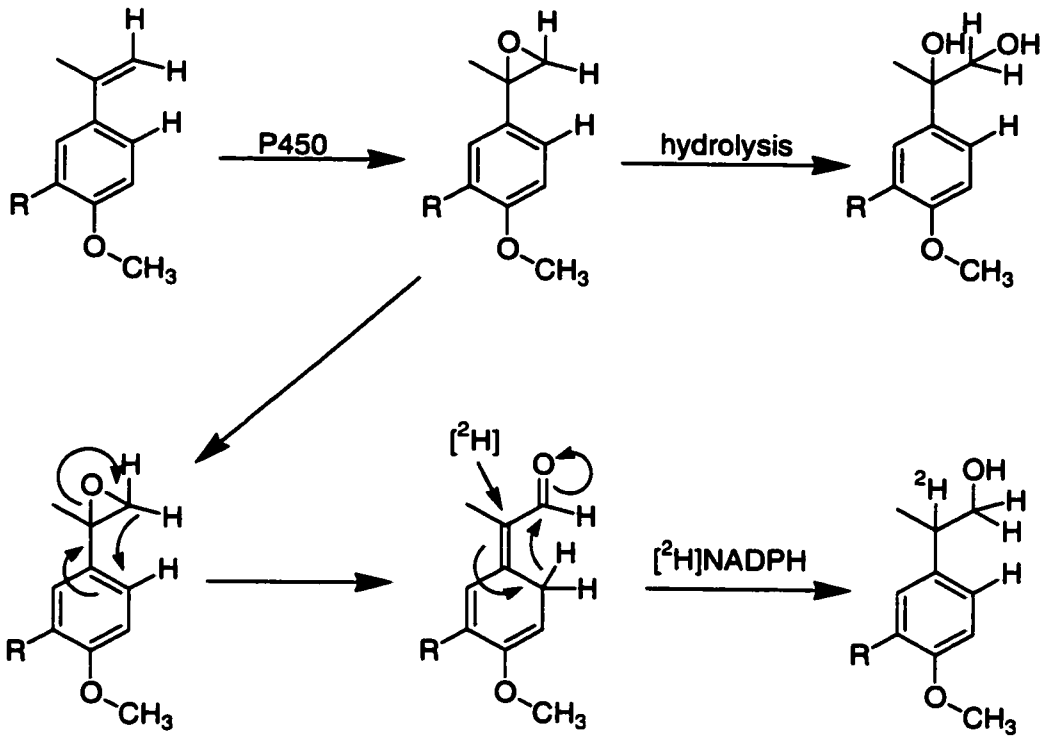

Figure 3.3 Proposed mechanism of Ezlopitant alkene metabolite conversion to a primary alcohol. [a]

[a] Figure adapted from (*91*).

Table 3.3 Observed D_3/D_2 ion ratios of metabolites formed in CYP1A2 incubations with stereoselectively trideuterated N^7-methyl-isopropylcyclohexylline substrates. [a]

Metabolite	N-methyl-pro-S-D_3-IPC **25**	N-methyl-pro-R-$^{13}CD_3$-IPC **23**
N-methyl-vinyl-IPC **28**	3.29 ± 0.03	0.66 ± 0.005
N^7-methyl-diol-IPC **29**	3.38 ± 0.02	0.65 ± 0.004
N^7-methyl-8″-OH-IPC **27**	2.78 ± 0.15	21.70 ± 1.55

[a] The ratios shown have been corrected for natural isotope contribution and incomplete deuteration of the substrates.

Table 3.4 Expected deuterium isotope effects for oxidation of the prochiral methyl groups of N^7-methyl-isopropylcyclohexylline **20** to its olefin and diol metabolites.

Metabolite	$^{D}V_{exp,pro\text{-}S}$	$^{D}V_{exp,pro\text{-}R}$
N^7-methyl-vinyl-IPC **28**	1.49 ± 0.09	1.46 ± 0.09
N^7-methyl-diol-IPC **29**	1.53 ± 0.09	1.43 ± 0.08

Table 3.5 Calculated $^{R/S}K_{eq}$ and expected isotope effects for formation of N^7-methyl-8″-OH-isopropylcyclohexylline **27** by ω-hydroxylation of the prochiral methyl groups of N^7-methyl-isopropylcycloheyxlline **20**. [a]

$^{R/S}K_{eq,calc}$ [b]	0.36 ± 0.02
$^{D}V_{exp,pro\text{-}S}$ [c]	6.17 ± 0.63
$^{D}V_{exp,pro\text{-}R}$ [d]	9.79 ± 1.19

[a] Formulas adapted from (*119*).

b $$^{R/S}K_{eq,calc} = \left(\frac{D_3/D_2\ pro-S-D_3-IPC}{D_3/D_2\ pro-R-^{13}CD_3-IPC} \right)^{1/2} = \left(\frac{\frac{pro-R-HAT}{pro-S-DAT}}{\frac{pro-S-HAT}{pro-R-DAT}} \right)$$

Assuming rapid equilibration of the prochiral methyl groups and that the energy of activation for hydroxylation is independent of stereochemistry. Where D_3/D_2 pro-S-D_3-IPC and D_3/D_2 pro-R-D_3-IPC are the experimentally observed D_3/D_2 ion ratios of N-methyl-8″-OH-IPC **27** generated from the stereoselectively trideuterated substrates, as shown in table 3.3. HAT is "hydrogen atom transfer" and DAT is "deuterium atom transfer," showing that the equation is simply placing R-oxidation over S-oxidation.

c $$^{D}V_{exp,pro-S} = \left(\frac{D_3}{D_2} \right) \Big/ \left(\frac{\alpha^{R/S}K_{eq,calc} + (1-\alpha)}{\alpha + (1-\alpha)^{R/S}K_{eq,calc}} \right)$$, see Figure 2.7 for more details.

d $$^{D}V_{exp,pro-R} = \left(\frac{D_3}{D_2} \right) \Big/ \left(\frac{\alpha + (1-\alpha)^{R/S}K_{eq,calc}}{\alpha^{R/S}K_{eq,calc} + (1-\alpha)} \right)$$, see Figure 2.6 for more details.

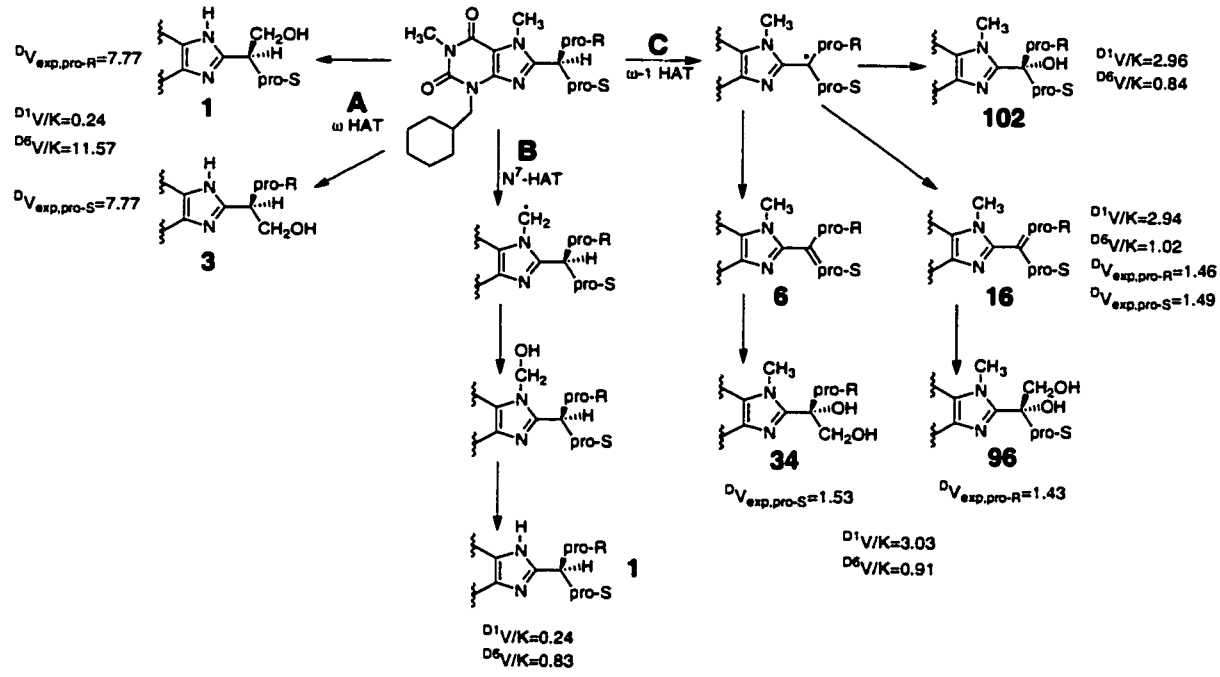

Figure 3.4 Proposed N^7-methyl-isopropylcyclohexylline **20** metabolic scheme, based on isotope effect profiles. A) stereoselective consensus P450 oxygen-rebound hydroxylation of ω-position, B) N-demethylation, and C) ω-1 hydrogen atom abstraction and partitioning of resultant 8′-carbon radical between consensus P450 oxygen-rebound hydroxylation of ω-1 position and desaturation via stereoselective abstraction of a second hydrogen atom from either prochiral ω-position. [a]

[a] Numbers in bold by observed metabolites are relative quantities of each produced in a typical incubation. The quantities of individual isomeric products were determined using the experimentally determined $^{R/S}P_S$ of desaturation or the calculated $^{R/S}P_S$ of ω hydroxylation.

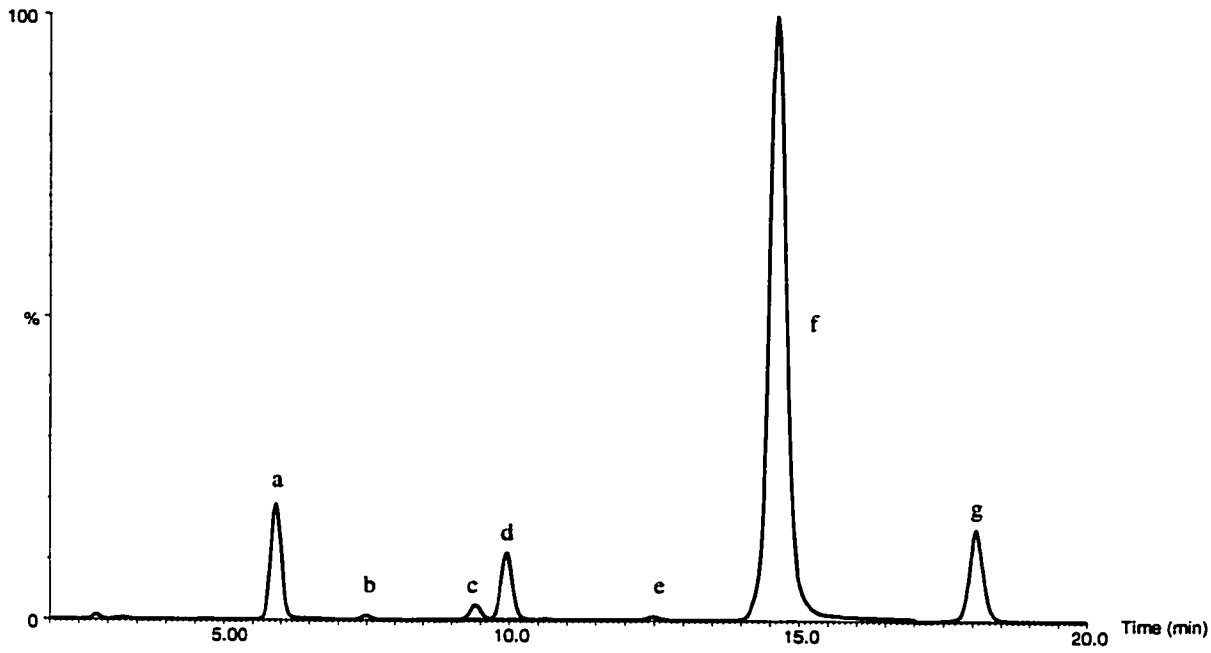

Figure 3.5 ESLC-MS-SIM chromatogram of CYP1A2 incubation (75 pmol Gentest lymphoblast expressed, 200 µl, 30 min) with isopropylcyclohexylline **2** (60 µM). Ion channels shown are those of the protonated parent ions: $[M + H]^+$ 321 (1.75 - 4.75 min), 337 (4.5 - 7 min), 321 (6.6 – 8.6 min), 319 & 321 (8.4 - 12 min), 305 (11.7 – 17 min), 303 (17 – 20 min). Amounts of identified metabolites provided were determined using an external standard curve and are corrected back to the original incubation mixture. (a) diol-isopropylcyclohexylline **18** (5.8 min, 1368 pmol), (b) 8″-OH-isopropylcyclohexylline **16** (7.4 min, 9 pmol), (c) unidentified metabolite (m/z 319) (9.3 min), (d) 8′-OH-isopropylcyclohexylline **15** (9.7 min, 351 pmol), (e) methylketone-cyclohexylline **19** (12.9 min, 83 pmol), (f) isopropylcyclohexylline **2** (14.9 min), (g) vinyl-isopropylcyclohexylline **17** (18.3 min, 435 pmol), (not shown) unidentified metabolite (m/z 319) (10.7 min).

Table 3.6 Incorporation of $H_2{}^{18}O$ into carbinol metabolites of isopropylcyclohexylline **2** and IPC isotopomers by CYP1A2.[a]

Substrate	8′-OH-IPC **15**	diol-IPC **18** [b]	8″-OH-IPC **16**	Methylketone-**19**	Metabolite c
Isopropylcyclohexylline **2**	43 ± 5	101 ± 9	5 ± 4	84 ± 13	1 ± 2
D_6-IPC **3**	54 ± 4	101 ± 13	1 ± 15	83 ± 18	1 ± 10
pro-(R)-$^{13}CD_3$-IPC **5**	46 ± 1	ND	ND	ND	ND
pro-(S)-D_3-IPC **10**	47 ± 3	ND	ND	ND	ND

[a] Values expressed as percent $H_2{}^{18}O$ incorporation into total of each carbinol.

[b] Incorporation of 2 equivalents of oxygen from the medium into the diol metabolite **18** is possible, but no evidence for incorporation of a second atom is seen. Therefore, the oxygen incorporation value for diol-IPC **18** is given as percent of one equivalent of $H_2{}^{18}O$ incorporation.

Table 3.7 Incorporation of $^{18}O_2$ into carbinol metabolites of isopropylcyclohexylline **2** in incubations with CYP1A2.[a,b,c]

Metabolite	% oxygen from O_2
8′-OH-IPC **15**	56 ± 1
diol-IPC **18** [d]	97 ± 6
8″-OH-IPC **16**	89 ± 3
Methylketone-cyclohexylline **19**	68 ± 4
Metabolite c	97 ± 1

[a] Determined from multiple measurements of one incubation using theoretical natural isotope contribution for appropriate corrections. Therefore, uncertainty is instrumental only.

[b] Incubations were terminated by extraction with ethyl acetate, and the residue brought back up in methanol for analysis.

[c] Values expressed as percent $^{18}O_2$ incorporation into total of each carbinol.

[d] Incorporation of 2 equivalents of oxygen from molecular oxygen into the diol metabolite **18** is possible, but no evidence for incorporation of a second atom is seen. Therefore, the oxygen incorporation value for the diol-IPC **18** is given as percent of one equivalent of $^{18}O_2$ incorporation.

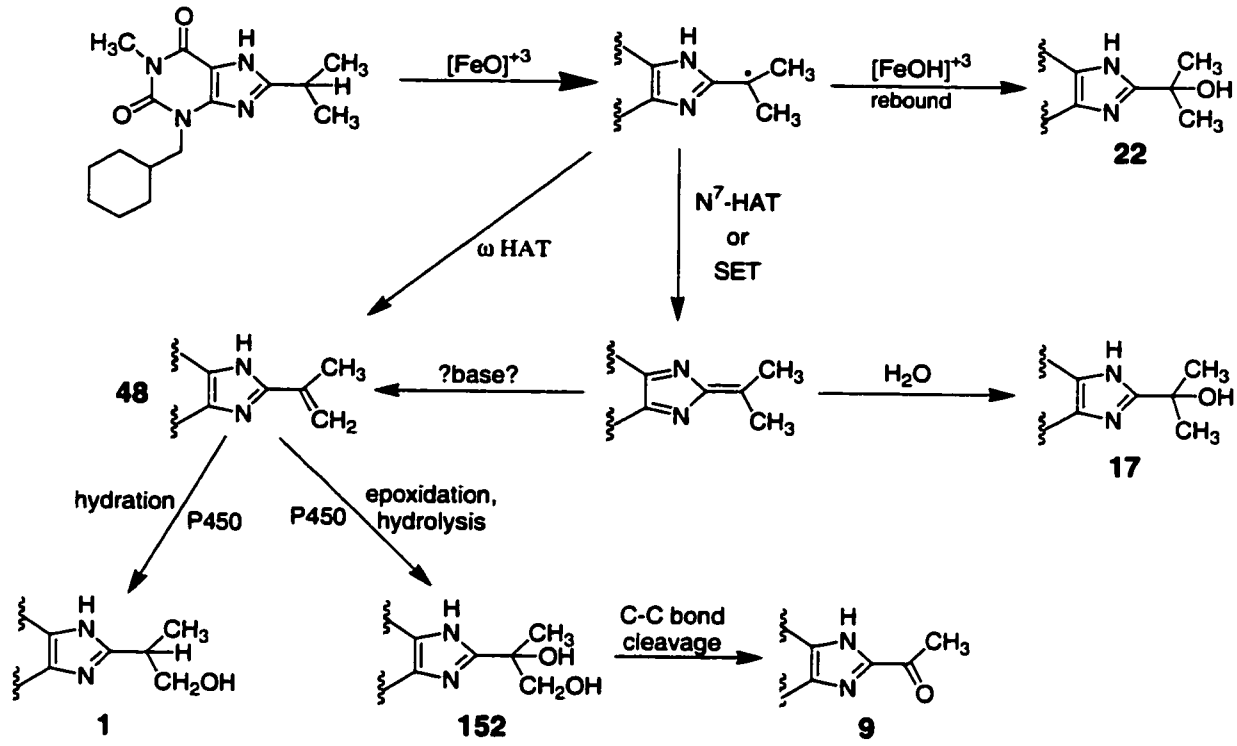

Figure 3.6 Metabolic scheme for CYP1A2-catalyzed metabolism of isopropylcyclohexylline **2**. [a]

[a] Numbers in bold by observed metabolites are relative quantities of each produced in a typical incubation (75 pmole Gentest lymphoblast expressed human CYP1A2, 200 μL, 60 μM IPC, 30 min).

Table 3.8 Competitive intermolecular deuterium isotope effects ($^{D}V/K$) for formation of isopropylcyclohexylline metabolites determined by CYP1A2 incubation with D_6-isopropylcyclohexylline **3**.

Metabolite	$^{D6}V/K$
vinyl-IPC **17**	1.45 ± 0.01
diol-IPC **18**	1.40 ± 0.02
8″-OH-IPC **16**	1.94 ± 0.05
8′-OH-IPC **15** (O_2)	0.34 ± 0.003
8′-OH-IPC **15** (H_2O)	0.27 ± 0.01
methylketone-cyclohexylline **19**	1.55 ± 0.03
metabolite c	5.54 ± 0.07

Table 3.9 Non-competitive intermolecular deuterium isotope effects (^{D}V) for formation of isopropylcyclohexylline metabolites determined by CYP1A2 incubation with D_1-isopropylcyclohexylline **4**.

Metabolite	$^{D6}V/K$
vinyl-IPC **17**	1.35 ± 0.26
diol-IPC **18**	1.08 ± 0.06
8″-OH-IPC **16**	0.43 ± 0.02
8′-OH-IPC **15**	1.24 ± 0.10
metabolite c	1.40 ± 0.48
methylketone-cyclohexylline **19**	1.11 ± 0.12
total metabolites	1.15 ± 0.12

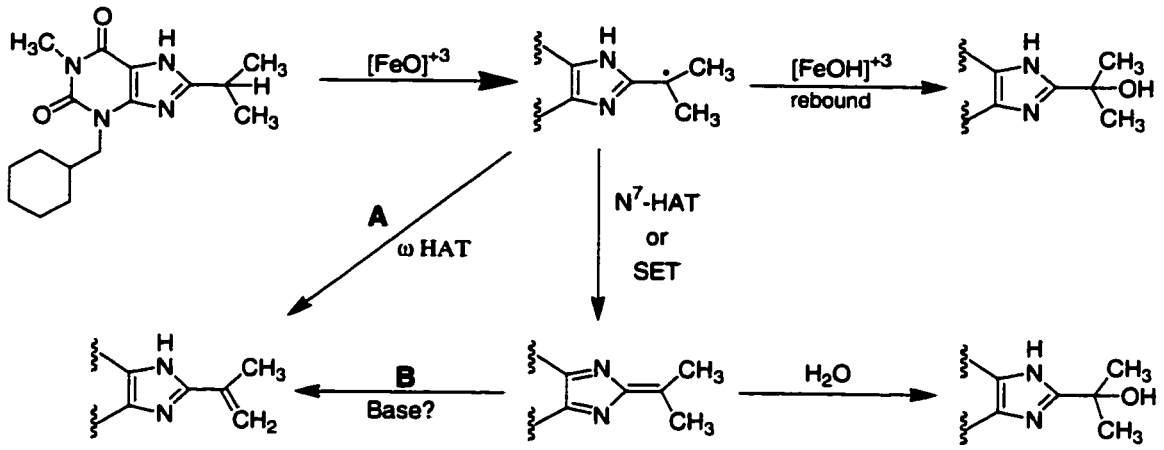

Figure 3.7 Possible mechanisms of vinyl-isopropylcyclohexylline **17** formation: a) dual hydrogen atom abstraction b) rearrangement of reactive intermediate

[a] dual hydrogen atom abstraction initiated by ω hydrogen atom transfer and dehydration of 8′-OH were excluded as mechanistic possibilities based on experimental observations.

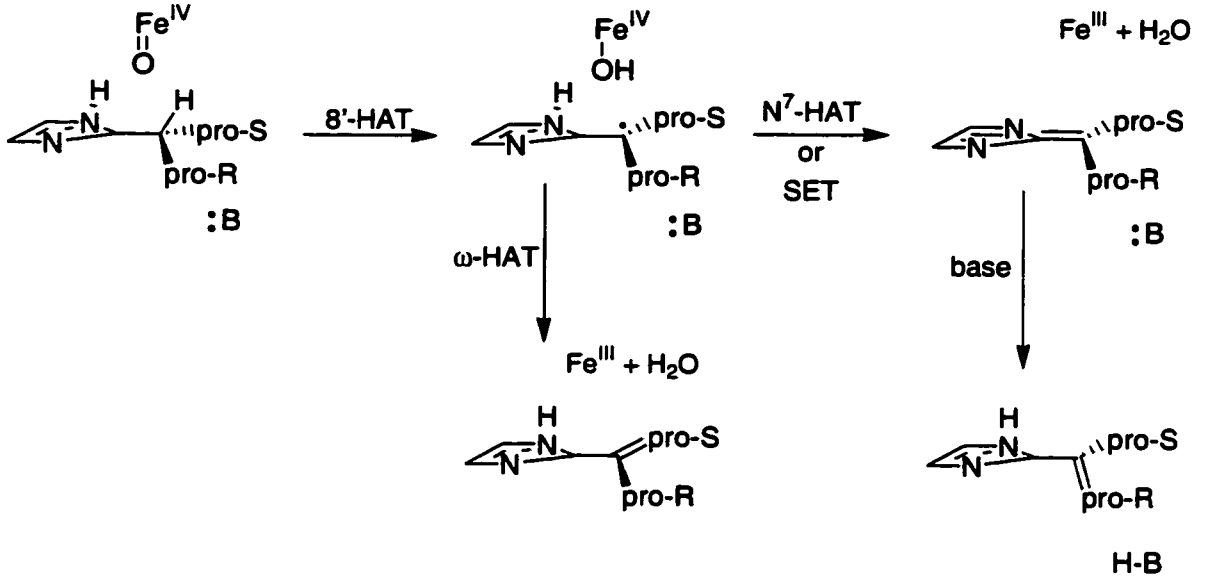

Figure 3.8 Planarity of 8′-carbon radical intermediate of isopropylcyclohexylline **2** and potentially different desaturation mechanisms for pro-R and pro-S methyl groups.

Table 3.10 Observed D_3/D_2 ion ratios of metabolites formed in CYP1A2 incubations with stereoselectively trideuterated isopropylcyclohexylline substrates.

Metabolite	pro-S-D_3-IPC **10**	pro-R-$^{13}CD_3$-IPC **5**
vinyl-IPC **17**	3.19 ± 0.03	7.19 ± 0.08
diol-IPC **18**	3.32 ± 0.05	6.93 ± 0.07
8″-OH-IPC **16**	4.10 ± 0.18	7.88 ± 0.36
Methylketone-cyclohexylline **19**	3.97 ± 0.10	7.76 ± 0.08

Table 3.11 Expected deuterium isotope effects for formation of isopropylcyclohexylline metabolites via oxidation of the individual prochiral methyl groups. [a]

Metabolite	$^{D}V_{exp,pro\text{-}S}$	$^{D}V_{exp,pro\text{-}R}$
vinyl-IPC **17**	4.25 ± 0.18	5.39 ± 0.24
diol-IPC **18**	4.42 ± 0.22	5.20 ± 0.23
8″-OH-IPC **16**	5.47 ± 0.43	5.91 ± 0.47
methylketone-cyclohexylline **19**	5.30 ± 0.32	5.83 ± 0.26

[a] All metabolites shown are believed to originate from the vinyl-IPC **17** desaturation pathway. Therefore, the experimentally determined $^{R/S}P_S$ or $^{R/S}K_{eq}$ for vinyl-IPC **17** and diol-IPC **18** formation are expected to be valid for 8″-OH-IPC **16** and methylketone-cyclohexylline **19** formation.

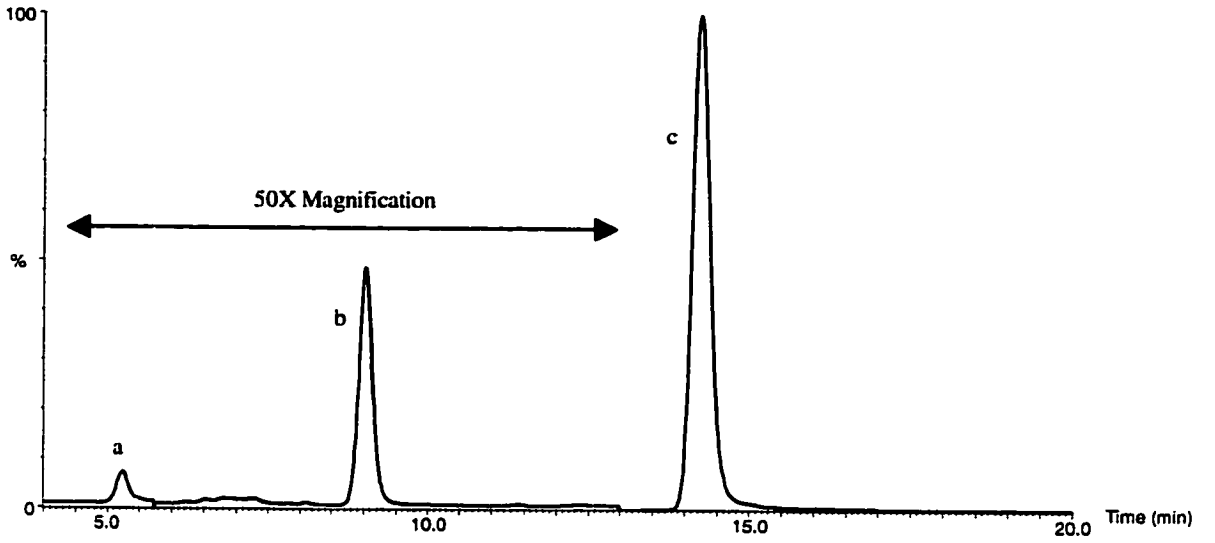

Figure 3.9 ESLC-MS-SIM chromatogram of CYP1A2 (75 pmole Gentest lymphoblast expressed) incubation with cyclopropylmethylcyclohexylline **30** (60 μM). Ion channels shown are those of the protonated parent ions: $[M + H]^+$ 349 (1 - 5.75 min), 333 (5.75 - 13 min), 317 (13 – 20 min), with 50X magnification from 4.0 – 13.0 min: (a) unidentified dual-hydroxylation product (5.5 min), (b) 8′-OH-cyclopropylmethylcyclohexylline **31** (8.9 min), (c) cyclopropylmethylcyclohexylline **30** (14.2 min).

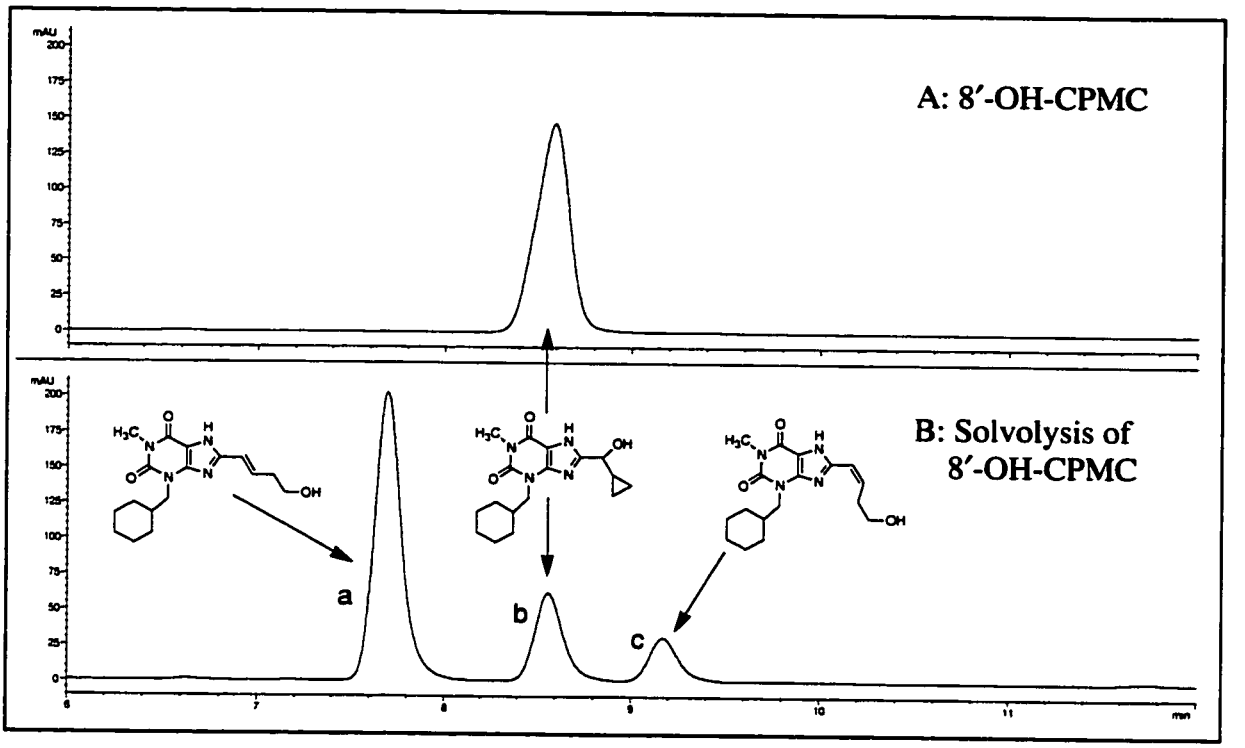

Figure 3.10 HPLC-UV (280 nm) chromatogram of 8′-OH-cyclopropylmethylcyclohexylline **31** solvolysis reaction. Panel A: recrystallized 8′-OH-CPMC **31** (8.5 min). Panel B: Solvolysis of 8′-OH-CPMC **31** after approximately 5 hr at 100 °C in 10% aqueous H_2SO_4, (a) trans-butenol-cyclohexylline **36** (7.7 min), (b) 8′-OH-cyclopropylmethylcyclohexylline **31** (8.5 min), (c) cis-butenol-cyclohexylline (9.2 min) **37**.

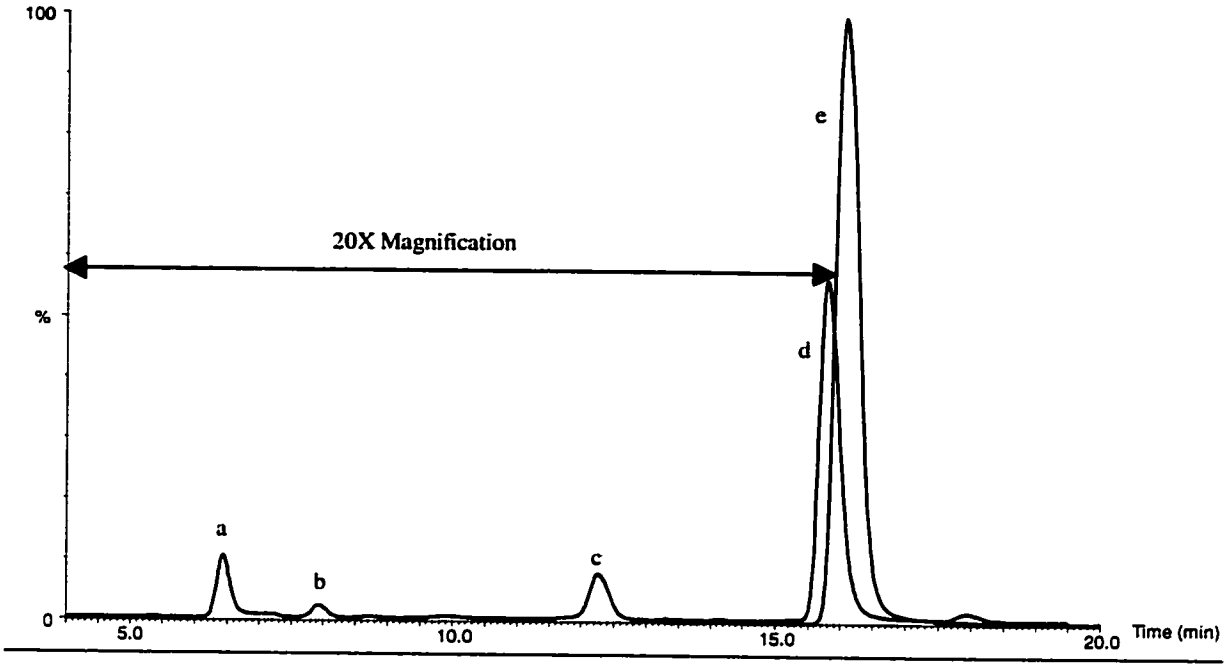

Figure 3.11 ESLC-MS-SIM chromatogram of CYP1A2 incubation (75 pmole Gentest lymphoblast expressed) with cyclobutylcyclohexylline **38** (60 μM). Ion channels shown are those of the protonated parent ions: $[M + H]^+$ 349 (1 - 5.75 min), 333 (5.75 - 13 min), 315 & 317 (13 – 20 min) with 20X magnification of all metabolite peaks: (a) unidentified mono-hydroxylation product (6.4 min), (b) unidentified minor metabolite (7.9 min), (c) 8′-OH-cyclobutylcyclohexylline **39** (12.2 min), (d) unidentified desaturation product (15.8 min), (e) cyclobutylcyclohexylline **38** (16.1 min).

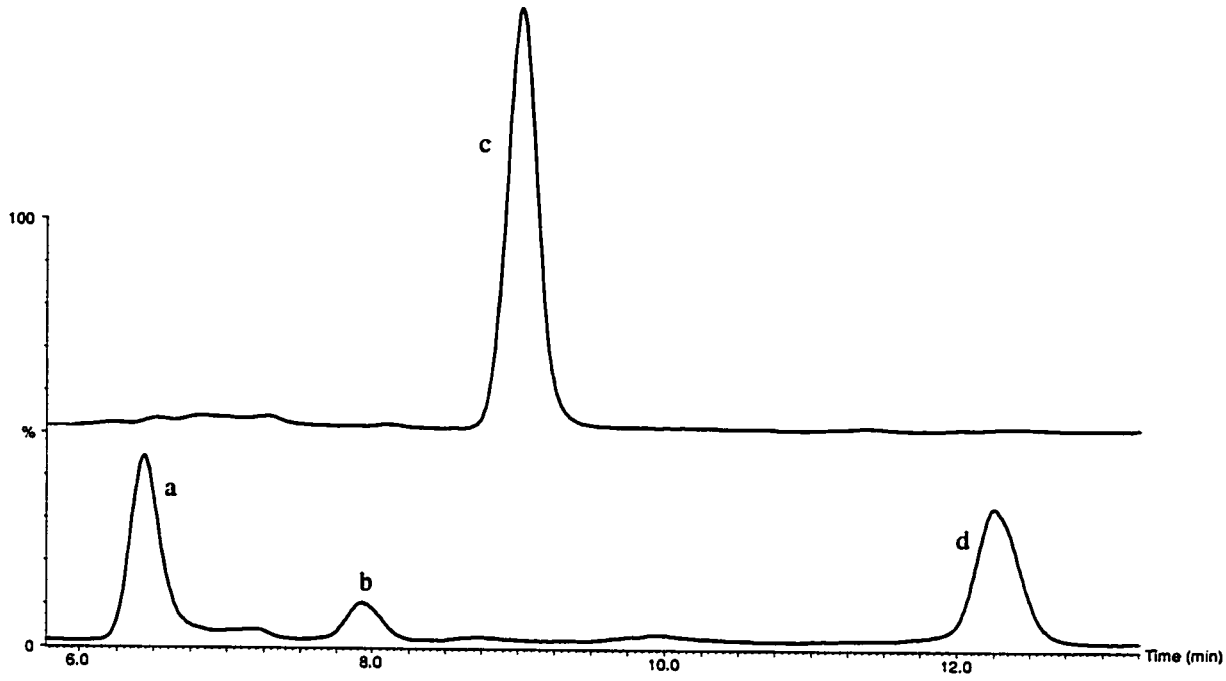

Figure 3.12 Overlay of ESLC-MS-SIM chromatograms of CYP1A2 incubation with cyclopropylmethylcyclohexylline **30** (top) and cyclobutylcyclohexylline **38** (bottom). . Ion channel shown in both chromatograms are those of the protonated carbinol parent ions: $[M + H]^+$ 333: (a) unidentified CBC mono-hydroxylation product (6.4 min), (b) unidentified minor CBC metabolite (7.9 min), (c) 8′-OH-CPMC **31** (8.9 min), (d) 8′-OH-CBC **39** (12.2 min).

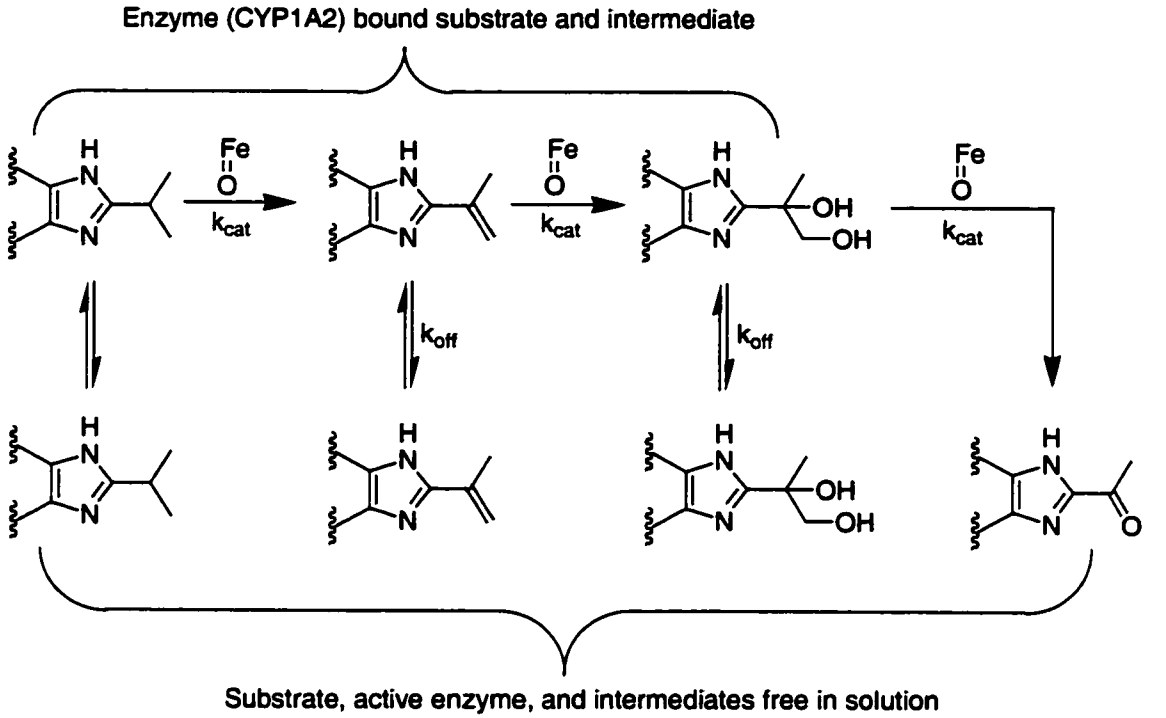

Figure 3.13 Scheme of IPC **2** metabolism by CYP1A2.

Table 3.12 $K_{M,app}$ and $k_{cat,app}$ determination for IPC **2**, vinyl-IPC **17**, and diol-IPC **18** with Gentest lymphoblast expressed CYP1A2 or Gentest CYP1A2 Supersomes. [a]

Lymphoblast Expressed CYP1A2						
	IPC **2**		Vinyl-IPC **17**		Diol-IPC **18**	
Metabolite [b]	$K_{M,app}$ [c]	$k_{cat,app}$ [d]	$K_{M,app}$	$k_{cat,app}$	$K_{M,app}$	$k_{cat,app}$
8'-OH-IPC **15**	24.6 ± 4.1	0.46 ± 0.03	NA [e]	NA	NA	NA
Vinyl-IPC **17**	14.1 ± 1.3	0.88 ± 0.03	NA	NA	NA	NA
Diol-IPC **18**	5.1 ± 0.4	0.60 ± 0.01	2.8 ± 0.3	2.51 ± 0.06	NA	NA
Ketone **19**	BLD [f]	BLD	8.7 ± 2.9	0.73 ± 0.07	ND [g]	ND
Summed [h]	10.3 ± 0.7	1.86 ± 0.04	3.3 ± 0.5	3.2 ± 0.1	NA	NA

CYP1A2 Supersomes						
	IPC **2**		Vinyl-IPC **17**		Diol-IPC **18**	
Metabolite	$K_{M,app}$	$k_{cat,app}$	$K_{M,app}$	$k_{cat,app}$	$K_{M,app}$	$k_{cat,app}$
8'-OH-IPC **15**	9.8 ± 1.6	2.0 ± 0.1	NA	NA	NA	NA
Vinyl-IPC **17**	13.2 ± 0.8	1.7 ± 0.03	NA	NA	NA	NA
Diol-IPC **18**	5.1 ± 0.9	3.8 ± 0.2	1.9 ± 0.2	6.7 ± 0.2	NA	NA
Ketone **19**	8.1 ± 2.7	2.0 ± 0.2	2.8 ± 0.6	3.3 ± 0.1	2800 ± 700	31.4 ± 6.5
Summed	7.4 ± 1.3	9.5 ± 0.5	2.2 ± 0.3	10.0 ± 0.3	NA	NA

[a] Nominal substrate concentrations were used in determinations, except when substrate depletion may have been a factor, in which case the average of the nominal and ending concentration of substrate was used. Plots of each data set fit classic Michaelis-Menton kinetics, in all cases.

[b] K_M and k_{cat} for the substrates were determined in terms of each individual metabolite.

[c] K_M is expressed as μM.

[d] k_{cat} is expressed as pmol/pmol CYP1A2/min.

[e] Not applicable.

[f] Below limit of detection in kinetic studies, where reduced P450 concentrations and incubation length were employed to minimize substrate depletion.

[g] Not determined. For calculations in which a value is needed, the rate of lymphoblast expressed CYP1A2 conversion of diol-IPC **18** to methylketone-cyclohexylline **19** is assumed to be approximately $1/5^{th}$ of CYP1A2 Supersome conversion, based on the difference in total turnover rate between the two enzyme sources.

[h] Values reported for are those obtained after summing the quantities of all metabolites.

Table 3.13 Steady state approximation of the fraction of total enzyme bound to IPC **2** substrate or metabolites in incubations with CYP1A2 from different sources of enzyme. [a]

CYP1A2 Preparation	E * IPC	E * Vinyl-IPC	E * Diol-IPC
Lymphoblast Expressed	0.66	0.24	0.10
Supersomes	0.33	0.57	0.10

[a] values based on ratios of k_{cat} values from Table 3.12.

Table 3.14 Metabolism of ^{15}N-isopropylcyclohexylline by Gentest lymphoblast expressed human CYP1A2 in the presence of unlabeled vinyl-IPC **17** or diol-IPC **18**.

Gentest Lymphoblast Expressed Human CYP1A2 [a]			
^{15}N-IPC + Vinyl-IPC **17**			
Time (min)	0	5	30
^{15}N-IPC	100	Concentration (μM)	
Vinyl-IPC	3.5	2.752 ± 0.136	2.621 ± 0.169
Diol-IPC		0.207 ± 0.003	1.306 ± 0.009
Ketone		0.024 ± 0.002	0.056 ± 0.001
^{15}N-Vinyl-IPC		0.491 ± 0.007	2.356 ± 0.081
^{15}N-Diol-IPC		0.288 ± 0.010	2.539 ± 0.035
^{15}N-Ketone		0.024 ± 0.002	0.126 ± 0.008
^{15}N-8′-OH-IPC		0.092 ± 0.006	0.519 ± 0.011
	A	0.612 ± 0.004	0.469 ± 0.005
	B	1.043 ± 0.002	1.285 ± 0.019
	(1-A*B)/(A*B)	0.567 ± 0.008	0.660 ± 0.013
^{15}N-IPC + Diol-IPC **18**			
Time (min)	0	5	30
^{15}N-IPC	100	Concentration (μM)	
Vinyl-IPC	NA		
Diol-IPC	2	2.290 ± 0.074	2.586 ± 0.022
Ketone		0.0015 ± 0.0005	0.0018 ± 0.0003
^{15}N-Vinyl-IPC		0.568 ± 0.012	2.346 ± 0.041
^{15}N-Diol-IPC		0.417 ± 0.011	2.926 ± 0.106
^{15}N-Ketone		0.025 ± 0.002	0.134 ± 0.006
^{15}N-8′-OH-IPC		0.107 ± 0.001	0.613 ± 0.016
	A	0.942 ± 0.005	0.956 ± 0.003
	B	1.0003 ± 0.0001	1.0004 ± 0.0001
	(1-A*B)/(A*B)	0.061 ± 0.006	0.046 ± 0.004

[a] Incubations (400 μl) contained 40 pmol CYP1A2.

Table 3.15 Metabolism of ^{15}N-isopropylcyclohexylline by Gentest CYP1A2 Supersomes in the presence of unlabeled vinyl-IPC **17** or diol-IPC **18**. [a]

Gentest CYP1A2 Supersomes			
^{15}N-IPC + Vinyl-IPC **17**			
Time (min)	0	5	30
^{15}N-IPC	100	Concentration (μM)	
Vinyl-IPC	3.2	2.977 ± 0.229	3.588 ± 0.217
Diol-IPC		0.140 ± 0.006	0.574 ± 0.009
Ketone		0.064 ± 0.002	0.199 ± 0.005
^{15}N-Vinyl-IPC		0.212 ± 0.001	0.899 ± 0.022
^{15}N-Diol-IPC		0.453 ± 0.019	2.051 ± 0.060
^{15}N-Ketone		0.299 ± 0.012	1.357 ± 0.033
^{15}N-8′-OH-IPC		0.121 ± 0.002	0.550 ± 0.012
	A	0.221 ± 0.006	0.210 ± 0.007
	B	1.035 ± 0.002	1.113 ± 0.007
	(1-A*B)/(A*B)	3.39 ± 0.13	3.28 ± 0.11
^{15}N-IPC + Diol-IPC **18**			
Time (min)	0	5	30
^{15}N-IPC	100	Concentration (μM)	
Vinyl-IPC	NA		
Diol-IPC	2.7	3.782 ± 0.113	4.013 ± 0.238
Ketone		0.0048 ± 0.0005	0.0170 ± 0.0006
^{15}N-Vinyl-IPC		0.243 ± 0.008	0.928 ± 0.039
^{15}N-Diol-IPC		0.705 ± 0.037	2.773 ± 0.114
^{15}N-Ketone		0.333 ± 0.006	1.474 ± 0.041
^{15}N-8′-OH-IPC		0.135 ± 0.007	0.659 ± 0.030
	A	0.678 ± 0.008	0.653 ± 0.003
	B	1.0006 ± 0.0001	1.0021 ± 0.0001
	(1-A*B)/(A*B)	0.473 ± 0.018	0.529 ± 0.007

[a] Incubations (400 μl) contained 10 pmol CYP1A2.

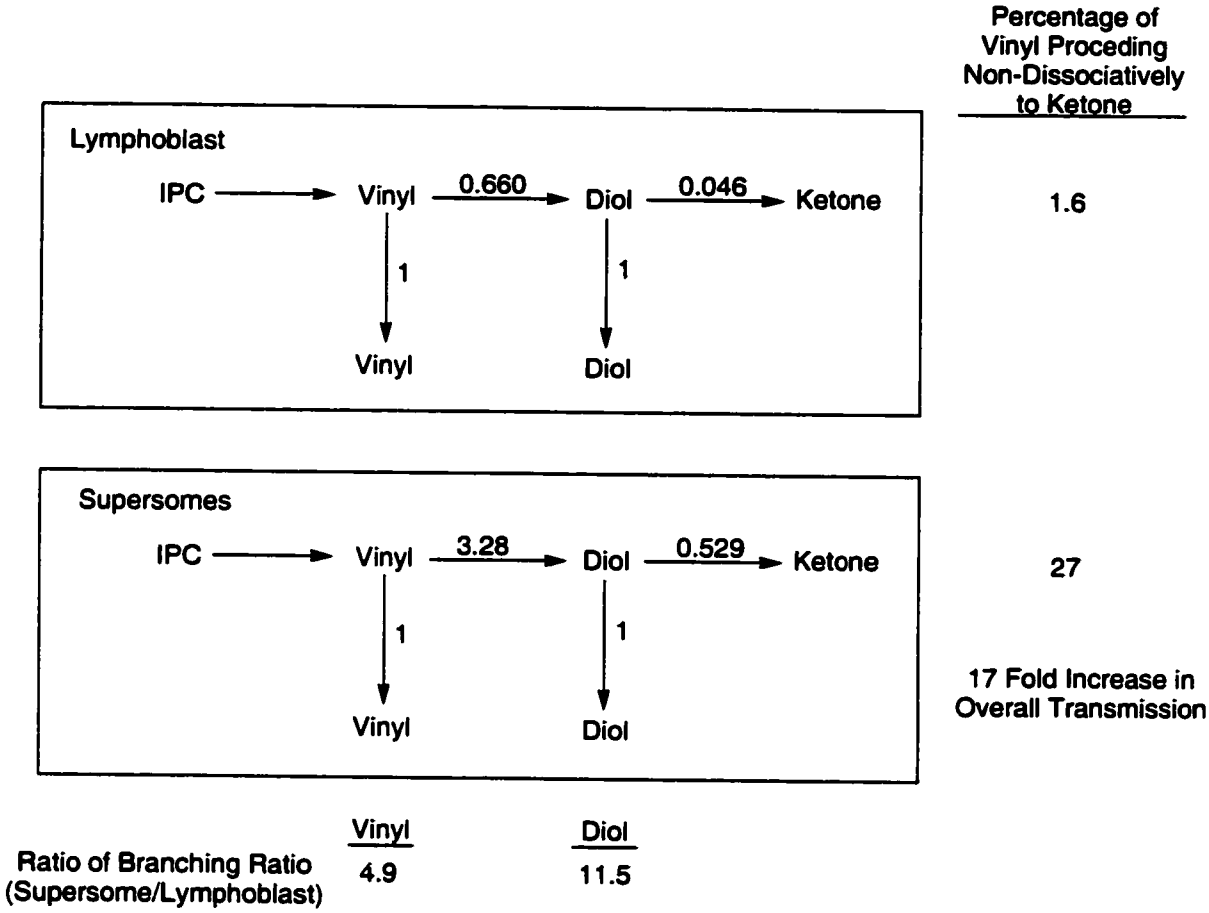

Figure 3.14 Branching ratios (k_{cat}/k_{off}) in Isopropylcyclohexylline metabolism by Gentest Lymphoblast Expressed CYP1A2 and Gentest CYP1A2 Supersomes. [a]

[a] Ratios calculated from isotope-tracing experiments results (see Tables 3.14 and 3.15).

CHAPTER 4

DISCUSSION

Mechanism-based inactivation of cytochromes P450 and substrate desaturation are often mechanistically intertwined metabolic events. CYP1A2-catalyzed desaturation of the highly potent and selective suicide substrates furafylline and cyclohexylline to their imidazomethide reactive intermediates has been proposed to account for formation of both 1:1 protein adduct and 8′-carbinol with the majority of its oxygen sourced to the medium (Figure 1.18) (*89*). CYP1A2-catalyzed dual-HAT or HAT/SET processes, resulting in an uncharged or cationic species, respectively, could form this putative iminium species (Figure 1.21). The absence of H_2O incorporation into the 8′-carbinols from N^7-methylated substrates suggests that reactive intermediate formation is dependent upon N^7-HAT (ie. the dual-HAT mechanism is operative). Though the results of CYP1A2 incubations with the carbocation-probe substrate, CPMC **30**, ostensibly support this mechanism, definitive reactive intermediate charge state assignment is not possible due to the complexity of cyclopropyl carbinyl cation chemistry and the resulting uncertainty about the course of rearrangement under experimental conditions. As expected, no radical rearrangement was observed in incubations of CPMC **30** with CYP1A2. A recent evaluation of 8-phenyltheophylline showed that it is a potent and selective competitive inhibitor of CYP1A2 (K_i = 0.11 μM) (*122*). Therefore, 8-phenylmethyl derivatives of furafylline and cyclohexylline may be CYP1A2 substrates. If benzylic oxidation of these derivatives were to occur, the combined charge/radical stabilizing effects of the adjacent imidazole and phenyl rings may allow spectrometric characterization of the reactive intermediate or the 8′-carbon radical intermediate. Even if 8′-radical delocalization to the phenyl ring were to alter normal metabolism and reactive intermediate formation, the results would still provide useful information by

supporting the oxygen rebound mechanism of hydroxylation. Thus, mechanistic tools remain available for future exploration of 8-alkylxanthine metabolism by CYP1A2.

Extension of the 8-alkyl side chain of FF by one methylene group, as in ethylcyclohexylline, virtually eliminates protein adduction, while desaturation to an iminium reactive intermediate remains evident due to H_2O incorporation into the 8′-carbinol (60%) (*90*). In addition, side chain desaturation to form vinylcyclohexylline emerges as a major metabolic pathway (Figure 1.19). Hence, CYP1A2 seemingly has a propensity for desaturation of 8-alkylxanthines. While desaturation by P450s is not an uncommon process, all evidence from the ethyl substrate supports the hypothesis that vinylcyclohexylline formation is not a typical P450-mediated desaturation reaction; rather, it is the result of rearrangement of the putative desaturated iminium reactive intermediate (Path C in Figure 1.20). Metabolic studies with isopropylcyclohexylline **2** provided a means to confirm these results with ETC, and therefore, test the hypothesis that the dominant side chain desaturation mechanism catalyzed by CYP1A2 on 8-alkylxanthines is an unusual base-catalyzed rearrangement process and a central player in the metabolism/decomposition of the iminium species common to all 8-alkylxathines studied thus far.

Prior investigation in our laboratory has shown that N^7-methylation of 8-alkylxanthines averts reactive intermediate formation (*89*). In accord with this, CYP1A2-catalyzed metabolism of N^7-methyl-isopropylcyclohexylline **20** displays three separate common P450-catalyzed metabolic pathways, all initiated by a distinct mechanistic event (Figures 3.2 and 3.4, Tables 3.1, 3.2, and 3.4): 1) consensus oxygen-rebound hydroxylation of ω and ω-1 positions displaying large normal isotope effects and

complete lack of water incorporation, 2) desaturation of both 8-alkyl side chain prochiral methyl groups, initiated by ω-1 hydrogen atom removal and displaying low normal isotope effects on ω hydrogen atom abstraction ($^{D}V/K$ = 1.2), consistent with consensus dual hydrogen atom transfer, and 3) a final metabolic switching site resulting in N-demethylation. Therefore, as expected, N-methyl-IPC **20** metabolism by CYP1A2 presents a simplified mechanistic baseline for comparison to the complex and atypical metabolism of IPC **2**.

At first glance, the deuterium isotope effect profile of IPC **2** metabolism by CYP1A2 (Table 3.8) suggests that vinyl-IPC **17**, diol-IPC **18**, 8″-OH-IPC **16**, and methylketone cyclohexylline **19** all originate from initial ω-hydrogen atom abstraction, with metabolic switching to the non-isotopically sensitive ω-1 site leading to formation of 8′-OH-IPC **15** from both water and molecular oxygen (Figure 4.1). This scheme would account for the normal isotope effects on all metabolites, save the 8′-carbinols. However, the lack of significant amounts of 8″-OH-IPC **16** formed following ω-HAT casts doubt upon this mechanism, even with attempted rationalization by considering the significant stabilization driving force behind generation of the conjugated vinyl metabolite. The deuterium retention data from incubations with D_1-IPC **4** indicates that at least 75 % of 8″-OH-IPC **16** is derived from vinyl-IPC **17**. In this case, only 0.1 % of all ω-HAT would result in 8″-OH-IPC **16** formation; an unlikely proposition. As a result, while the scheme shown in figure 4.1 may contribute, a more probable mechanism for IPC **2** metabolism by CYP1A2 is shown in figure 3.6.

In figure 3.6, the intermolecular deuterium isotope effect analysis of IPC metabolism by CYP1A2 using ω D_6-IPC **3** (Table 3.8) is interpreted as indicating isotopically sensitive branching between vinyl-IPC **17** and 8′-OH-IPC **15** from both water and molecular oxygen. Thus, unlike the mechanism proposed for vinylcyclohexylline formation from ETC, both dual hydrogen atom transfer and rearrangement of the iminium reactive intermediate evidently contribute to vinyl-IPC **17** formation. The similarity in isotope effects on the 8′-carbinols formation may lead to the conclusion that dual hydrogen atom transfer is the sole mechanism of IPC **2** side chain desaturation, as discussed in the introduction. However, this possibility is ruled out based on the large normal isotope effects for ω hydrogen atom abstraction (4.3 & 5.4) calculated from these results, which are inconsistent with literature values for the second HAT of a dual HAT desaturation process ($^{D}V/K \approx 1$-2) (*32*, *35*). These isotope effect values suggest that a significant proportion of IPC side chain desaturation must be attributable to a mechanism other than dual HAT. Unfortunately, the composite nature of these intermolecular isotope effects (both mechanisms contribute to the normal isotope effect on olefin formation) prohibited determination of the intrinsic isotope effect for the individual desaturation mechanisms.

Attempts to disentangle the intrinsic isotope effects for each separate desaturation mechanism using deuterium isotope effect analysis with stereoselectively trideuterated IPC substrates (**5** and **10**, Table 3.11, and Figure 3.8) showed that the isotope effects associated with desaturation of both prochiral methyl groups of IPC **2** are large and normal (4.3 and 5.4). Thus, in contrast to the substrate/enzyme interaction hypothesis shown in figure 3.8, the fixed planar orientation of the 8′-radical and iminium

intermediates apparently allows each active agent (Fe^{IV}-OH or active site base) nearly equal access to both methyl groups. That is, there is no clear demarcation of the desaturation mechanism due to stereochemistry; both prochiral methyl groups of IPC appear to experience similar desaturation processes, which display isotope effects that are not consistent with a dual hydrogen atom transfer mechanism. In the end, deuterium isotope effect analysis leaves us with a scenario in which the magnitudes of all isotope effects for vinyl-IPC **17** formation are consistent with base-catalyzed rearrangement of the iminium reactive intermediate, as in the mechanism proposed for ETC, while the inverse isotope effect on 8′-carbinol from oxygen rebound suggests that consensus dual hydrogen atom transfer is a participating process.

An intriguing mechanistic possibility, which may explain the inconsistent isotope effect results, is that like ETC, consensus dual HAT desaturation (path A in figure 3.7) is not operative in IPC metabolism; rather, we have mixed sources of water in the active site giving misleading results. With the preponderance of desaturation reactions catalyzed by CYP1A2 on 8-alkylxanthines, each of which will generate two water molecules with oxygen originating from molecular oxygen (one while generating the active iron-oxene oxidant as shown in figure 1.3, and one during the desaturation reaction), it seems likely that a portion of the water present in the active site would be derived from molecular oxygen (depending upon the rate of exchange with the external bulk medium). This "sham-H_2O" scenario (Figure 4.2) would overestimate the amount of 8′-carbinol from oxygen rebound, and account for the large inverse isotope effect on formation of this metabolite. In the extreme case, all observed 8′-carbinol with its oxygen sourced to O_2 could actually be from incorporation of sham H_2O, meaning that all IPC **2** metabolism by

CYP1A2 involves a desaturation reaction, with complete evasion of consensus P450-catalyzed oxygen rebound hydroxylation. The similarity and the magnitude of the inverse isotope effects on 8′-carbinol formation from O_2 and H_2O incorporation support both having the same isotopically sensitive branching point at the iminium reactive intermediate. In addition, the highly stereoselective CYP1A2-catalyzed formation of ETC's (S)-8′-carbinol from both oxygen sources supports the sham-water mechanism (*90*); both processes occur on the same face of the desaturated intermediate, suggesting that the active site water is in close proximity to the heme, and therefore could be a water molecule derived from the P450 catalytic cycle. However, an explanation for the observation of sham-H_2O incorporation with IPC **2** but not with ETC (no isotope effect on 8′-carbinol from O_2) is not forthcoming. While we have no clear means at this time to differentiate between 8′-OH-IPC **15** containing oxygen from molecular oxygen via P450 oxygen rebound hydroxylation or from sham-H_2O added to the reactive intermediate, in theory, water incorporation into diol metabolites would provide a measure of the sham-H_2O/ H_2O ratio within the CYP1A2 active site.

Isotope-tracing experiments (Tables 3.14 and 3.15) with IPC indicate that at saturating substrate concentrations virtually 100% of the methylketone metabolite **19** is formed as a result of non-dissociative sequential metabolism of diol-IPC **18**. Thus, a portion of the putative epoxide formed from vinyl-IPC **17** must be hydrolyzed to the diol within the enzyme active site. Interestingly, the discounted $P450_{SCC}$ mechanism of cholesterol conversion to pregnenolone proposed by Kraaipoel, *et al.* (see Figure 1.15) bears surprising similarities to this possible mechanism of IPC **2** metabolism by CYP1A2 (*61*). In both cases, epoxide hydrolysis by active site water is proposed to account for

diol metabolite formation. However, contrary to what would be expected if sham-H_2O were present, oxygen-tracing experiments with IPC show that 100% of one equivalent of $H_2{}^{18}O$ is incorporated into diol-IPC **18**. A key difference in the two enzymatic systems is the amount of metabolic intermediate "leakage" from the catalytic sequence. In the case of $P450_{SCC}$, the highly directed metabolism of cholesterol ensures that very little of the intermediates are released *in route* to pregnenolone formation. Therefore, the vast majority of 20,22-epoxycholesterol hydrolysis must take place within the $P450_{SCC}$ active site, allowing for an accurate sham-H_2O/H_2O ratio measurement (0.67) (*60*). CYP1A2-catalyzed conversion of IPC **2** to methylketone-cyclohexylline **19**, on the other hand, is very "leaky," with less than 2% IPC substrate metabolism resulting in conversion to the ketone end product when incubated with Gentest lymphoblast expressed CYP1A2. The oxygen tracing experiments with IPC may then reflect this leakiness and indicate that most IPC epoxide hydrolysis occurs in the bulk solvent. Interestingly, N-methyl-diol-IPC **29** shows only 68% $H_2{}^{18}O$ incorporation (Tables 3.1 and 3.6, respectively). It is also interesting to note the nearly equivalent $H_2{}^{18}O$ incorporation value for 8′-OH-CPMC **31** (64 ± 8 %). Therefore, it is a distinct possibility that the oxygen-tracing results with N-methyl-diol-IPC **29** and 8′-OH-CPMC **31** provide a measure of sham-H_2O proportions present in the enzyme active site. The validity of using N-methyl-IPC and CPMC results to draw conclusions about IPC/CYP1A2 sham-water levels is uncertain though, because CYP1A2 three-dimensional modeling studies indicate that the number and location of active site water molecules is substrate dependent (*123*).

Uncertainties aside, a potential explanation for the difference between diol-IPC **18** and N-methyl-diol-IPC **29** water incorporation is alluded to by the difference in

metabolic profile between IPC **2** and N-methyl-IPC **20**. Only CYP1A2-catalyzed metabolism of IPC **2** forms detectable quantities of the methylketone metabolite **19**. Because ketone formation is dependent upon retention of the diol metabolite within the active site for additional catalytic processing, it is possible that, in the case of IPC **2**, epoxide decomposition is accomplished by two separate processes 1) external (outside enzyme active site) hydrolysis by H_2O, resulting in 100% $H_2{}^{18}O$ incorporation into diol-IPC **18**, and 2) internal (inside enzyme active site) decomposition by interception of Fe-O-O^- as it is generated for the next catalytic cycle (Figure 4.3). In this case, diol is formed solely from released epoxide, while ketone is formed from intercepted epoxide that is effectively anchored within the active site. It is notable that the intermediate formed by Fe-O-O^- addition to the epoxide is the same intermediate that would be expected for heterolytic C-C bond cleavage, as proposed for the mechanism of $P450_{SCC}$ (Figure 1.16). On the other hand, no N-methyl-ketone metabolite formation has been detected from the N-methyl substrate. Thus, if this mechanism is operative, the lack of putative N-methyl-epoxide intermediate interception by the iron-peroxide anion may permit its hydrolysis within the enzyme active site by sham-H_2O, accounting for the less than complete $H_2{}^{18}O$ incorporation into N-methyl-diol-IPC **29**. Evidence already exists for differences in active site binding orientations between IPC **2** and N-methyl-IPC **20**, with their opposite prochiral stereoselectivities of desaturation and the dramatic increases in cyclohexyl ring hydroxylation products with the N-methylated substrate. In the case of IPC, its binding orientations may also promote epoxide interception by Fe-O-O^-.

Oxygen-tracing experiments of IPC metabolism by Gentest lymphoblast expressed CYP1A2 and CYP1A2 Supersomes (results not shown) show different

amounts of H_2O incorporation into 8'-OH-IPC **15** (lymphoblasts = 40 %, Supersomes = 25 %). One explanation for this observation is that the faster CYP1A2 turnover in Supersomes compared to lymphoblast microsomes somehow results in reduced exchange of active site water with the medium, leading to Supersome CYP1A2 active site enrichment with water from the P450 catalytic cycle. Comparable experiments with N-methyl-IPC **20** monitoring N-methyl-diol $H_2{}^{18}O$ incorporation would possibly provide more evidence for sham-H_2O residence in the active site and it's incorporation into metabolites.

Finally, additional studies to determine the stereochemistry of the diol products of IPC and N-methyl-IPC may prove useful in testing the sham-H_2O incorporation hypothesis. Hydrolysis of the epoxide products in the bulk solvent would be expected to result in a racemic mixture of the diol stereoisomers, while any degree of stereochemical control would support the role of active site water. Thus, if the oxygen-tracing results with N-methyl-diol-IPC do provide a measure of sham-H_2O within the enzyme active site, the stereochemistry of the ^{16}O- and ^{18}O-containing N-methyl-diol should be similar and not racemic. Additionally, if the oxygen-tracing results with diol-IPC are a result of IPC epoxide hydrolysis after leaving the active site, a racemic diol mixture should be observed.

Even without the sham water mechanism, all evidence indicates that the predominant mechanism of 8-alkylxanthine side chain desaturation involves base-catalyzed rearrangement of the iminium reactive intermediate. The mechanism most consistent with the observed isotope effects and the structure of the putative iminium reactive intermediate is $(E_1cB)_I$, or (Elimination, first-order, conjugate-base)Irreversible

(*124*). This mechanism, in general, involves removal of a proton by a base and subsequent loss of a leaving group:

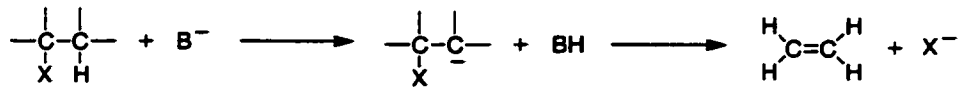

Because loss of the leaving group is facile, proton abstraction becomes rate-limiting. In the case of IPC **2** and ETC, base-catalyzed proton removal would result in rearrangement of the reactive intermediate, rather than loss of a leaving group. Rearrangement of the imidazomethide-type intermediate of IPC **2** and ETC forms the respective olefin metabolites, which are relatively stable products. Thus, the reverse reaction should be minimal, and proton removal is again rate-limiting. From this, the isotope effects on the base-catalyzed rearrangement of the reactive intermediates should not be masked and the magnitude of the isotope effect should directly reflect the transition state structure of the mechanism. General base catalyzed removal of protons from carbon acids reveal maximum isotope effects when the difference in pK_a between the catalyst and substrate is close to zero. Finally, the ranges of isotope effects for proton and hydrogen atom transfer are large and show no consistent difference between the two types of reactions. From this, the observed isotope effects for base-catalyzed rearrangement of the reactive intermediate of IPC (4.2-5.4) and ETC (5-6) indicate a symmetrical transition state and therefore, participation of a base whose conjugate acid has a pK_a nearly equivalent to that of the ω proton. Unfortunately, at this point, we do not have an estimate of this pK_a, however formation of the conjugated double bond in vinyl-IPC **17** would be expected to

provide a considerable driving force for proton removal, and therefore, the pK_a of the a terminal methyl group proton would be expected to be considerably lower than a normal alkyl methyl group. Accordingly, any of the active site amino acids with a conjugate acid pK_a in the physiological range, such as glutamate and aspartate, are potential base catalysts of iminium reactive intermediate rearrangement.

While the highly lipophilic and membrane-associated nature of mammalian P450s has impeded crystallization efforts, three-dimensional models based on sequence homologies with several crystallized water-soluble bacterial isoforms have provided some insight into the active site architecture. Homology modeling and mutational studies on CYP1A2 enzyme/substrate interactions have predicted a number of amino acids with nucleophilic/basic side chains within the active site (*123, 125-127*). For example, a model of furafylline within the human CYP1A2 active site by Lewis, *et al.* (Figure 4.4) shows furafylline held in position for oxidation at the 8-methyl group by hydrogen bonds with several threonine residues (Thr78, Thr87, and Thr438) and by π-π stacking with aromatic amino acid side chains (Tyr437 and Phe181) (*126*). Additional polar active site residues, not indicated in figure 4.4, include the highly conserved Thr321 and Asp320, which are believed to participate in the proton delivery conduit necessary for heterolytic cleavage of the O-O bond to generate the iron-oxene species (see Figure 1.3) (*128, 129*). Finally, mutational studies conducted by Hadjokar, *et al.* indicate Arg108, Asp313, and Thr385 are critical sites of substrate/enzyme interaction (*127*). Therefore, while there is some conjecture on the active site architecture and the amino acids that interact with or are in the vicinity of substrates, the general statement that several potential active site bases/nucleophiles are in close proximity with the substrate can easily be made. These

same amino acids could be the active participants in protein adduction with FF and CH and in base-catalyzed proton removal from the iminium reactive intermediate of ETC and IPC. Unfortunately, efforts to isolate and characterize the CYP1A2-furafylline protein adduct have been unsuccessful. If identification of the adducting residue were accomplished, CYP1A2 mutation studies and knowledge of its pK_a would clearly aid determination of its role in the proposed base-catalyzed rearrangement of ETC and IPC.

To this point, we have focused on active site amino acid side chains as the putative base involved in 8-alkylxanthine metabolism. However, the catalytic power of P450s is dependent on the generation of highly reactive heme-oxygen species. In addition to the iron-oxene species, a growing body of evidence implicates the participation of the iron-peroxide anion and iron-hydroperoxide species in some P450-catalyzed reactions (Figure 1.13) (*49-53*). In light of this, even though 1:1 protein adduct formation in CYP1A2-catalyzed metabolism of FF and CH dictates the participation of active site amino acid side chains, it behooves us to consider the possibility that some of the observed metabolic reactions are due to the spectrum of reactions potentially catalyzed by the multiple heme-oxygen species of the P450 catalytic cycle. In particular, the nucleophilic nature of the iron-peroxide anion, Fe-O-O$^-$ (see Figure 1.13), makes it an attractive alternative active site base for ω proton removal from the iminium reactive intermediate of IPC and ETC (Figure 4.5). Interestingly, as shown in figure 4.5, ω proton removal by Fe-O-O$^-$ would generate the iron-hydroperoxy species (Fe-O-O-H), which is implicated in epoxidation reactions (Figure 1.13) (*49-53*). In this way, the reactant necessary for further oxidation of the olefin metabolite to the putative epoxide is generated in the process of olefin formation. The lack of dual HAT desaturation of ETC

and the lack of differentiation between desaturation mechanisms based on IPC substrate stereochemistry lend credence to this hypothesis; similar stereochemical constraints would apply to both dual HAT by Fe=O/Fe-OH and reactive intermediate ω proton removal by Fe-O-O$^{\cdot}$, while the difference in "reach" of the Fe-O-O$^{\cdot}$ and Fe-OH species would lead to a difference in reaction sites available to the oxidants (Figure 4.6). CYP1A2's proclivity for reactive intermediate formation with all studied 8-alkylxanthines suggests that the imidazole nitrogen (N^7) is readily accessible to the Fe-OH species generated after initial 8′-HAT, and delocalization of the 8′-radical to the adjacent imidazole ring would promote this reaction. Radical delocalization would also require that the 8-alkyl side chain adopt a planar sp^2-hybridization structure from the original tetrahedral sp^3-hybridized configuration (Figures 4.6 and 3.8). In this way, one of the methyl groups of IPC (presumably pro-S, based on the slightly lower isotope effect for desaturation determined with the stereoselectively labeled substrates, Table 3.11) may be close enough to permit subsequent ω-HAT by Fe-OH, and thus direct olefin formation via dual HAT (Figure 4.6a). However, the majority of metabolic flux is directed to the planar reactive intermediate, and as shown in figure 4.6a, the greater "reach" of Fe-O-O$^{\cdot}$, over that of Fe-OH, would allow it access to both methyl groups of IPC for ω proton removal. Therefore, consistent with our original hypothesis, the additional methyl group of IPC may allow us to observe both desaturation processes after all, albeit both are catalyzed from the same location by different heme iron-oxygen species. This same logic may be applied to the lack of dual HAT desaturation of ETC (Figure 4.6b). The terminal methyl group of ETC may be oriented such that, even after initial 8′-HAT, it is

inaccessible to the Fe-OH species. Therefore, only reactive intermediate formation followed by ω proton removal by Fe-O-O$^-$ is observed.

Lastly, we consider intramolecular base-catalyzed rearrangement of the iminium reactive intermediate to the olefin (Figure 4.7). This mechanism is appealing for a couple of reasons 1) formation of a 5-member ring transition state should encourage such a reaction and 2) base-catalyzed rearrangement would be a substrate-dependent phenomenon, thus enabling testing of the mechanism. Vinylcyclohexylline formation and H_2O incorporation into the 8′-carbinol has been observed in incubations of ETC with different CYPs and CYP preparations (unpublished results), suggesting that reactive intermediate formation is not limited to CYP1A2-catalyzed metabolism. If so, and if reactive intermediate rearrangement is an intramolecular process, similar isotope effects as with CYP1A2 should be observed. Unfortunately, deuterium isotope effect analysis of ETC and IPC metabolism by other P450s has not yet been carried out. Finally, as discussed above, the nearly equivalent isotope effects for desaturation of the prochiral methyl groups of IPC, as well as the isotopically sensitive switching between methyl groups, suggests that the oxidant responsible for catalysis of ω proton removal must have access to both methyl groups. Because the planarity of the reactive intermediate would not permit the N^7 imidazole ring nitrogen access to both methyl groups of IPC, in order for this intramolecular process to occur, either nitrogen atom of the imidazole ring must be able to act as the base.

Figure 4.8 compiles all of the more feasible mechanistic possibilities for CYP1A2-mediated metabolism of IPC **2** into one comprehensive scheme, which will be a useful tool for future mechanistic investigation. With the discussion of multiple oxidants

participating in ETC and IPC metabolism, future experiments will most likely include CYP1A2 mutation studies. For instance, if Fe-O-O$^-$ and/or Fe-O-O-H are participating oxidants, mutation of the active site amino acids believed to be involved in the proton shuttle necessary for generation of the iron-oxene species (Thr321 and Asp320) would be expected to change product ratios. However, the sheer complexity of the IPC/CYP1A2 system makes prediction of the results difficult, at best. Similar experiments with ETC would provide a simplified starting point because of the absence of sham-H_2O incorporation and dual HAT ethyl side chain desaturation. The information gained from studies with ETC and mutated CYP1A2 would aid interpretation of the undoubtedly complex results with IPC.

The unusual nature of 8-alkylxanthine metabolism by CYP1A2 is not limited to its propensity for desaturation and its atypical catalytic mechanisms. Incubations of CYP1A2 with saturating concentrations of IPC **2** and ETC produce significant amounts of multiply oxidized metabolites (see Figures 3.6 and 1.19, respectively), implicating non-dissociative sequential metabolism, an uncommon observation with xenobiotic metabolizing P450 enzymes. Evidence from the literature (*72-74*), as well as from unpublished results with ETC, suggests that the amount of non-dissociative sequential metabolism catalyzed by cytochromes P450 is dependent on the concentration of NADPH P450-reductase and on the rate of reducing equivalent transfer from the reductase to the P450. Thus, a competition exists between intermediate release (k_{off}) and rearming of the enzyme to catalyze the formation of the subsequent metabolite (k_{cat}) (see Figure 3.13). Characterization of IPC **2** metabolism with Gentest lymphoblast expressed CYP1A2 and Gentest CYP1A2 Supersomes, allowed us to explore the effects of electron

transfer rate on the observed sequential metabolism. A combination of kinetic studies with each intermediate (Table 3.12) and isotope tracing experiments (Tables 3.14 and 3.15) reveal that CYP1A2 Supersomes' higher activity generates a disproportionately large improvement in the efficiency of diol-IPC conversion to ketone, over that of vinyl-IPC conversion to diol-IPC and the overall rate of metabolism. This interesting result suggests that the electron transfer rate from NADPH P450-reductase affects individual metabolic steps and mechanisms differently. The mechanistic implications of these findings are not clear, in particular with the possibility that a number of the metabolic reactions are catalyzed by non-consensus mechanisms. Kinetic modeling experiments are being conducted to further explore the non-dissociative sequential metabolism of IPC by CYP1A2.

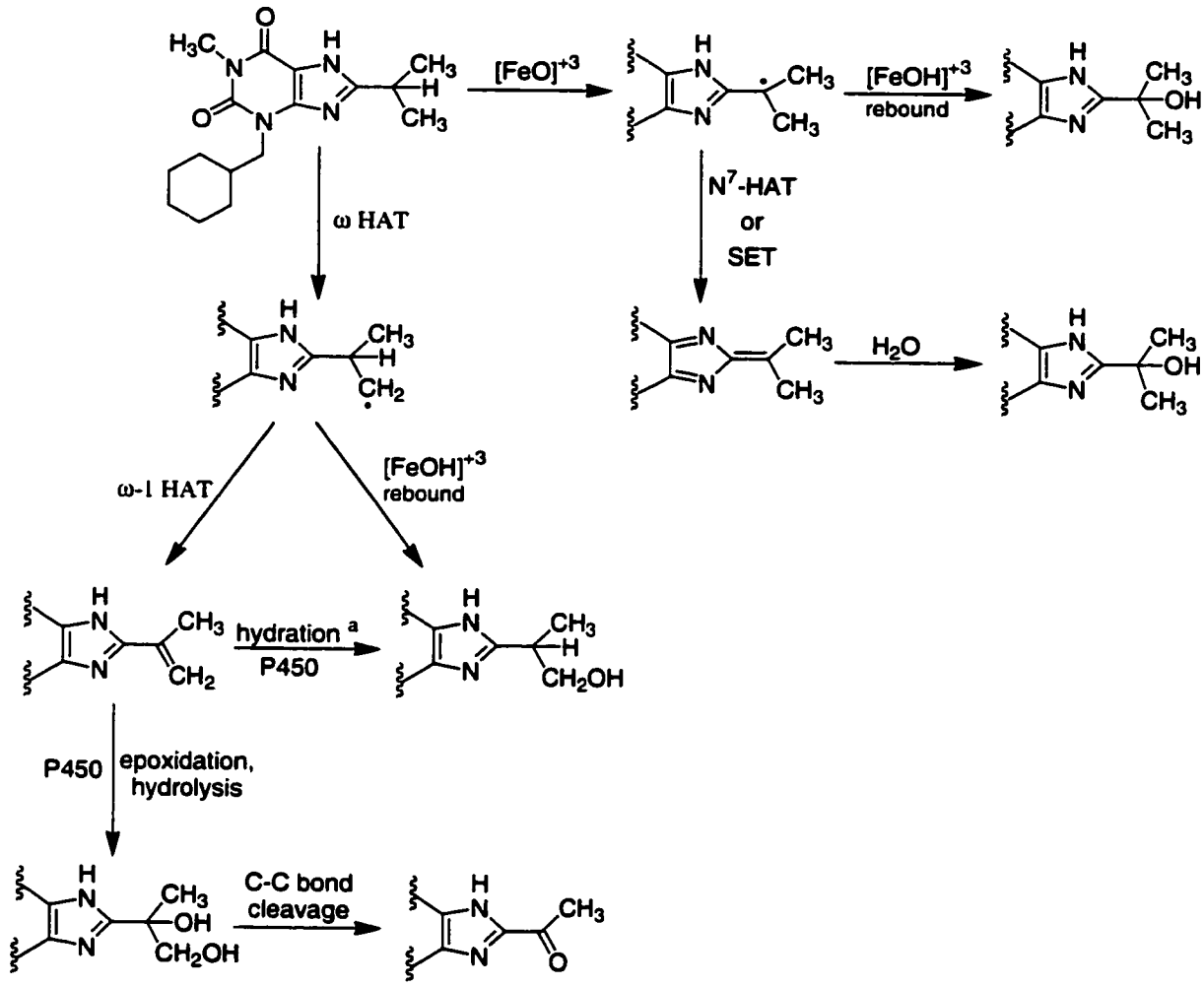

Figure 4.1 Improbable contributing mechanism of IPC 2 metabolism by CYP1A2 initiated by either ω or ω-1 hydrogen atom transfer.

[a] Alkene hydration mechanism like that proposed for Ezlopitant (*91*).

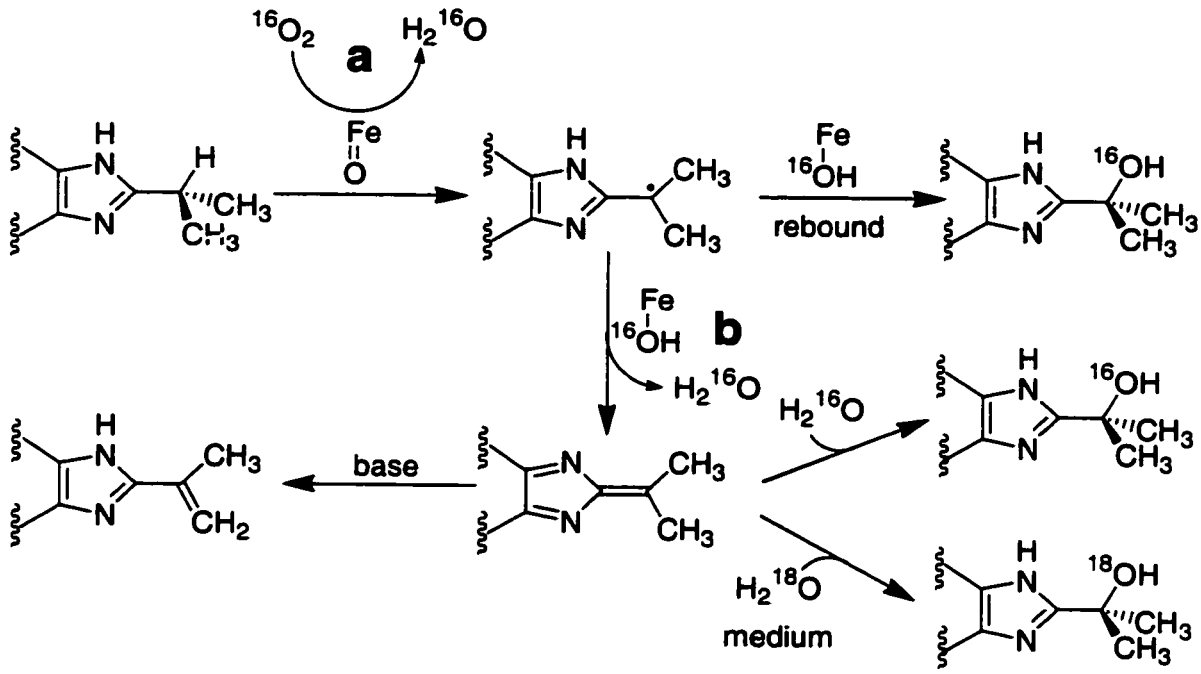

Figure 4.2 Sham-H_2O incorporation hypothesis for CYP1A2-catalyzed metabolism of isopropylcyclohexylline **2**. H_2O generated from the P450 catalytic cycle (**a**, see figure 1.3) and from the CYP-catalyzed desaturation reaction (**b**) results in enrichment of the enzyme active site with water molecules that stem from molecular oxygen. This in turn, leads to over estimation of 8′-OH-IPC from oxygen rebound.

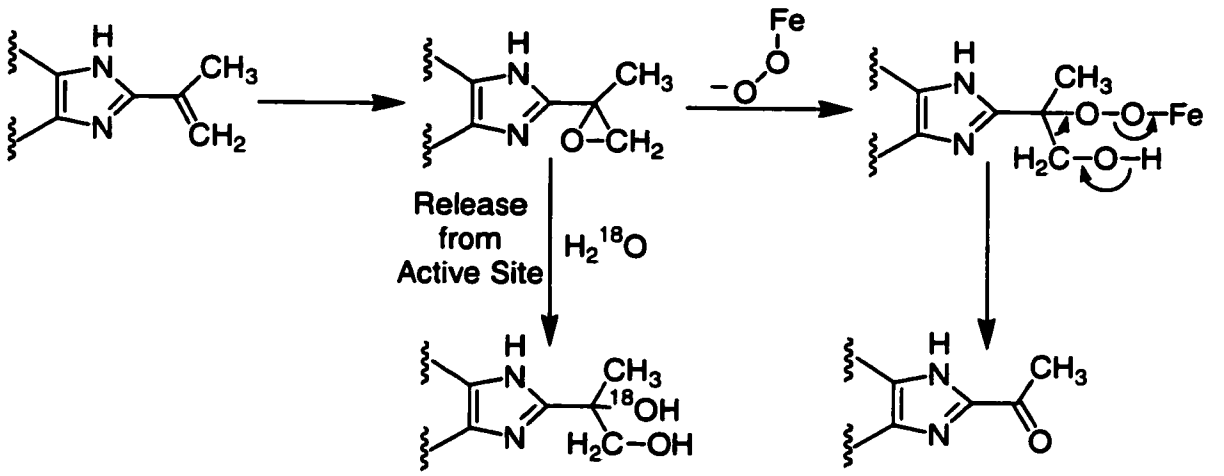

Figure 4.3 Possible mechanisms of IPC **2** epoxide decomposition 1) hydrolysis by solvent water after release from the active site, or 2) interception and active site retention by the iron-peroxy species of the P450 catalytic cycle. Ketone formation is shown to proceed in a similar manner to the heterolytic mechanism proposed for $P450_{SCC}$, as shown in figure 1.16.

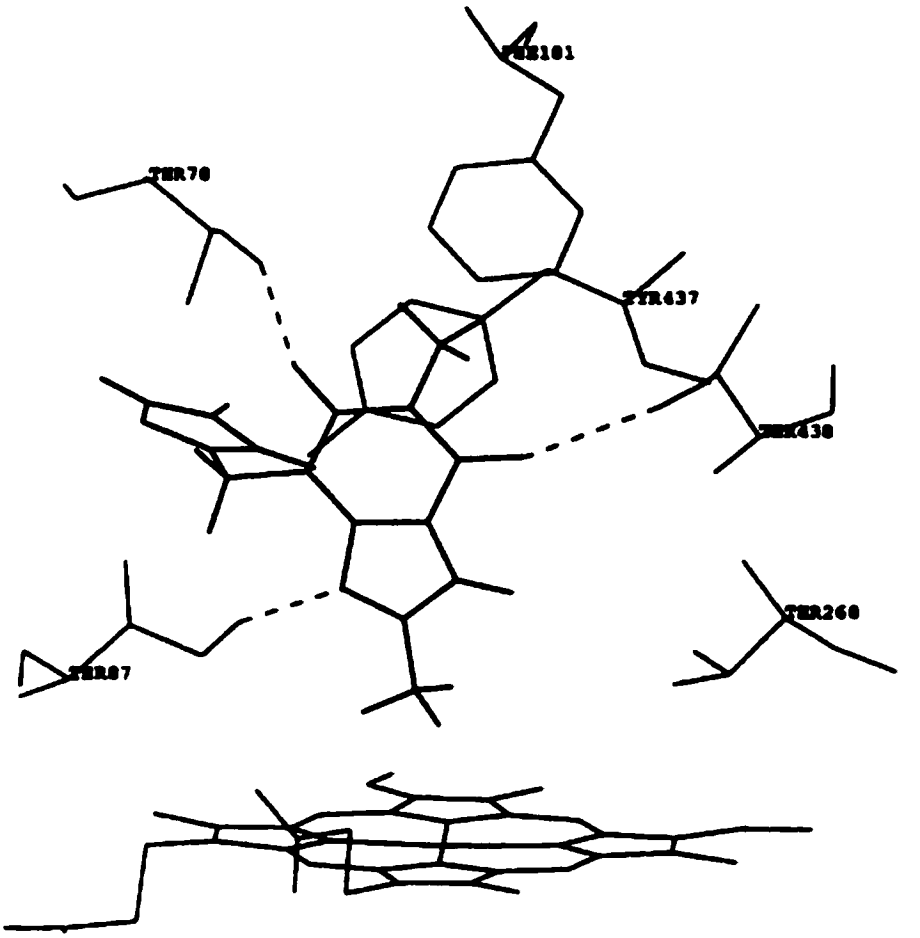

Figure 4.4 Molecular modeling of furafylline within the human CYP1A2 active site, showing protein amino acids that could act as an active site base for rearrangement or quenching of the desaturated iminium reactive intermediate.

[a] Figure taken from (*126*).

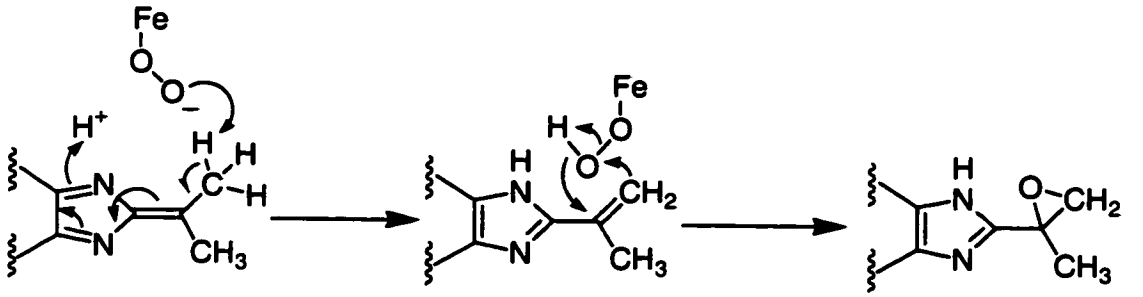

Figure 4.5 Base-catalyzed rearrangement of the desaturated iminium reactive intermediate with the iron-peroxide anion, resulting in formation of the iron-hydroperoxy species, which may be the active epoxidation species, as indicated in figure 1.13.

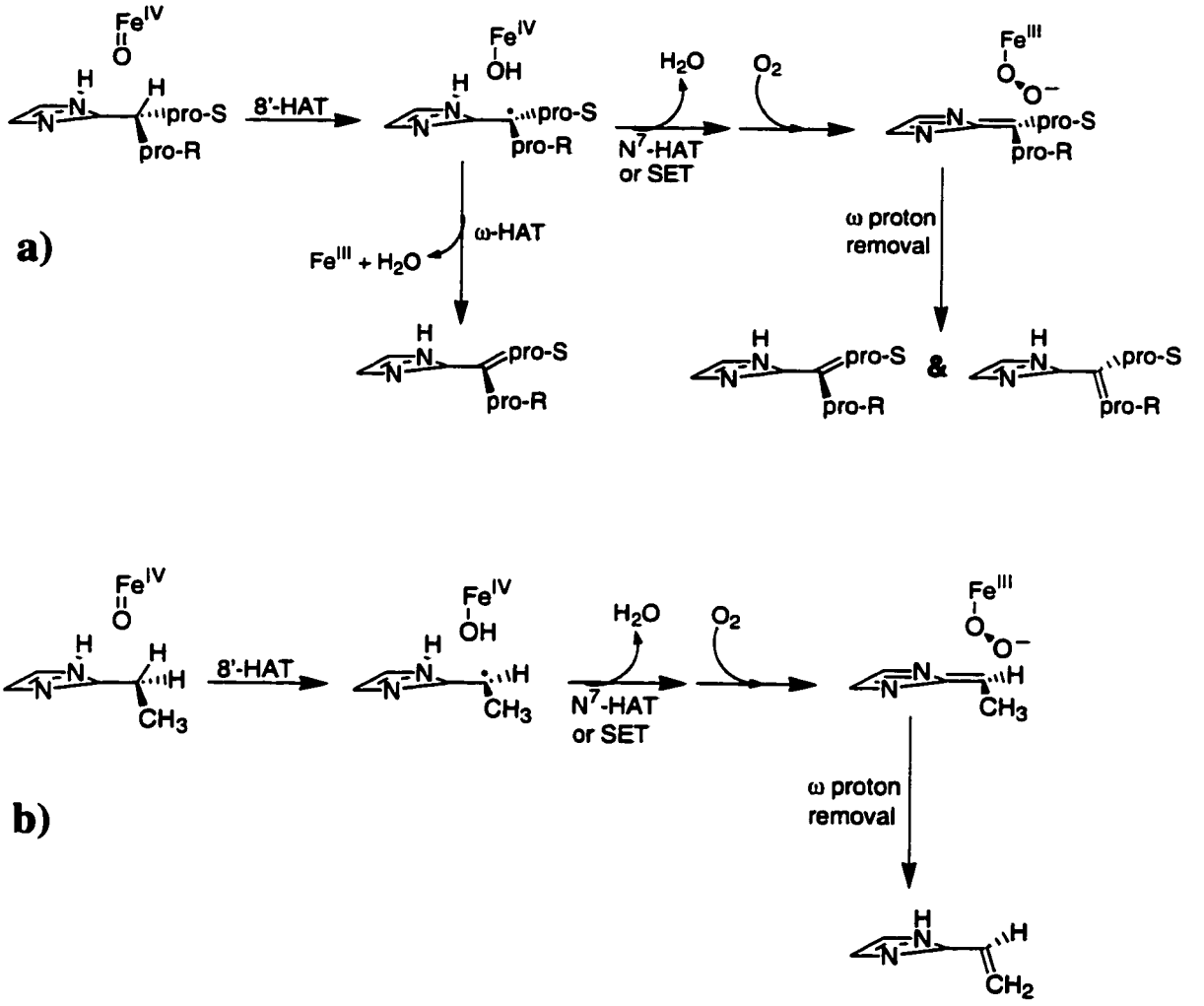

Figure 4.6 Mechanism of 8-alkylxanthine side chain desaturation by CYP1A2 dictated by intermediate orientation in relation to two possible P450 heme iron-oxygen species. a) IPC **2** pro-S methyl group orientation allows for dual HAT desaturation, potentially accounting for its slightly lower desaturation isotope effect (table 3.11), while the increased reach of Fe-O-O$^{\cdot}$ enables ω proton removal from both prochiral methyl groups. b) ETC terminal methyl group orientation prevents dual HAT desaturation, while allowing base-catalyzed rearrangement of the iminium reactive intermediate by Fe-O-O$^{\cdot}$.

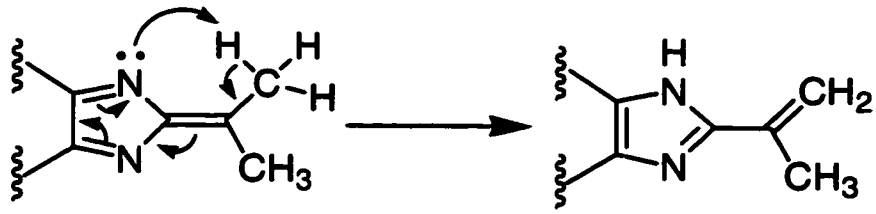

Figure 4.7 Intramolecular base-catalyzed rearrangement of the desaturated iminium reactive intermediate of IPC **2**.

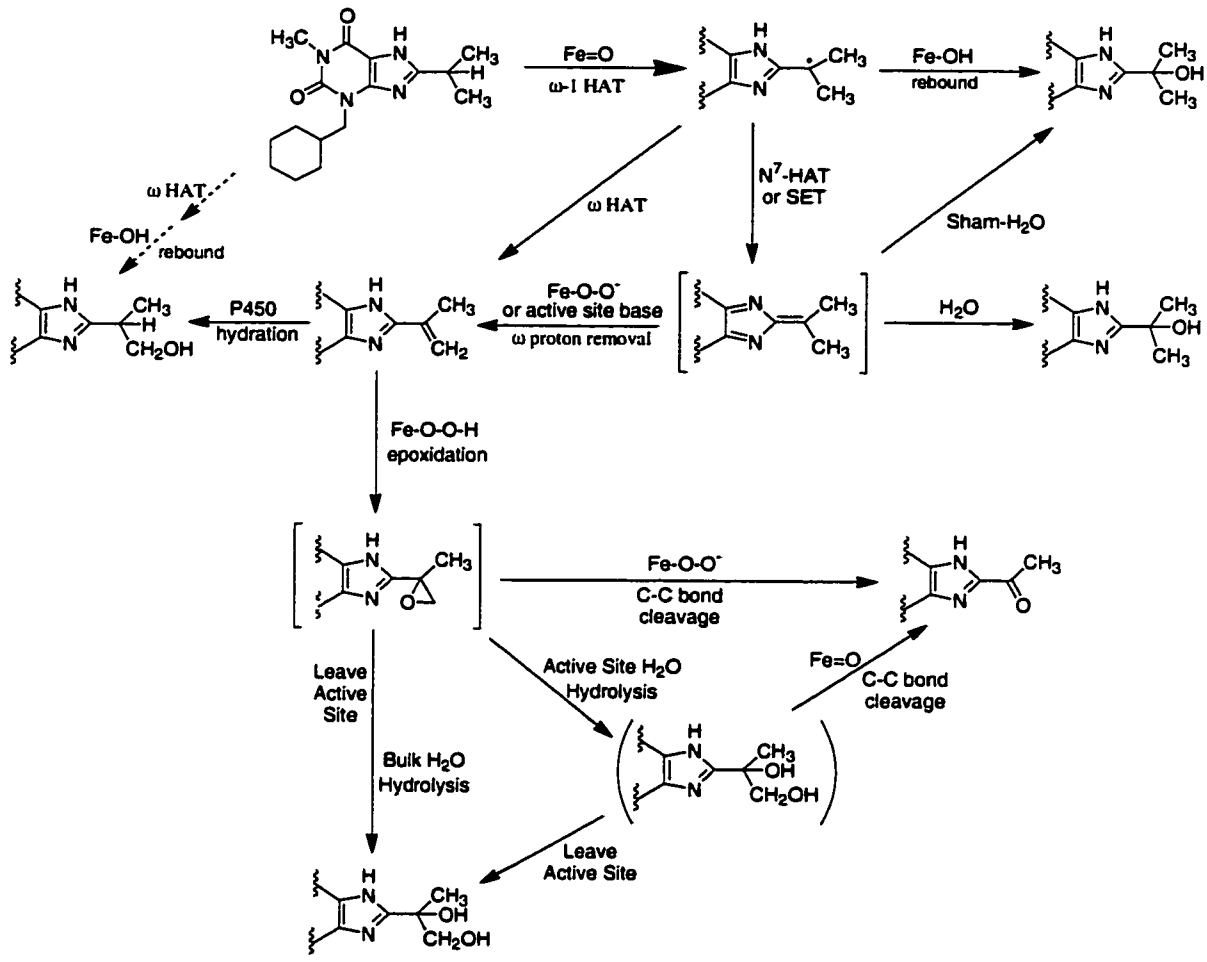

Figure 4.8 Comprehensive metabolic scheme for CYP1A2-catalyzed metabolism of isopropylcyclohexylline **2**, including all feasible mechanisms deduced from experimental data. [a, b]

[a] Dashed arrows between the substrate and primary alcohol metabolite indicate that this mechanism is a minor contributor to total formation.

[b] Diol metabolite shown in parentheses is to indicate its formation and residence within the enzyme active site and to distinguish it from diol formed in the medium.

List of References

1. Ortiz de Montellano, P. R. (1995) *Cytochrome P450 Structure, Mechanism, and Biochemistry*, 2nd ed., Plenum Press, New York.

2. Williams, P. A., Cosme, J., Sridhar, V., Johnson, E. F., and McRee, D. E. (2000) *Mol Cell 5*, 121-31.

3. Williams, P. A., Cosme, J., Sridhar, V., Johnson, E. F., and McRee, D. E. (2000) *J Inorg Biochem 81*, 183-90.

4. Dai, R., Pincus, M. R., and Friedman, F. K. (2000) *Cell Mol Life Sci 57*, 487-99.

5. Ortiz de Montellano, P. R. (1995) in *Cytochrome P450 Structure, Mechanism, and Biochemistry* (Ortiz de Montellano, P. R., Ed.) pp 245-303, Plenum Press, New York.

6. Akhtar, M., and Wright, J. N. (1991) *Nat Prod Rep 8*, 527-51.

7. Guengerich, F. P. (2001) *Chem Res Toxicol 14*, 611-50.

8. Sono, M., Roach, M. P., Coulter, E. D., and Dawson, J. H. (1996) *Chem Rev 96*, 2841-2888.

9. Schlichting, I., Berendzen, J., Chu, K., Stock, A. M., Maves, S. A., Benson, D. E., Sweet, R. M., Ringe, D., Petsko, G. A., and Sligar, S. G. (2000) *Science 287*, 1615-22.

10. Berkowitz, J., Ellison, G.B., Gutman, D. (1994) *J. Phys. Chem. 98*, 2744-2765.

11. Shapiro, S., Piper, J.U., and Caspi, E. (1982) *J. Am. Chem. Soc. 104*, 2301-2305.

12. McMahon, R. E., Sullivan, H. R., Craig, J. C., and Pereira, W. E., Jr. (1969) *Arch Biochem Biophys 132*, 575-7.

13. Hamberg, M., and Bjorkhem, I. (1971) *J Biol Chem 246*, 7411-6.

14. Groves, J. T., and McClusky, G. A. (1978) *Biochem Biophys Res Commun 81*, 154-60.

15. Groves, J. T. a. S., D.V. (1984) *J. Am. Chem. Soc. 106*, 2177-2181.

16. White, R. E., Miller, J.P., Favreau, L.V., and Bhattacharyya, A. (1986) *J. Am. Chem. Soc. 108*, 6024-6031.

17. Griller, D. a. I., K.U. (1980) *Acc. Chem. Res. 13*, 317-323.

18. Ortiz de Montellano, P. R. a. S., R.A. (1987) *J. Am. Chem. Soc. 109*, 3415-3420.

19. Bowry, V. W., Lusztyk, J., and Ingold, K.U. (1989) *J. Am. Chem. Soc. 111*, 1927-1928.

20. Bowry, V. W. a. I., K.U. (1991) *J. Am. Chem. Soc. 113*, 5699-5707.

21. Atkinson, J. K. a. I., K.U. (1993) *Biochemistry 32*, 9209-9214.

22. Newcomb, M., Le Tadic, M.-H., Putt, D.A., and Hollenberg, P.F. (1995) *J. Am. Chem. Soc. 117*, 3312-3313.

23. Toy, P. H., Dhanabalasingam, B., Newcomb, M., Hanna, I.H., and Hollenberg, P.F. (1997) *J. Org. Chem. 62*, 9114-9122.

24. Newcomb, M., Le Tadic-Biadatti, M.-H., Chestney, D.L., Roberts, E.S., and Hollenberg, P.F. (1995) *J. Am. Chem. Soc. 117*, 12085-12091.

25. Toy, P. H., Newcomb, M., and Hollenberg, P.F. (1998) *J. Am. Chem. Soc. 120*, 7719-7729.

26. Newcomb, M., Shen, R., Choi, S.-Y., Toy, P.H., Hollenberg, P.F., Vaz, A.D.N., and Coon, M.J. (2000) *J. Am. Chem. Soc. 122*, 2677-2686.

27. Shaik, S., Filatov, M., Schroder, D., and Schwartz, H. (1998) *Chem. Eur. J. 4*, 193-199.

28. Ogliaro, F., Filatov, M., and Shaik, S. (2000) *Eur. J. Inorg. Chem.*, 2455-2458.

29. Ogliaro, F., Harris, N., Cohen, S., Filatov, M., de Visser, S.P., and Shaik, S. (2000) *J. Am. Chem. Soc. 122*, 8977-8989.

30. Harris, N., Cohen, S., Filatov, M., Ogliaro, F., and Shaik, S. (2000) *Angew. Chem. Int. Ed. 39*, 2003-2007.

31. Auclair, K., Hu, Z., Little, D.M., Ortiz de Montellano, P.R., and Groves, J.T. (2002) *J. Am. Chem. Soc. 124*, 6020-6027.

32. Fisher, M. B., Thompson, S. J., Ribeiro, V., Lechner, M. C., and Rettie, A. E. (1998) *Arch Biochem Biophys 356*, 63-70.

33. Rettenmeier, A. W., Gordon, W. P., Barnes, H., and Baillie, T. A. (1987) *Xenobiotica 17*, 1147-57.

34. Rettie, A. E., Rettenmeier, A. W., Howald, W. N., and Baillie, T. A. (1987) *Science 235*, 890-3.

35. Rettie, A. E., Boberg, M., Rettenmeier, A. W., and Baillie, T. A. (1988) *J Biol Chem 263*, 13733-8.

36. Porubek, D. J., Barnes, H., Meier, G. P., Theodore, L. J., and Baillie, T. A. (1989) *Chem Res Toxicol 2*, 35-40.

37. Kassahun, K., and Baillie, T. A. (1993) *Drug Metab Dispos 21*, 242-8.

38. Rettie, A. E., Sheffels, P. R., Korzekwa, K. R., Gonzalez, F. J., Philpot, R. M., and Baillie, T. A. (1995) *Biochemistry 34*, 7889-95.

39. Korzekwa, K. R., Trager, W. F., Nagata, K., Parkinson, A., and Gillette, J. R. (1990) *Drug Metab Dispos 18*, 974-9.

40. Skiles, G. L., and Yost, G. S. (1996) *Chem Res Toxicol 9*, 291-7.

41. Okazaki, O., and Guengerich, F. P. (1993) *J Biol Chem 268*, 1546-52.

42. Guengerich, F. P., and Bocker, R. H. (1988) *J Biol Chem 263*, 8168-75.

43. Miwa, G. T., Walsh, J. S., Kedderis, G. L., and Hollenberg, P. F. (1983) *J Biol Chem 258*, 14445-9.

44. Ortiz de Montellano, P. R. (1989) *Trends Pharmacol Sci 10*, 354-9.

45. Guengerich, F. P., Okazaki, O., Seto, Y., and Macdonald, T. L. (1995) *Xenobiotica 25*, 689-709.

46. Augusto, O., Beilan, H. S., and Ortiz de Montellano, P. R. (1982) *J Biol Chem 257*, 11288-95.

47. Hanzlik, R. P., and Shearer, G. O. (1978) *Biochem Pharmacol 27*, 1441-4.

48. Groves, J. T., Avaria-Neisser, G.E., Fish, K.M., Imachi, M., and Kuczkowski, R.L. (1986) *J. Am. Chem. Soc. 108*, 3837-3838.

49. Vaz, A. D., Pernecky, S. J., Raner, G. M., and Coon, M. J. (1996) *Proc Natl Acad Sci U S A 93*, 4644-8.

50. Vaz, A. D., McGinnity, D. F., and Coon, M. J. (1998) *Proc Natl Acad Sci U S A 95*, 3555-60.

51. Coon, M. J., Vaz, A. D., McGinnity, D. F., and Peng, H. M. (1998) *Drug Metab Dispos 26*, 1190-3.

52. Nam, W., Lee, H. J., Oh, S. Y., Kim, C., and Jang, H. G. (2000) *J Inorg Biochem 80*, 219-25.

53. Nam, W., Lim, M.H., Lee, H.J., and Kim, C. (2000) *J. Am. Chem. Soc. 122*, 6641-6647.

54. Ogliaro, F., de Visser, S. P., Cohen, S., Sharma, P. K., and Shaik, S. (2002) *J Am Chem Soc 124*, 2806-17.

55. de Visser, S. P., Ogliaro, F., Harris, N., and Shaik, S. (2001) *J Am Chem Soc 123*, 3037-47.

56. Sugiyama, K., Nagata, K., Gillette, J. R., and Darbyshire, J. F. (1994) *Drug Metab Dispos 22*, 584-91.

57. Shikita, M., and Hall, P. F. (1974) *Proc Natl Acad Sci U S A 71*, 1441-5.

58. Burstein, S., and Middleditch, B. S. (1974) *Biochem Biophys Res Commun 61*, 692-7.

59. Burstein, S., Middleditch, B. S., and Gut, M. (1975) *J Biol Chem 250*, 9028-37.

60. Kraaipoel, R. J., Degenhart, H. J., and Leferink, J. G. (1975) *FEBS Lett 57*, 294-300.

61. Kraaipoel, R. J., Degenhart, H. J., van Beek, V., de Leeuw-Boon, H., Abeln, G., Visser, H. K., and Leferink, J. G. (1975) *FEBS Lett 54*, 172-9.

62. Kraaipoel, R. J., Degenhart, H. J., Leferink, J. G., Van Beek, V., De Leeuw-Boon, H., and Visser, H. K. (1975) *FEBS Lett 50*, 204-9.

63. Burstein, S., Byon, C. Y., Kimball, H. L., and Gut, M. (1976) *Steroids 27*, 691-701.

64. Morisaki, M., Bannai, K., Ikekawa, N., and Shikita, M. (1976) *Biochem Biophys Res Commun 69*, 481-8.

65. Teicher, B. A., Koizumi, N., Koreeda, M., Shikita, M., and Talalay, P. (1978) *Eur J Biochem 91*, 11-9.

66. Lambeth, J. D., Kitchen, S. E., Farooqui, A. A., Tuckey, R., and Kamin, H. (1982) *J Biol Chem 257*, 1876-84.

67. Tuckey, R. C., and Kamin, H. (1982) *J Biol Chem 257*, 9309-14.

68. Tuckey, R. C., and Kamin, H. (1983) *J Biol Chem 258*, 4232-7.

69. Turesky, R. J., Parisod, V., Huynh-Ba, T., Langouet, S., and Guengerich, F. P. (2001) *Chem Res Toxicol 14*, 901-11.

70. Bondon, A., Macdonald, T. L., Harris, T. M., and Guengerich, F. P. (1989) *J Biol Chem 264*, 1988-97.

71. Bell-Parikh, L. C., and Guengerich, F. P. (1999) *J Biol Chem 274*, 23833-40.

72. Tagashira, H., Kominami, S., and Takemori, S. (1995) *Biochemistry 34*, 10939-45.

73. Grogan, J., Shou, M., Zhou, D., Chen, S., and Korzekwa, K. R. (1993) *Biochemistry 32*, 12007-12.

74. Yamazaki, T., Ohno, T., Sakaki, T., Akiyoshi-Shibata, M., Yabusaki, Y., Imai, T., and Kominami, S. (1998) *Biochemistry 37*, 2800-6.

75. Rendic, S., and Di Carlo, F. J. (1997) *Drug Metab Rev 29*, 413-580.

76. Eaton, D. L., Gallagher, E. P., Bammler, T. K., and Kunze, K. L. (1995) *Pharmacogenetics 5*, 259-74.

77. Jencks, W. P. (1987) in *Catalysis in Chemistry and Enzymology* pp 243-281, Dover Publications, Inc., Mineola, N.Y.

78. Westheimer, F. H. (1961) *Chem. Rev. 61*, 265-273.

79. Higgins, L., Bennett, G. A., Shimoji, M., and Jones, J. P. (1998) *Biochemistry 37*, 7039-46.

80. Northrop, D. B. (1981) *Annu Rev Biochem 50*, 103-31.

81. Gillette, J. R. a. K., K. (1990) in *Biological Reactive Intermediates IV* (Witmer, C. M., *et al.*, Ed.), Plenum Press, New York.

82. Jones, J. P., Korzekwa, K.R., Rettie, A.E., and Trager, W.F. (1986) *J. Am. Chem. Soc. 108*, 7074-7078.

83. Korzekwa, K. R., Trager, W. F., and Gillette, J. R. (1989) *Biochemistry 28*, 9012-8.

84. Miwa, G. T., Garland, W. A., Hodshon, B. J., Lu, A. Y., and Northrop, D. B. (1980) *J Biol Chem 255*, 6049-54.

85. Segura, J., Garcia, I., and Tarrus, E. (1986) *J Pharm Pharmacol 38*, 615-8.

86. Sesardic, D., Boobis, A. R., Murray, B. P., Murray, S., Segura, J., de la Torre, R., and Davies, D. S. (1990) *Br J Clin Pharmacol 29*, 651-63.

87. Tarrus, E., Cami, J., Roberts, D. J., Spickett, R. G., Celdran, E., and Segura, J. (1987) *Br J Clin Pharmacol 23*, 9-18.

88. Kunze, K. L., and Trager, W. F. (1993) *Chem Res Toxicol 6*, 649-56.

89. Racha, J. K., Rettie, A. E., and Kunze, K. L. (1998) *Biochemistry 37*, 7407-19.

90. Kunze, J. K. R. a. K. L. (1998) *J. Am. Chem. Soc. 120*, 5337-5338.

91. Obach, R. S. (2001) *Drug Metab Dispos 29*, 1057-67.

92. Mazur, R. H., White, W.N., Semenow, D.A., Lee, C.C., Silver, M.S., and Roberts, J.D. (1959) *J. Am. Chem. Soc. 81*, 4390-4398.

93. Olah, G. A., Jeuell, C.L., Kelly, D.P., and Porter, R.D. (1972) *J. Am. Chem. Soc. 94*, 146-156.

94. Winstein, S. (1972) in *Carbonium Ions* (Olah, G. A., and Schleyer, P. R., Eds.) pp 965-1005, Wiley-Interscience, New York.

95. Olah, G. A., White, A.M., DeMember, J.R., Commeyras, A., and Lui, C.Y. (1970) *J. Am. Chem. Soc. 92*, 4627-4640.

96. Roberts, J. D. a. M., R.H. (1951) *J. Am. Chem. Soc. 73*, 2509-2520.

97. Olah, G. A. (1973) *Angew. Chem. internat. Edit. 12*, 173.

98. Olah, G. A., and Schleyer, P. R. (1972) *Nonclassical Ions and Homoaromaticity*, Vol. III, Wiley-Interscience, New York.

99. Caserio, M. C., Graham, W.H., and Roberts, J.D. (1960) *Tetrahedron 11*, 171-182.

100. Hanack, M. a. S., H.-J. (1967) *Angew. Chem. internat. Edit. 6*, 666-677.

101. Wiberg, K. B., Shobe, D., and Nelson, G.L. (1993) *J. Am. Chem. Soc. 115*, 10645-10652.

102. Holland, H. L., Chernishenko, M.J., Conn, M., Munoz, A., Manoharan, T.S., and Zawadski, M.A. (1990) *Can. J. Chem. 68*, 696-700.

103. Bowry, V. W., Lusztyk, J., and Ingold, K.U. (1990) *J. Chem. Soc., Chem. Commun.*, 923-925.

104. Halgren, T. A., Roberts, J.D., Horner, J.H., Martinez, F.N., Tronche, C., and Newcomb, M. (2000) *J. Am. Chem. Soc. 122*, 2988-2994.

105. Beckwith, A. L. J. a. B., V.W. (1994) *J. Am. Chem. Soc. 116*, 2710-2716.

106. Guroff, G., Daly, J. W., Jerina, D. M., Renson, J., Witkop, B., and Udenfriend, S. (1967) *Science 157*, 1524-30.

107. Olah, G. A. (1995) *Angew. Chem. Int. Ed. Engl. 34*, 1393-1405.

108. Reynolds, K. A., O'Hagan, D., Gani, D., Robinson, J.A. (1988) *J. Chem. Soc., Perkin Trans. 1 12*, 3195-3207.

109. Atkinson, J. G., Csakvary, J.J., Herbert, G.T., Stuart, R.S. (1968) *J. Am. Chem. Soc. 90*, 498-499.

110. Evans, D. A., Bartroli, J., and Shih, T.L. (1981) *J. Am. Chem. Soc. 103*, 2127-2129.

111. Fletcher, M. D., Harding, J.R., Hughes, R.A., Kelly, N.M., Schmalz, H., Sutherland, A., and Willis, C.L. (2000) *J. Chem. Soc., Perkin Trans. 1*, 43-52.

112. Kelly, N. M., Reid, R.G., Willis, C.L., and Winton, P.L. (1995) *Tetrahedron Lett. 36*, 8315-8318.

113. Evans, D. A., Britton, T.C., and Ellman, J.A. (1987) *Tetrahedron Lett. 28*, 6141-6144.

114. Harding, J. R., Hughes, R.A., Kelly, N.M., Sutherland, A., and Willis, C.L. (2000) *J. Chem. Soc., Perkin Trans. 1*, 3406-3416.

115. (1989) in *Vogel's Textbook of Practical Organic Chemistry* (Furniss, B. S., Hannaford, A.J., Smith, P.W.G., Tatchell, A.R., Ed.) pp 609: exp. 5.86, Longman Scientific & Technical, Essex, England.

116. Dahn, H., Dao, Le H., Hunma, R. (1982) *Helv.Chim.Acta 65*, 2458-2463.

117. Jackman, M., Bergman, A.J., and Archer, S. (1948) *J. Am. Chem. Soc. 70*, 497.

118. Harnden, M. R. (1971) in *Chemical Abstracts*, Abbott Laboratories, US.

119. Sugiyama, K., Trager, W.F. (1986) *Biochemistry 25*, 7336-7343.

120. Obach, R. S. (2000) *Drug Metab Dispos 28*, 1069-76.

121. Obach, R. S. (2001) *Drug Metab Dispos 29*, 1599-607.

122. Murray, S., Odupitan, A. O., Murray, B. P., Boobis, A. R., and Edwards, R. J. (2001) *Xenobiotica 31*, 135-51.

123. Lozano, J. J., Lopez-de-Brinas, E., Centeno, N.B., Guigo, R., and Sanz, F. (1997) *Journal of Computer-Aided Molecular Design 11*, 395-408.

124. Lowry, T. H. a. R., K.S. (1976) *Mechanism and Theory in Organic Chemistry*, Harper & Row, New York.

125. Lewis, D. f. V. a. L., B.G. (1996) *Xenobiotica 26*, 723-753.

126. Lewis, D. F. V., Lake, B.G., George, S.G., Dickins, M., Eddershaw, P.J., Tarbit, M.H., Beresford, A.P., Goldfarb, P.S., Guengerich, F.P. (1999) *Toxicology 139*, 53-79.

127. Hadjokas, N. E., Dai, R., Friedman, F. K., Spence, M. J., Cusack, B. J., Vestal, R. E., and Ma, Y. (2002) *Br J Pharmacol 136*, 347-52.

128. Vidakovic, M., Sligar, S.G., Li, H., and Poulos, T.L. (1998) *Biochemistry 37*, 9211-9219.

129. Aikens, J., Sligar, S.G. (1994) *J Am Chem Soc 116*, 1143-1144.

Vita

Jason Boer was born in Sioux Center, Iowa. He lived in Lyons, South Dakota for the majority of his life. He currently calls Colchester, Connecticut his home. At the University of Minnesota, Morris he earned Bachelor of Arts degrees in Chemistry and Biology. In 2003 he earned a Doctor of Philosophy at the University of Washington in Medicinal Chemistry.